High Heat Flux Tolerant and Radiation Resistant Materials Based on Mo and SiC Coatings

By

Nisar Ahmed

Reg # 00000203786

Session 2017-19

Supervised by

Prof. Dr. Zuhair S. Khan

A Thesis Submitted to the US Pakistan Centre for Advanced Studies in Energy in partial fulfillment of the requirements for the degree of

MASTERS of SCIENCE in

THERMAL ENERGY ENGINEERING

US Pakistan Center for Advanced Studies in Energy (USPCASE)

National University of Sciences and Technology (NUST)

H-12, Islamabad 44000, Pakistan

July 2020

THESIS ACCEPTANCE CERTIFICATE

Certified that final copy of MS thesis written by **Mr. Nisar Ahmed**, (Registration No. 00000203786), of U.S.-Pakistan Center for Advanced Studies in Energy (USPCAS-E), NUST has been vetted by undersigned, found complete in all respects as per NUST Statues/Regulations, is in the allowable limits of plagiarism, errors, and mistakes and is accepted as partial fulfillment for award of MS degree. It is further certified that necessary amendments as pointed out by GEC members of the scholar have also been incorporated in the said thesis.

Signature: Zskhan

Name of Supervisor: Dr Zuhair S. Khan

Date: 26 July, 2020

Signature (HoD TEE): _____

Date: _____

Signature (Principal/Dean): _____

Date: _____

Certificate

This is to certify that work in this thesis has been carried out by **Mr. Nisar Ahmed** and completed under my supervision in Advanced Energy Materials and Systems laboratory, USPCAS-E, National University of Sciences and Technology, H-12, Islamabad, Pakistan.

Supervisor:

Dr. Zuhair S. Khan
USPCAS-E
NUST, Islamabad

GEC member 1: _____

Dr. Majid Ali
USPCAS-E
NUST, Islamabad

GEC member 2: _____

Dr. Nadia Shahzad
USPCAS-E
NUST, Islamabad

GEC member 3:

Dr. Malik Adeel Umer
SCME
NUST, Islamabad

HOD-TEE: _____

Dr. Adeel Javed
USPCAS-E
NUST, Islamabad

Principal: _____

Dr. Adeel Waqas
USPCAS-E
NUST, Islamabad

Dedication

All praise to Allah Almighty who gave me the strength and knowledge to do the work presented in this thesis. I would like to express my sincere gratitude to my research supervisor, Prof. Dr. Zuhair S. Khan for letting me be part of the research group at Advanced Energy Materials Lab, USPCAS-E, NUST, Islamabad. I feel privileged to have worked under his kind Supervision. It's the blend of his patience, persistence, guidance and motivation that made me accomplish my research aims in due time. He polished my research skills and I have learned a lot under his supervision and guidance.

I would also like to thank the members of my GEC committee, Dr. Majid Ali, Dr. Nadia Shehzad, and Dr. Malik Adeel who honored my committee's presence. I would like to sincerely thank my senior Mr. Azhar Iqbal, my fellows and friends for their unconditional support. Specially, I pay gratitude to Lab Engineers Mr. Asghar ali, Mr. Aamir Satti and Mr. Qamar sahib for their unmatchable support during the whole research work.

I gratefully acknowledge the financial support provided by the Research and PGP Directorates of NUST and the US-AID.

Abstract

Fulfilling energy demand is very vital for every nation. But using fossil fuels to meet it has turned the global environment on a destructive path. The high level of greenhouse gas (GHG) emissions and the impacts of global warming have stimulated humans to find environmentally friendly energy practices. Apart from renewable sources, nuclear fusion and advanced nuclear fission are the aspiring alternative to fossil fuels. Scientists are considering fusion as a future of energy. The aim is the development of such a facility that can run the process for a long period of time. In order to sustain in a high-temperature plasma environment, it is needed to make plasma-facing components that are high heat flux tolerant and erosion resistive. Molybdenum (Mo) is a high Z refractory metal. It has a high melting temperature of 2617°C and a low coefficient of thermal expansion of 4.8 μm/m°C. Combination of thermo-mechanical and chemical properties makes it suitable for various applications that involve high heat flux. In Generation IV nuclear fission reactors, molten salt reactor will play a significant role in the exploration of nuclear energy. These reactors will employ graphite as a reflector and moderator. Owing to the high porosity of the graphite matrix, it undergoes oxidation at high temperatures. However, several opportunities exist to enhance graphite's utility as a moderator in Generation IV nuclear reactors. One of them is by developing an oxidation-resistant coating. This work consists of two major portions. At first, DC magnetron sputtering was employed to deposit molybdenum coatings on the graphite substrate. The impact of process parameters like sputtering power and working gas pressure has been investigated to get a suitable match between physical and mechanical characteristics of coating and substrate. Adequate class thin film was achieved at high deposition power and low working gas pressure. The optimum thin film was irradiated with He ion of 0.8 MeV and 1.6 MeV with an equivalent dose of 0.0765 and 0.645 DPA respectively. Different analytical techniques were employed to analyze the structure and morphological evolution occurred as a result of irradiation. Significant deterioration in crystallanity was observed as crystallite size was decreased at high irradiation dose. Surface roughness was increased and electrical conductivity was dropped. However, no delamination was observed. Micro-hardness of Mo thin film increased with an increase in irradiation dose. In the second part of this research one-micron silicon carbide (SiC) coating was developed on Graphite using RF

Magnetron Sputtering to serve as an anti-corrosion layer. Crystallanity of deposited thin film was enhanced by high-temperature annealing at 1000, 1200 and 1400 °C. The dependence of corrosion resistance on the annealing temperature of coatings has been analyzed. Corrosion resistance of SiC thin film increased with an increase in annealing temperature as sample annealed at 1400 °C showed the lowest corrosion rate as compared to low temperature annealed thin films.

Keywords: Molybdenum, Magnetron Sputtering, Irradiation, Tokamak, Thin Films, Silicon Carbide

Table of Contents

List of figures

List of Tables

List of Abbreviations/ Nomenclature

GHG	Green House Gasses
CPEC	China-Pakistan economic corridor
UNDP	United Nation Development Program
CIGS	Copper indium gallium selenide
PVD	Physical vapor deposition
CVD	Chemical vapor deposition
PAEC	Pakistan Atomic Energy Commission
AEDB	Alternative Energy Development Board
PCRET	Pakistan Council of Renewable Energy
ITER	International Thermonuclear
TOKAMAK	Torus-shaped vacuum chamber surrounded by magnetic coils
Mo	Molybdenum
SiC	Silicon Carbide
DCMS	Direct Current Magnetron Sputtering
SLG	Soda lime Glass
NBI	neutral beam injection
PFC	Plasma Facing Component
XRD	X ray Diffraction
AFM	Atomic Force Microscopy
SEM	Scanning Electron Microscopy
E	Energy
EIS	Electrochemical impedance spectroscopy
OCPT	Open circuit potential time
PECVD	Plasma enhanced Chemical Vapor Deposition
B	Magnetic field
E	Electric Field
F	Force
v	Velocity
Ω	Ohm sign
p	Resistivity
L	Crystallite Size
MeV	Mega electron volt
KeV	Kilo electron volt
RFMS	Direct Current Magnetron Sputtering
K	Scherrer Constant
OCPT	Open Circuit Potential Time

List of Journal Papers from this research work

1. DC magnetron sputtered Mo thin films with high adhesion, conductivity and reflectance
   Nisar Ahmed, Azhar Iqbal, Zuhair S. Khan, Ahmed Qayyum
   Published in **"Journal of Electronic Materials"** on 16th April, 2020
   Volume: 49, Page No: 4221-4230 **(DOI:** 10.1007/s11664-020-08138-2)
2. Effects of process parameters on the microstructural characteristics of DC magnetron sputtered molybdenum films on graphite substrate
   M Azhar Iqbal, Zuhair S. Khan, **Nisar Ahmed**
   Published in **"AJSE"** (**DOI:** 10.1007/s13369-020-04888-7)
3. Structural evaluation and irradiation hardening in α-particles irradiated DC magnetron sputtered Mo thin film
   Nisar Ahmed, Zuhair S. Khan, Azhar Iqbal, Asghar Ali
   To be submitted in **"Nuclear Engineering and Design"**
4. Impact of high temperature annealing on corrosion resistance & Adhesion of RF Magnetron sputtered SiC thin film on graphite
   Nisar Ahmed, Zuhair S. Khan
5. Fabrication of Molybdenum carbide by reactive annealing of DC sputtered Mo Thin Film on graphite substrate
   Nisar Ahmed, Zuhair S. Khan

Chapter 1: Introduction

1.1 Problem of Energy

The world's population has grown faster than ever in the last century. With advancement in science, our life standards improved a lot, which ultimately leads to increase in energy demand. Human being always tends to find an easy and economical ways of energy to meet those requirements. In last 12 decades human being relied mostly on fossil fuels, as they were the most economical and easiest to access. The present and predicted global energy mix is given in the figure 1-1. Electric power demand is meet mostly by coal power plants and transportation needs are meet by crude oil derivatives. But things were not as easy as they were looking [1].

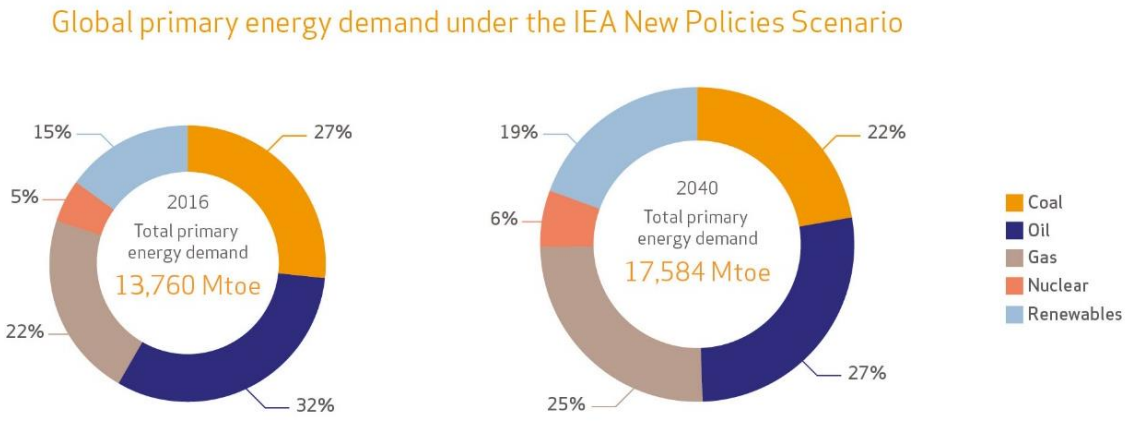

Figure 1-1: Global energy mix

Those fossil fuel reserves are not only depleting but humanity is paying huge price due to climate changes cause by carbon dioxide emission. These major environmental issues have compelled humanity to find out nature friendly energy sources. Solar, Wind, Biomass, hydro energy and fission based nuclear plants are one of them. The world is moving towards those technologies. Now days, the major portion of worlds electrical demand is meet by renewable sources. But due to their shorter availability and ever-increasing demand in energy have compelled us to establish most advanced energy technologies [2].

Nuclear fusion-based power plants can be potential candidate to meet such up rise in energy demand.

1.2 Climate Change

Many people still doubt that climate change is real thing. In previous century, greenhouse effect was discovered. According to which Carbon dioxide in our atmosphere is continuously heating our atmosphere. Majority of them came from burning of fossil fuels as shown in the figure 1-2. Usually total heat it gains from sun is released to space in the form of different radiations majorly in the form of infrared radiation. But presence of carbon dioxide in abundance disturbs this balance as it has ability to entrap the heat. Most of Carbon dioxide is consumed by vegetation and forests [2]. But green belts are decreasing due to increase in urbanization and carbon dioxide emission is increasing on the other hand.

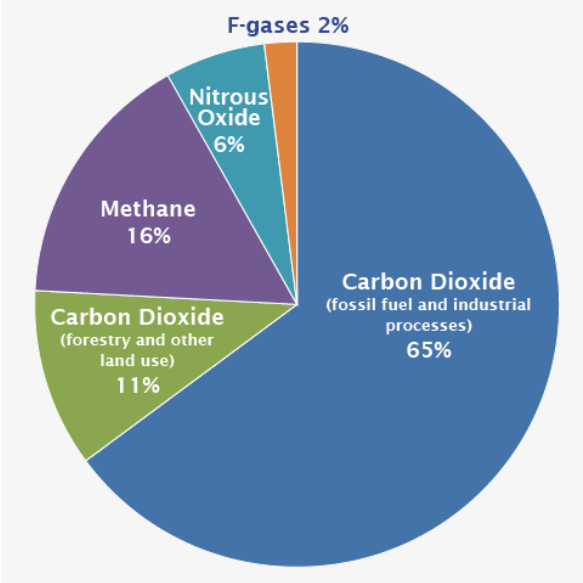

Figure 1-2 Global greenhouse gas emission

This is leading us toward surplus CO_2 formation. Current CO_2 concentration in our environment is about 407 ppm, which is 3 times more than average CO_2 concentration in last 100000 years of earth. Scientists predict that if we keep releasing CO_2 at this particular rate, the earth will become inhabitable and turns into planet like Venus.

Talking about Pakistan carbon dioxide is a main cause behind greenhouse gas emission. which accounts about 60%. Carbon dioxide emission which was about 30 million tons in

1980s is now 170 million tons per year. Trends show we are increasing CO2 emission by 6 to 8 percent every year [3].

1.3 Energy shortage in Pakistan

Pakistan always has power and energy shortage problems. Situation was worse few year back. Most of power demand in Pakistan is meet by coal and fossil fuels in the form of thermal power plants. Pakistan oil production is very limited, so most of energy demand meets by importing the oil. Which is not only increases the import bill but also causing environmental issues [2]. Pakistan is one of the top ten countries vulnerable countries that are most affected by climate change, increase in energy demands and depletion in fossil fuel is the major concern that compelled us to start thinking about such kind of energy facilities that can give abundant, sustainable and environment friendly energy [3]. Currently, Pakistan's energy mix from fossil fuels and hydrocarbons is 63 % (Natural gas 29 %, Oil 22 %, Coal 12 %) as shown in figure 1-3. Power generated from Fission based nuclear reactor accommodate 2 % of national need. Renewable have very small portion [4].

It is well noticeable that Pakistan in not a poor nation as far as accessibility of natural resources yet, it is a nation that falls behind at the administration end. It is shocking to express that about 15% of population have no access to power. Energy shortfall is presently the reason of numerous different issues the present circumstance requests to fathom not just the energy crises yet in addition to the human advancement which are enormously interlinked. Advance power generation technologies, for example, hydrogen based novel assets for Fusion reactors are in reality on of the answer for these musings. In this system Pakistan has officially settled Nation Tokamak Program which requires a great deal of devoted work to make it ready to begin vitality creation in not so distant future and this examination is step towards goal.

1.4 Solution to problem

Pakistan is facing huge electrical power crisis. Per capita electric power consumption of Pakistan is three times less than world's average. This problem needs to resolve as soon as possible, because industrial growth and Gross domestic product of any country is directly related to power consumption [4]. We need to install those power sources that can provide

sustainable solution to this problem. They must be not only economical but environment friendly. Pakistan is taking some positive steps in this regard. Share of renewable energy is increasing every year. Nuclear energy also has significant share in accommodating national grid, which is about 1300 MW. Pakistan is planning to increase nuclear power capacity to 8000 by the year 2025.

Many departments have been established to do feasibility, research and development of energy sector in Pakistan. Those departments include AEDB (Alternative Energy Development Board) and PCRET (Pakistan Council of Renewable Energy) are established to work for sustainable and renewable energy. Moreover, Center for Advance Studies in Energy has been established in National University of Sciences and Technology and University of Engineering Technology, Peshawar with the collaboration of USAID. The purpose of these institutes is to do R&D in energy sector and to produce trained personals.

Pakistan needs to rely on all possible power solution. All the conventional and renewable sources need to be utilized together [5]. Currently Pakistan's installed capacity is about 25000 MW. And our demand varies between 17000 to 23000 MW, which is expected to rise by 4 times till 2050.

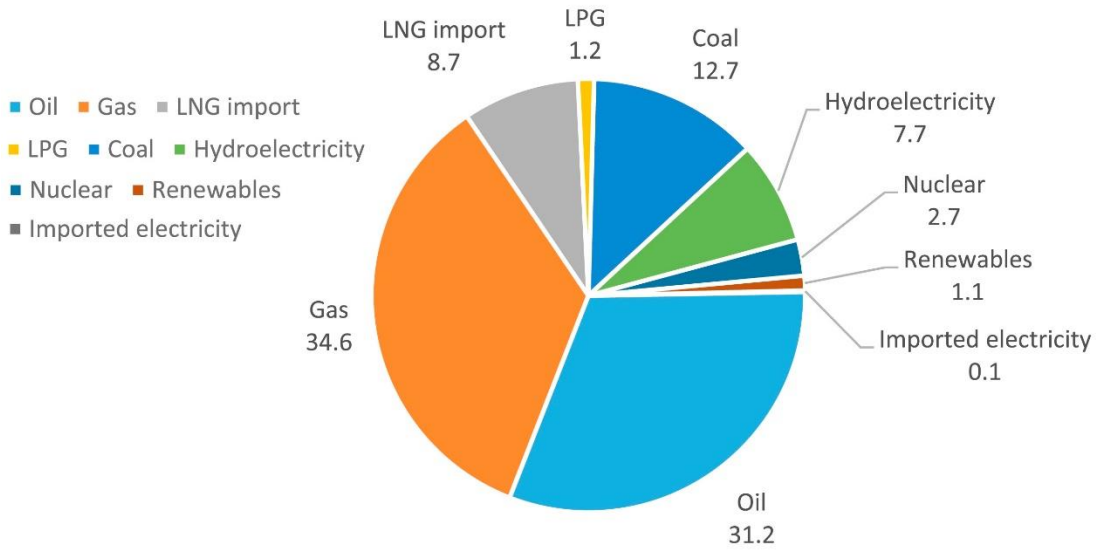

Figure 1-3 Energy Mix of Pakistan by Sector

1.5 Renewable source of energy

When it comes to renewable source of energy, solar energy is the first thing came to mind. Solar energy evolves significantly in last 20 years. Efficiency has increased and cost of production reduced by 80 %. Solar PV is capitalizing on its position in the renewable market [6]. Currently, Global PV power capacity is about 250 GW. 100 times more than 20 years. Solar PV is fastest growing source among the renewable, with an annual average growth rate of 8%. Many classes of Solar PV have been introduced to the market. But the most efficient are CIGS and CZTR based solar cells, with efficiency exceeding 20 % [7]. Other than that wind energy is also one of aspiring source of renewable energy.

1.6 Nuclear power as an alternative source of energy

Solar energy is good prospect for renewable energy. But it is only available at the day time. Thermal storage devices to store solar energy for nights have low conversion efficiency. Similarly, Wind energy is limited to coastal areas only. Due to these limitations in solar and wind power energy, we can't completely rely on these sources. We have to look at another alternative source for continues power supply [2]. The convention sources of energy burning fossil fuels is comparatively a reliable mode but this energy production is at the cost of distraction in environment is not bearable. In addition to depletion of oil and gas reserves is a sure fact, one day fossil fuels are going to be depleted. Nuclear energy can be good option to meet continuous power demand. Nuclear energy can be extracted by two ways, by nuclear fission and nuclear fusion reactions [8]. After advancement in nuclear energy in last century, hundreds of fissions based nuclear power plants are working in different countries producing thousands of Megawatts. Fusion based nuclear power plants are still in research phase. It is considered as one the safe and abundant source of energy for future.

Nuclear energy was considered as myth in mid-20^{th} century. But now it is very much included in daily life. Nuclear radiation usually exists naturally and can be produced artificially for many applications like medical in diagnosis and research purpose [9]. They are utilized to kill cancer cells. Currently 400 nuclear reactors are active producing about 10 % of world's total power. At present, cost of 1 kilo watt hour of nuclear power costs around 0.033 US dollars. This cost includes fuel cost and all the operational and

maintenance cost. But these nuclear reactors are producing nuclear waste which is a public fear; there is no safe method to dispose this nuclear waste.

1.7 Energy from Fusion

According to scientists start of universe happened 14 billion years ago after big bang. It was predicted to produce in very dense hydrogen gas cloud at ultra-high temperature. Hydrogen clouds spread throughout in the universe. When different clouds got critical mass and volume, they collapsed to fewer volume due to gravitational force. Owing to high temperature and pressure at their core, fusion reaction begins and new stars formed. After millions of years those larger stars turn to super nova due to shortage of hydrogen [9]. And large portion of that gas spread out in the space, which was enough to form smaller stars like our sun [8]. Our star is about 6 billion old, like each star it is having nuclear fusion in its core where temperature is about 15 million degree Celsius. Hydrogen atoms collide with each other very abruptly and repulsive force overcomes and as result to form larger nuclei releasing huge amount of energy [10]. Figure 1-4 illustrates the phenomena of fusion reaction. Deuterium and tritium are the feed stock of Tokamak based magnetic confinement nuclear device. Deuterium is available in every source of water. About 0.9 % of hydrogen is comprised of deuterium. Sea water will be main source of Deuterium and can be sufficient for millions of years [11]. Talking about Tritium, it is not abundant in the earth as it has shorter half-life. It is extracted from lithium in tritium breeder inventory inside Tokamak device. Technically speaking, one basket of water and lithium present in your battery can provide power to your entire house for 50 years.

In order to produce control fusion reaction at earth we need more critical conditions. We need to raise temperature up to 100-million-degree Celsius degree to start that reaction. This temperature can be achieved by different methods but maintain that plasma and temperature for long time is the actual issue [12]. No material can handle temperature more than 4000 Celsius. So, the idea of nuclear magnetic confinement was presented in the last century. This idea is gone through gradual improvements

PTL device from the production of first watt of electricity to 16,000,000 watts using the JET device at United Kingdom in year 1997. Internal Thermonuclear experiment reactor (ITER) is currently in development phase [13], which is expected to produce ≈500,000,000

Watts after its complete operation. Energy output will be at the order of 10 and this productivity is planned to be proved after 2030. Yet there are decades to reach the destination of this dream. Not only the electrical production but fusion has application in other aspects also, through which it can give benefits to mankind.

In 1985 after the proposal of collaborative international fusion project, Fusion made a remarkable appearance to the common world through a series of science fiction movies and it has remained a fascinating art in many blockbuster creations in one or another way even till now fusion is a subject of many famous latest movies [9]. Peoples perceive fusion technology as fiction but it has real deep roots in actual science. Combination of different field of science has turned this dream to reality. Moreover, fusion machine was ready on drawing board in the era of World War II. of shining stars was tried to explain by a British astrophysicist Arthur Eddington in 1920. He proposed that this energy is produced due to fusion reaction between hydrogen atoms [14], which was further elaborated by "proton-proton chain" described by 1967 Nobel Prize in Physics winner Hans Bethe in 1939. Other major contributor to the modern fusion research was Ernest Rutherford from his explanation of atomic structure. Furthermore, Australian scientist Mark Oliphant discovered the second heavy isotope of hydrogen named tritium, which played a main role towards aleuronic fusion [10].

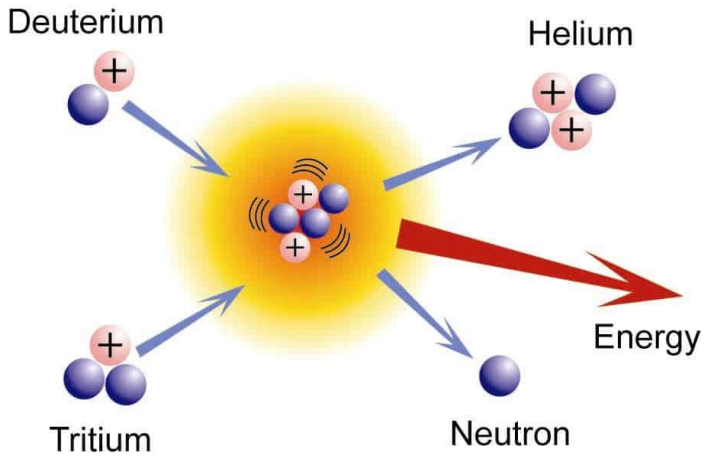

Figure 1-4 Schematic of nuclear Fusion reaction

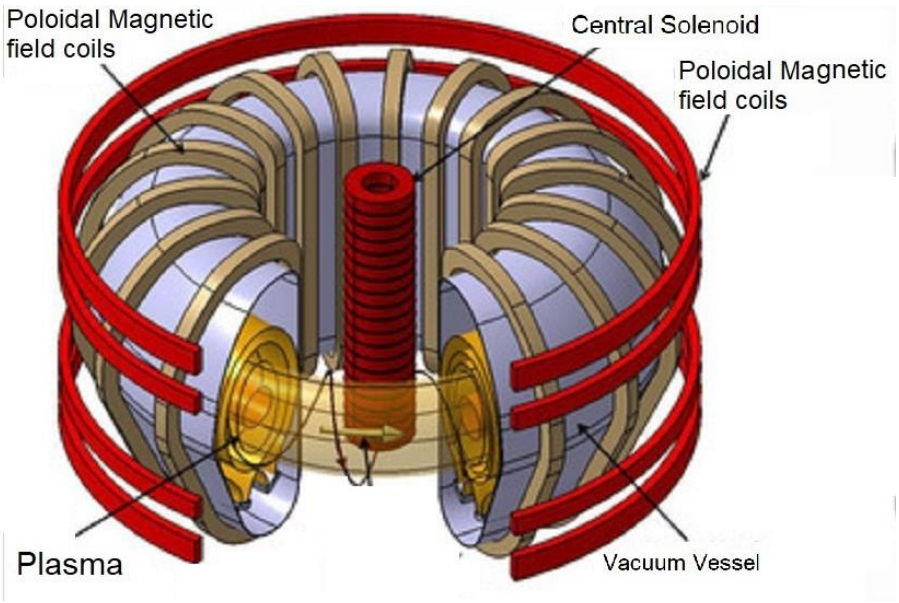

Figure 1-5 Schematic of Tokamak reactor

1.7.1 Fusion reactor

Many classes of magnetic confinement based nuclear fusion devices were proposed and made. But Tokamak is one of the most reliable designs due to its most successful configuration to make nuclear fusion device [12]. The word tokamak is derived from Russian language which means torus shaped vacuum chamber cover by magnets. It was initially developed by Russian scientist in 1960. It is still considered as the most reliable design for magnetic confinement [15]. Schematic of tokamak is given in the figure 1-5.

Deuterium and tritium are the feed stock of Tokamak based magnetic confinement nuclear device. Deuterium is available in every source of water. About 0.9 % of hydrogen is comprised of deuterium. Seawater will be main source of Deuterium and can be sufficient for millions of years. Talking about Tritium, it is not abundant in the earth as it has shorter half-life [13]. It is extracted from lithium in tritium breeder inventory inside Tokamak device. Technically speaking, one basket of water and lithium present in your battery can provide power to your entire house for 50 years.

Tokamak is comprised of experimental setup which produces energy as a result of nuclear fusion. As the plasma forms at 100 million degree Celsius so reactants cannot be directly in contact with any chamber material. For this purpose, magnetic field is applied in poloidal and toroidal forms. Gigantic coil around the chamber confined the plasma in central part

by virtue of powerful magnetic field. As plasma is comprised of charged particles so it leads to confinement of plasma in vacuum chamber. Absence of air leads to no heat transfer through conduction and convection. The only mean of heat transfer is radiation. The coolant running in cooling pipes in the first wall collects the heat and converts it into steam. This steam then runs the turbine to produce electrical power by induction.

ITER (International Thermonuclear Experimental Reactor) will be one of the largest TOKAMAK devices in the world and it is under construction. This project begins in 1985 and construction has started in 2010. 35 countries are collaborating to develop ITER. They are planning to ignite plasma in the mid of next decade. Scientists are planning to generate 500 MW power from this reactor. This project will be followed by DEMO, which will be first commercial reactor to product electricity for public use. It is estimated that tokamak will be commercialized by the end of next decade [11]. By 2050, nuclear fusion will have good share in world's total electrical power output. According to US department of energy fusion is a carbon free source of energy that has abundant fuel with no chance of melt down destruction along with it a very low radioactive waste. Moreover, the challenge in the development of this facility is to run the process for long period of time.

1.7.2 Working of the Tokamak

ITER will be worked as mini sun on the earth. Out of all possible reactions between hydrogen isotopes, deuterium and tritium reaction will be most feasible, because DT fusion reaction produces the highest energy gain at lowest temperature. The threshold temperature to achieve this fusion reaction is 100 to 150 million degree Celsius. As, no material can hold that temperature so magnetic confinement is employed. It provides two advantages; it not only prevents plasma through alignment to touch first wall but it also keeps plasma ignited [14]. Absence of air leads to no heat transfer through conduction and convection. The only mean of heat transfer is radiation. The coolant running in cooling pipes in the first wall collects the heat and converts it into steam. This steam then runs the turbine to produce electrical power.

1.7.3 Divertor in the Tokamak

Divertor is one of plasma facing component of Tokamak, installed at bottom of vacuum vessel. Purpose of divertor is to maintain plasma purity and extraction of heat power coming in the form of scrap off layer [16]. The divertor component should be able to tolerate high heat flux as it is main interface between plasma and material surface. The choice of the armor ingredients for the Plasma Facing Materials of the ITER tokamak is very critical because of very exclusive characteristics of a burning fusion plasma atmosphere. The parameters that affect the choice come primarily from the necessities of plasma behavior for example minimization of impurities in the confined plasma, engineering integrity, material age (how much it can bear thermal stress and erosion) & protection (minimization radioactive dust and tritium inventories).

The divertor has two major sections, one is armor section and other is structural section which is supporting castellated tungsten plate. But our research will deal with enhancing material for armor section [2]. Each of Divertor cassette have variety of components which includes lower vertical target and dump, upper vertical target, dome and divertor liner.

1.7.4 Challenges towards a successful dream

Designing of plasma facing component is one of the key challenges towards successful operation of ITER reactor. So, in order to tolerate high temperature plasma environment for specified time, we need to make plasma facing components that are high heat flux tolerant and erosion resistive. In early days all the focus was on low Z materials like carbon-based materials such as graphite, because of their high melting temperature but they encounter high chemical erosion due to hydrogen and oxygen atmosphere that put question mark on the credibility of graphite PFCs [16]. In such situations high Z materials were purposed as alternative that include: Tungsten, Molybdenum, zirconium, niobium, hafnium, and tantalum Molybdenum is a potential candidate material for plasma facing components in the fusion reactors. Refractory metals are well known because of high melting temperatures. These metals have been defined by their cutoff temperature. The most commercially accepted definition to the refractory metals is that they should have body centered cubic crystallite structure as well as the ratio of melting temperature of metal oxide to that of respective metal should be less than one [16]. They are being utilized

because of their chemical electrical and mechanical properties. Among the rest of high Z materials, Tungsten caught the sight due to superior melting temperature and threshold to sputter erosion. In addition to it, there found disadvantages linked with using tungsten. Brittleness and dense heavy structure make it difficult to mold in required shapes. This issue was tried to resolve by using tungsten coating on graphite and CFC substrate [16].

However, the difference in CTE of graphite and tungsten instigate adhesion loses, which results instability of PFCs. Despite of thermal conductivity and mechanical strengths of the candidate materials, there are other challenges to meet in extreme plasma environment [13]. High fluence radiation of Helium, Deuterium and Neutron cause formation of bubbles, crack [17], blister and fuzz [18], that deteriorate the process efficiency [19]. There is a need to understand the phenomena that cause such type of material degradation, this emphasis us to test other candidate materials with similar properties [20]. Mo is similar to tungsten in terms of thermo electrical properties. Therefore, Mo is a potential substitute contender for PFCs. Difference in CTE of Mo (4.8 µm/m °C) and graphite (5.9 µm/m °C) is less than tungsten (4.5 µm/m °C), that enhance stability of Mo films [21].

Each component face extreme environment in the form of high heat flux and neutrons. Starting with vertical plate and dump components, their purpose is to accommodate high heat flux of 10 MW/m^2 at normal conditions and about 20 MW/m^2 at slow transient, which can reach up to 100 $MW/m^2$for few milliseconds during disruption period [21]. Temperature can vary from 500 K to 2800 K this section. Usually CFCs or graphite are used as component materials. CFCs are generally preferred because they give some advantages over other materials which includes no melting, thermal shock resistance and ability to bear high heat flux. The drawback of CFCs is chemical erosion and sputtering that's why they are used with coating of any suitable metal. Tungsten or molybdenum are potential candidate for its coating.

However, the divertor components usually experience high irradiation dose. Erosion is one of critical issue cause irradiation effect. Sputtering erosion is result of alfa particles [20]. Chemical erosion can only happen in CFCs and graphite base components [19]. Thermal erosion is caused by thermal quench disruption and runaway electrons emission effect. Thermal quench disruption can cause substantial erosion of coated surface due to

vaporization which results into loss of material. Plasma facing components have to bear runaway electron impact. Runaway electron impact causes melting of components.

Neutrons also have significant effect on component life spam. It affects both CFCs and coated tungsten. The critical changes in tungsten properties are cause by displacement damage. As tungsten has body center structure so displacement damages lead to increase in ductile brittle transient temperature [19]. Which makes tungsten more brittle? In CFCs based components, irradiation decreases the thermal conductivity. Irradiation also causes atomic collision cascades creating lattice defects that can increase retention of hydrogen isotopes in material exposed to plasmas. This can possibly impact tritium inventory in reactor where tungsten plasma facing components will be damaged by ion irradiation. Another impact of high energy neutron is that it can cause transmutation of tungsten to rhenium and osmium [20]. Osmium being a very high oxidizing agent will act as impurity. It will have very complex impact on tungsten inventory.

Age of various graphite-based components depend on erosion rate, which means age can be enhanced by overcoming these issues. Purpose of my research will be formation of such a material by physical vapor deposition, and determination of most reliable plasma facing armor material for Tokomak divertor components that can withstand long enough during normal and of design conditions.

1.8 Energy from fission

Fission energy is obtained from fission nuclear reaction. In fission nuclear reaction heavy radioactive nucleus splits into two smaller nuclei and releases huge amount of energy. Heavy radioactive element can be uranium or plutonium. Those newly formed nuclei further splits into new nuclei [22]. This reaction also produced neutrons and other radioactive rays like alfa particles, beta rays and gamma rays. Neutron produced in this reaction further reacts with other nuclei to initiate nuclear chain reaction. In nuclear power plant normally 3 neutrons produced in the single reaction and 2 of them usually lost or consumed by control rods. 1 neutron takes apart in reaction thus control nuclear chain reaction happens. Energy produced in nuclear chain reaction is predicted by mass loss of reactant and product. Fission based nuclear reaction is illustrated in the figure below.

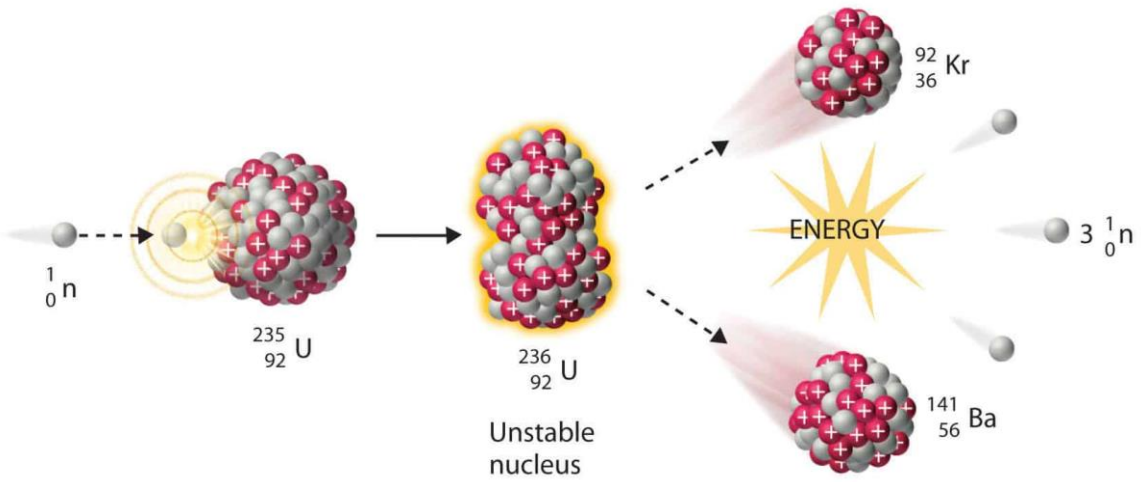

Figure 1-6 Schematic of nuclear fission reaction

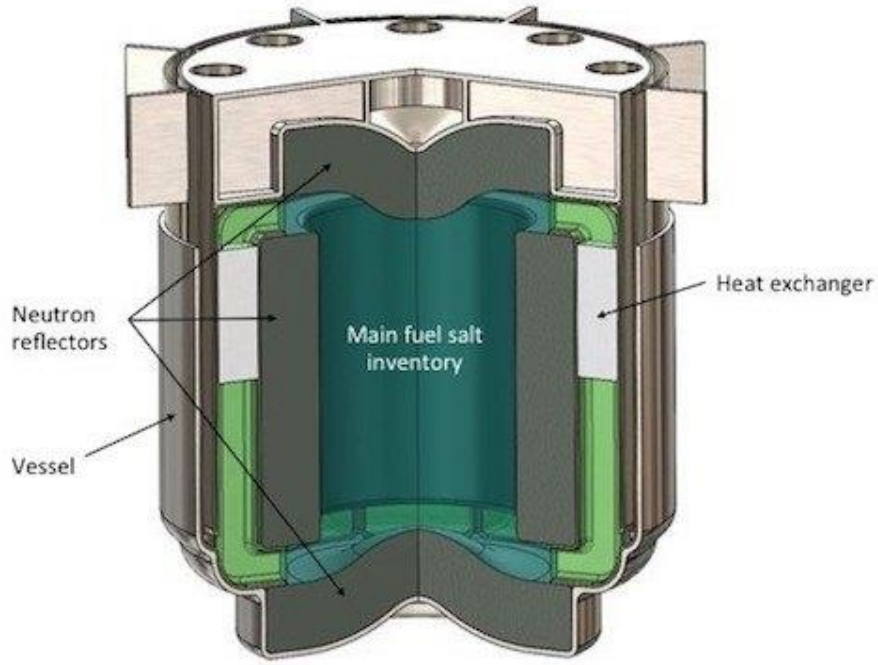

Figure 1-7 Schematic of Gen IV molten salt reactor core

1.8.1 Generation IV fission reactors

Generation IV nuclear reactors are the researched based nuclear reactors and are considered as the future of commercial fission based nuclear reactor. Generation IV nuclear reactors are expected to safer, efficient, sustainable and economical [23]. Another aspect of Gen nuclear reactor is that they will be closed fuel cycle followed by gas turbine for power

generation. Sodium fast reactors are the most developed fourth generation nuclear reactors. The molten-salt reactor, a less developed technology, is considered as potentially having the greatest inherent safety of the all 6 models [24]. These reactors have a lot of research potential.

1.8.2 Moderator in Fission reactors

One of the crucial components of fission based nuclear reactor is moderator. The purpose of neutron moderator is to slow down the speed of neutrons released during the nuclear fission process. Much high energy neutrons are released during nuclear fission reaction. But fissile material only interacts with slow or low energy neutrons, which are also referred as thermal neutrons. So, in order to make chain reaction sustainable, the neutrons speed is slowed down by mean of nuclear moderator [24]. Different kinds of materials are used to moderate neutron speed these days. They include Light water, heavy water and graphite. About one fifth of current nuclear reactors are using graphite as a moderator.

Graphite was often used in 1^{st} and 2^{nd} Generation nuclear power like RBMK reactors. In this reactor fuel rods are encased with graphite wall. It slows down the speed and reduce the energy of fast-moving neutrons emitted from fuel elements. It allows the chain reaction to extend throughout the fuel rods.

1.8.3 Problems in fission based nuclear reactors

The use of graphite moderator has declined in 2^{nd} and 3^{rd} generation nuclear plants. Only 20 % of current nuclear reactors work on graphite moderator. More declines are expected in the next few decades [25]. Several issues associated with graphite as moderator made it unpopular. Chernobyl incident was one of the causes of public fear.

During emergency scenario, especially when loss of coolant event occurs, reactor operating on graphite moderator will carry on the nuclear fission reaction, as graphite has extremely high heat of sublimation and thus it will be remained working, heat accumulation inside reactor core will occur and it could lead catastrophic scenario of core melt down. But in 3^{rd} generation nuclear reactors, Coolant (Water) itself acts as moderator. During loss of coolant scenario, there will be no coolant along with moderator and Reactor will stop working. The Chernobyl nuclear disaster occurred in RMBK reactor which used graphite as a moderator. The loss of coolant event leads to catastrophic scenario as core was still

active as nuclear reaction keeps happening because of moderation by graphite. It leads to core melt down. On the other hand, both Three Mile Island and Fukushima disaster occurred in light water reactors. Their coolant which itself was moderator was evaporated and nuclear reaction stopped.

Another problem associated with graphite-based reactor is that graphite is life limiting component of the reactor Cracks propagated by irradiated neutrons and creep cause from high temperature fluctuations cause loss in structural integrity by time. Although many challenges are associated with graphite to be used as moderator and other components in nuclear fission-based power plants [22]. But this doesn't render graphite use obsolete. Graphite moderator is supposed to slow down the speed of neutrons by scattering them. Its moderation ability is way more than light water. In future many opportunities exist for graphite to be used in nuclear power plants. One of them is their potential use in molten salt based nuclear reactors, where graphite can be utilized as reflector.

1.9 Summary

With beginning of 21st century, energy demand has been increased significantly. Especially in developing countries energy shortage is one of critical issue. Most of energy demand in the world is met by fossil fuels. These fuels are not only depleting but Carbon dioxide emission into environment fuels is producing greenhouse effect which is increasing global temperature. So, world is looking for alternative clean and economical source for energy. Energy from nuclear fusion is one of those alternatives and it is most promising one, because few kilograms of fuel in nuclear fusion can light up thousands of houses for months. This technology is under development and expected to be commercialized by 2040. Deuterium and tritium, isotopes of hydrogen are reactant for that reaction. This reaction has very small cross section, so it starts at 100-million-degree Kelvin. No material can sustain that temperature, that's why plasma is confined using strong magnetic field. These devices are referred as Tokamak.

Currently scientists are developing a new Tokamak device named as ITER. ITER will develop by2025 and it will be first prototype that will generate more power than consumption. But it will be not an easy job. Dozens of hurdles are still there which includes

selectivity of most suitable materials for its manufacturing. Selection of most reliable material for plasma facing divertor component is one of those hurdles.

1.10 Flowchart of thesis

The remainder of the thesis can be grouped into five major sections.

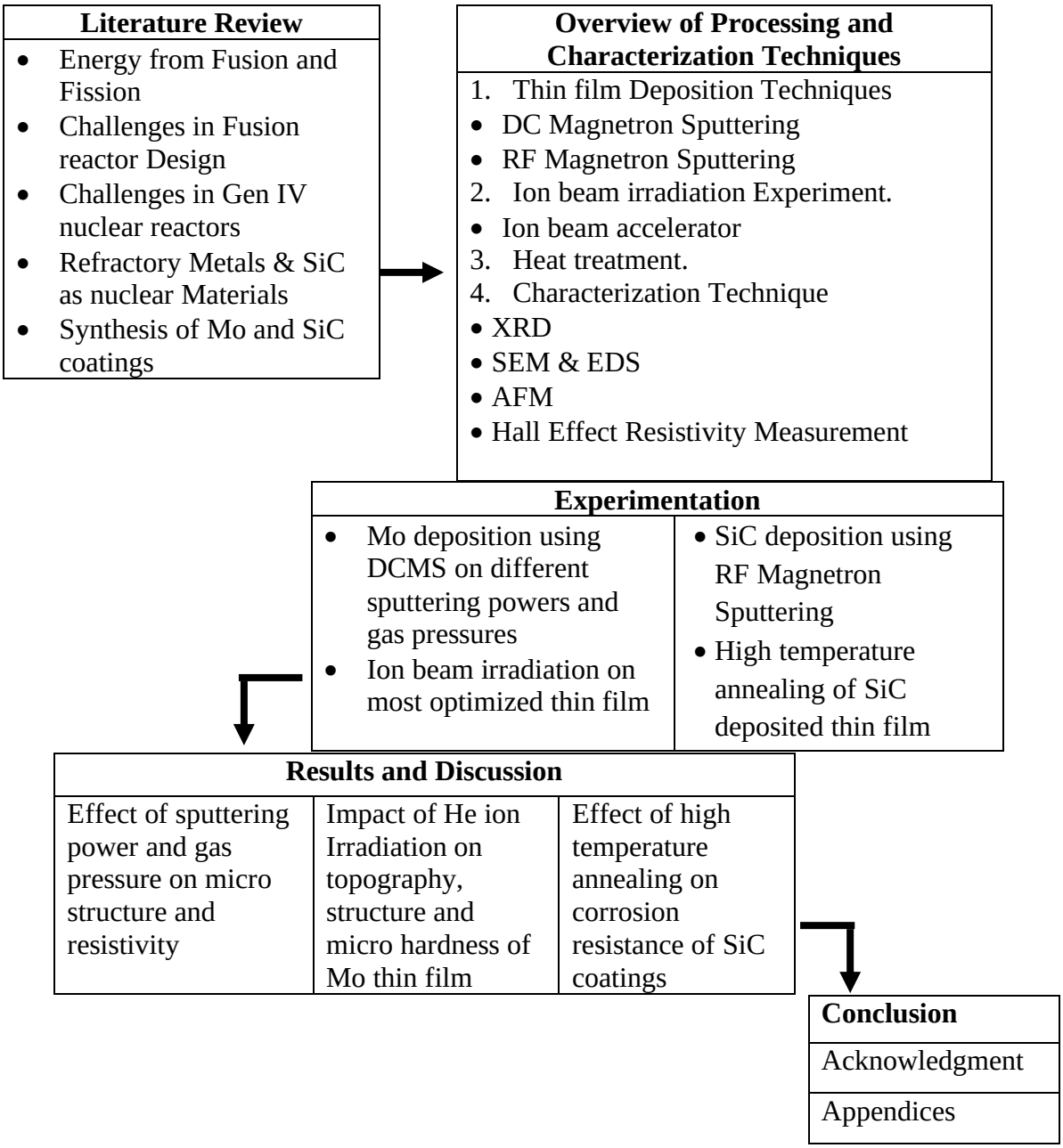

We begin with a literary review of advances in fusion and fission technology. It is followed by an overview of the processing and characterization tools and techniques. Next comes the experimentation section. The experimentation section is a combination of t**wo** basic subsections; In first section, deposition at different process parameters and ion beam irradiation is given. In second part, Deposition of SiC along with heat treatment is explained. Following the experimentation section is the results and discussion section. Which is distributed in three subsections; First subsections contain analysis of effects produced due to changing sputtering parameters. second part consist of variations in films properties produced by helium ion irradiations. Third subsection explain the impact of high temperature annealing on corrosion resistance of SiC coatings. Then there are some conclusions as concrete interpretations from the results and discussion section. Here this thesis is warped up with the acknowledgements to all the individuals without whom this worked could never be done followed by the appendices, which comprises of the research articles that emerged as a consequence of this study.

References

[1] A. Rehman, A. Rauf, M. Ahmad, A. A. Chandio, and Z. Deyuan, "The effect of carbon dioxide emission and the consumption of electrical energy, fossil fuel energy, and renewable energy, on economic performance: evidence from Pakistan," *Environ. Sci. Pollut. Res.*, vol. 26, no. 21, pp. 21760–21773, 2019, doi: 10.1007/s11356-019-05550-y.

[2] Z. Wang, Danish, B. Zhang, and B. Wang, "Renewable energy consumption, economic growth and human development index in Pakistan: Evidence form simultaneous equation model," *J. Clean. Prod.*, vol. 184, pp. 1081–1090, 2018, doi: 10.1016/j.jclepro.2018.02.260.

[3] N. Ahmad, L. Du, J. Lu, J. Wang, H. Z. Li, and M. Z. Hashmi, "Modelling the CO2 emissions and economic growth in Croatia: Is there any environmental Kuznets curve?," *Energy*, vol. 123, pp. 164–172, 2017, doi: 10.1016/j.energy.2016.12.106.

[4] R. Maqbool and Y. Sudong, "Critical success factors for renewable energy projects; empirical evidence from Pakistan," *J. Clean. Prod.*, vol. 195, pp. 991–1002, 2018, doi: 10.1016/j.jclepro.2018.05.274.

[5] M. A. Sheikh, "Energy and renewable energy scenario of Pakistan," *Renew. Sustain. Energy Rev.*, vol. 14, no. 1, pp. 354–363, 2010, doi: 10.1016/j.rser.2009.07.037.

[6] J. Khan and M. H. Arsalan, "Solar power technologies for sustainable electricity generation - A review," *Renew. Sustain. Energy Rev.*, vol. 55, pp. 414–425, 2016, doi: 10.1016/j.rser.2015.10.135.

[7] N. Ahmed, M. A. Iqbal, Z. S. Khan, and A. A. Qayyum, "DC Magnetron-Sputtered Mo Thin Films with High Adhesion, Conductivity and Reflectance," *J. Electron. Mater.*, 2020, doi: 10.1007/s11664-020-08138-2.

[8] J. Vujić, D. P. Antić, and Z. Vukmirović, "Environmental impact and cost analysis of coal versus nuclear power: The U.S. case," *Energy*, vol. 45, no. 1, pp. 31–42, 2012, doi: 10.1016/j.energy.2012.02.011.

[9] C. H. Skinner, "Atomic physics in the quest for fusion energy and ITER," *Phys. Scr. T*, vol. T134, 2009, doi: 10.1088/0031-8949/2009/T134/014022.

[10] P. Weng *et al.*, "The Engineering Commissioning of EAST Superconducting Tokomak," pp. 2–5.

[11] J. Bucalossi *et al.*, "The WEST project: Testing ITER divertor high heat flux component technology in a steady state tokamak environment," *Fusion Eng. Des.*, vol. 89, no. 7–8, pp. 907–912, 2014, doi: 10.1016/j.fusengdes.2014.01.062.

[12] H. Maier, J. Luthin, M. Balden, J. Linke, F. Koch, and H. Bolt, "Properties of tungsten coatings deposited onto the fine grain graphite by different methods," *Surf. Coatings Technol.*, vol. 142–144, pp. 733–737, 2001, doi: 10.1016/S0257-8972(01)01177-X.

[13] J. N. Brooks, L. El-Guebaly, A. Hassanein, and T. Sizyuk, "Plasma-facing material alternatives to tungsten," *Nucl. Fusion*, vol. 55, no. 4, p. 43002, 2015, doi: 10.1088/0029-5515/55/4/043002.

[14] J. Matějíček, Y. Koza, and V. Weinzettl, "Plasma sprayed tungsten-based coatings and their performance under fusion relevant conditions," *Fusion Eng. Des.*, vol. 75–79, no. SUPPL., pp. 395–399, 2005, doi: 10.1016/j.fusengdes.2005.06.006.

[15] G. S. Cho and K. H. Choe, "Characterization of plasma-sprayed tungsten coating on graphite with intermediate layers," *Surf. Coatings Technol.*, vol. 209, pp. 131–136, 2012, doi: 10.1016/j.surfcoat.2012.08.051.

[16] C. Ruset *et al.*, "Development of W coatings for fusion applications," *Fusion Eng. Des.*, vol. 86, no. 9–11, pp. 1677–1680, 2011, doi: 10.1016/j.fusengdes.2011.04.031.

[17] W. Hu *et al.*, "Hydrogen bubble formation and evolution in tungsten under different hydrogen irradiation conditions," *Fusion Eng. Des.*, vol. 90, pp. 23–28, 2015, doi: 10.1016/j.fusengdes.2014.10.007.

[18] A. Manuscript, "ce pte d M us," pp. 0–12, 2017, doi: https://doi.org/10.1088/1361-6528/aa8b39.

[19] M. Rubel *et al.*, "Overview of erosion-deposition diagnostic tools for the ITER-Like Wall in the JET tokamak," *J. Nucl. Mater.*, vol. 438, no. SUPPL, pp. S1204–S1207, 2013, doi: 10.1016/j.jnucmat.2013.01.266.

[20] J. K. Tripathi, T. J. Novakowski, G. Joseph, J. Linke, and A. Hassanein, "Temperature dependent surface modification of molybdenum due to low energy He+ ion irradiation," *J. Nucl. Mater.*, vol. 464, pp. 97–106, 2015, doi: 10.1016/j.jnucmat.2015.04.022.

[21] R. A. Causey, C. L. Kunz, and D. F. Cowgill, "Deuterium retention and release from molybdenum exposed to a Penning discharge," *J. Nucl. Mater.*, vol. 337–339, no. 1-3 SPEC. ISS., pp. 600–603, 2005, doi: 10.1016/j.jnucmat.2004.10.005.

[22] W. Frisch and G. Gros, "Improving the safety of future nuclear fission power plants," *Fusion Eng. Des.*, vol. 56–57, pp. 83–93, 2001, doi: 10.1016/S0920-3796(01)00238-1.

[23] K. Tuček *et al.*, "Generation IV reactor safety and materials research by the Institute for

Energy and Transport at the European Commission's Joint Research Centre," *Nucl. Eng. Des.*, vol. 265, pp. 1181–1193, 2013, doi: 10.1016/j.nucengdes.2013.06.018.

[24] J. Serp *et al.*, "The molten salt reactor (MSR) in generation IV: Overview and perspectives," *Prog. Nucl. Energy*, vol. 77, pp. 308–319, 2014, doi: 10.1016/j.pnucene.2014.02.014.

[25] J. J. Lee, J. D. Arregui-Mena, C. I. Contescu, T. D. Burchell, Y. Katoh, and S. K. Loyalka, "Protection of graphite from salt and gas permeation in molten salt reactors," *J. Nucl. Mater.*, vol. 534, 2020, doi: 10.1016/j.jnucmat.2020.152119.

[26] M. Zhao *et al.*, "Fluence dependence of helium ion irradiation effects on the microstructure and mechanical properties of tungsten," *Nucl. Instruments Methods Phys. Res. Sect. B Beam Interact. with Mater. Atoms*, vol. 414, pp. 121–125, 2018, doi: 10.1016/j.nimb.2017.09.002.

Chapter 2: Literature Review

2.1 Challenges in Fusion reactor Design

In nuclear reactions rather than electrons, nuclear particles (neutrons and protons) take part in the reactions and they release or absorb huge amount of energy. Hence, they are totally different from chemical reactions. It is important to fuse two smaller and less stable nuclei. As a result, the released energy is equal to the difference in the binding of the parent and daughter nuclei. According to the mass to energy conversion relation of Einstein, the small difference in initial and final component is actually due the conversion of this small mass into large amount of energy [1]. High demand of temperature is required for the fusion reaction but pressure conditions are also vital that it why, at sun fusion occurs at 10 to 15 million °C whereas, in the designed reactor it demands about 100 million °C because of the near atmospheric pressure. This is the consequence of small fuel used in tokamak. For power production at wanted reaction rate and achievable temperature the suggested fuel is isotopes of hydrogen like deuterium and tritium [1]. Intrinsically, hydrogen has one electron and one proton with no neutron in its nuclei. Isotopes carry one neutron in deuterium and two neutrons in tritium.

These isotopes are heated to form plasma. Plasma is a quasi-neutral gas of charged and neutral particles which exhibits collective behavior [2]. Since the fuel atoms are positively charges so they repel each other. In order to fuse both ions together the strong electrostatic force of repulsion is needed to overcome this force, to make them sufficiently close for sufficient amount of time. This is done by maintaining high temperature and by confining the plasma by strong external electromagnetic fields [3]. Stability of fusion reaction is important for power production that requires consideration in the field of plasma science, electric field controlling and protection of inner wall divertors and blankets of chamber [4]. The worldwide fusion community is currently building the International. Thermonuclear Experimental Reactor which has expectation to produces ≈500,000,000Watts of fusion power.

2.2 Plasma facing Component

The successful recognition of ITER project is critically based upon the efficient material, as well as to verify the credibility of all the integrated system for commercialization of fusion energy devices. Selection on material should be according to their ability to sustain n high heat flux resulting complex thermo mechanical loads and heavy neutron irradiation. Materials properties are subjected to change with increasing temperature which causes degradation of process efficiency that might lead to the failure [5]. Goal of plasma facing components and first wall of tokamak is to: protect of back structure, insure readily heat transfer as well as to keep the plasma clean. In addition to in ITER design demands the PFCs to safeguard sufficiently low tritium retention in the presence of high fuel throughput. Along with it they must sustain in the long-term operation that is considered as a matter of concern [6]. Figure 2-3 illustrates the schematic of ITER divertor.

Plasma facing components are one of the chief parts of fusion reactor design. PFCs will be exposed in highly adverse environment which is not fully predictable. So, it is vital to mold PFCs design in such a way that could not only with stand all the severe conditions but to achieve required process efficiency. For this purpose, multiple materials with various configurations are employed to test ITER like condition. Initially, carbon base compounds are used but the erosion and chemical stability issues along with the impurities of plasma made the scientist to search for other material in which refractory metals are the promising candidates [7].

2.3 Ion beam irradiation effect:

Sustainability concerns in high temperature plasma situation are the ability of material to bear hydrogen isotopes i.e. hydrogen, Deuterium and Tritium. First wall components must possess less sputter erosion and low solubility in hydrogen as it is the chief concern in future long pulse reactors. First walls are at front of high heat flux of the range 10^{22} to 10^{24} $m^{-2}s^{-1}$. Ion and neutrons of MeV energy ranges strike on the faces that create lattice imperfection. It requires focused set of extensive modeling to judge the simulation of environment and strains in materials [8]. Material examination points neutron induce activation, sputter erosion, plasma transient response. Solution must fulfill the criteria of an environmentally friendly product with minimum harms to the surroundings, reusable, tolerant to degradation of sputtering and persistent in operation demand [9]. The issue of

activated material in fusion process due to neutrons flux creates environmental concerns. This problem can be coped either by geological disposal or by reusing the material in the facility or by selling in market if it is radioactively safe. Geological dumping and commercializing is not encouraged rather it is more feasible to reutilize the material in same facility [10]. In the context of waste disposal Mo and Nb creates high level waste whereas Tungsten, Molybdenum and Hafnium can be recycled immediately. Talking to sputter erosion of Molybdenum, it has no much difference as that of tungsten. The average erosion is 1 mm per burn per year creating insignificant core plasma contamination. For elastic recoil detection (ERD) 0.1 mm thick annealed stainless steel, Molybdenum, Tungsten and Copper were annealed and mounted as first wall equivalent position. Samples were exposed to the successive helium discharges sustained by neutral beam injection (NBI) and plasma condition was: Ti = 0.7– 1.7 keV, ne = 0.3–8.1×10_{19} m^{-3} for the discharge time of 2s and the total reached 87s by repeating discharges with similar plasma parameters. The probe and samples temperature were kept at room temperature. Later on, small damaged was observed and depth profile of helium in W was estimated [11]. Smart alloy of tungsten chromium and yttrium was fabricated by using three different sputtering targets to get 3 to 7 um thick films. Samples were exposed to ion beam in simulated plasma condition to test oxidation behaviors in it. Steady plasma conditions at 576°C was provided keeping ion energy 200 ev with total fluence was 1.3×10^{22} ions/cm^2. Sputtering yield for pure tungsten and alloy was 1 and 1.1 mg. Controlled isothermal oxidation concluded the three-fold decrease in oxidation of alloyed sample, which represent the good diffusion in W-Cr-Y alloy [12]. Powder metallurgy tungsten and plasma-sprayed tungsten samples were exposed to high heat and particle fluxes to observe the morphological stresses. Specimens were irradiated with Hydrogen, Helium, and mixed proposition beams. Power densities ranges between of 2 MWm^{-2} to10 MWm^{-2} Changes in surface morphologies due to effect of H and He beam strongly depend on temperature and number of thermal load cycles. Effect of 1.3×10^{24} He cm^{-2} results the formation of coral like structures of μm ranges on samples. In case of actively cooled samples exposure to hydrogen irradiation no blisters formation was observed rather pores were found of nanometer ranges [13].

2.4 Refractory metals as plasma facing materials

Refractory metals are well known because of high melting temperatures. These metal shaves been defined by their cutoff temperature. The most commercially accepted definition to the refractory metals is that they should has body centered cubic crystallite structure as well as the ratio of melting temperature of metal oxide to that of respective metal should be less than one [14]. They are being utilized because of their chemical electrical and mechanical properties. High Z materials that includes: Tungsten, Molybdenum, zirconium, niobium, hafnium, and tantalum. Mo belongs to the Group six, it is a block d element of periodic table. Its atomic number is 42, It is one of the distinguish refractory metal because of thermo-mechanical properties as it has melting temperature of 2617°C which make him good candidate for high heat flux application. Moreover, to fulfill the need of high thermal conductivity Mo conductivity is100 W $m^{-1}K^{-1}$which is just 10 W less than as that of tungsten 110 $Wm^{-1}K^{-1}$. Whereas, boiling point of Mo is 4612°C and density is 10.2 g cm^{-3} . Mo is a valuable material to gain efficient CIGS based solar cell. Mo is used as back contact electrode due to its robust thermal stability and low resistive and low recombination properties [15].

Tungsten coating of micron size thickness was developed on graphite using three different techniques electron beam evaporation, magnetron sputtering, and arc deposition, the purpose was to select a reliable method for industrial needs. Sputtering has problem with adhesion due to compressive stress which can be cope by plasma etch cleaning. No adhesion losses were observed in later two methods, whereas oxygen impurities were detected in case of electron beam method and carbon impurity is in equal value for all three methods [16].

Mo is one of the distinguish refractory metal because of thermo-mechanical properties as it has high melting temperature. Thermal conductivity of Molybdenum at 1000°C is about 2.5 times higher than graphite [17]. Molybdenum is cheaper than tungsten as well as ease in its fabrication make Mo to surpass W. Mo is as anti-erosion metal. It resists the formation of oxides as well as remains non-reactive with hydrogen, nitrogen and ammonia up to 1110°C. However, at elevated temperature ammonia and nitrogen forms nitrides but still it

resists the formation of hydrides till the melting point reaches [14]. The comparison between properties of Mo and W is given in the Table 2-1.

Table 2-1: Properties of Mo, W are given in Table

Property	Units	Molybdenum	Tungsten
Melting Point	(°C)	2,617	3,410
Density	(g/cc)	10.2	19.3
Thermal Expansion	(ppm/°C)	4.8	4.5
Specific Heat	(J/g-°C)	0.25	0.13
Resistivity	(µohm-cm)	5.4	5.3
Tensile Stress	(1,000°C, Ksi)	20–30	50–75
Stiffness	(20°C, Msi)	48	60
Stiffness	(1,000°C, Msi)	41	53
Crystal Structure	(20°C)	BCC	BCC

Mo is a valuable material to gain efficient CIGS based solar cell. Mo is used as back contact electrode due to the fact that it provides robust thermal stability and low resistive and low recombination properties [15]. Silicon has been proved a revolutionary material in semiconductor industries. Matching thermo-mechanical properties of molybdenum and silicon enable us to use it in power application. This type of application demands good conductivity and high temperature tolerance and Mo possess such qualities. Soft errors cause lack in efficiency due to the creation of defects in silicon layers [18]. Molybdenum is used in the fabrication of high capacity memory chips as it eliminated the soft error [19]. These defects are originated as result radioactive alpha particles that penetration into metallic layer. Metallization of Mo on substrate enables the fabrication of thousands of high-performance electronic components [20]. Use of pure Mo

metallic also stops the diffusion of alkaline earth impurities. It is appropriate candidate to be utilized in flexible display applications. Moreover, to prevent from dewetting and adhesion issues for the formation of metal matrix composite Mo interlayer give beneficial results [21].

Soft errors cause lack in efficiency due to the creation of defects in silicon layers. Molybdenum is used in the fabrication of high capacity memory chips as it eliminated the soft errors. These defects are originated as result radioactive alpha particles that penetration into metallic layer. Metallization of Mo on substrate enables the fabrication of thousands of high-performance electronic components. Use of pure Mo metallic also stops the diffusion of alkaline earth impurities [19]. The use of molybdenum is well proven back contact electrode for CIGS because they are good conductor. The issues to get good adhesion and less resistivity was tried to overcome. Sputtering deposition technique was used in different modes of operation by varying operational parameter like power gas pressure. By changing parameters and modes of sputtering, samples were characterized to get morphological profiles. RF sputtering give greater resistivity then DC. It reveals that the crystallanity of the Mo films is inversely proportional to the deposition pressure. When the deposition pressure increases, the kinetic energy of Mo ions reduces because of the increased particle scattering; when the deposition power increases, the kinetic energy of Mo ions also increases. Larger grain size with higher deposition rate incorporated more foreign atoms in DC sputtering and produced rough surface. Mixed RF and DC sputter deposition fashion to form bi and tri layered composition gives better resistivity value of 61×10^{-6} Ω and 61×10^{-6} Ω respectively [22]. Electro deposition is one of the reliable techniques for synthesis of PFC, due to good coating coverage in all sides.

Tungsten was coated on Al_2O_3-Cu by electro deposition. Deposition parameters such as current density, duty cycles and periods were optimized. It was concluded that nucleation and electro-crystallization of tungsten coating greatly depend on the above-mentioned factors. Surface morphological study showed that: smooth grain characters were obtained at 2 ms period and 0.1 duty cycles, whereas, thickest coating was achieved at 0.5 duty cycles and 1 ms period. Moreover, the current density was 40 $mAcm^{-2}$ [23].

2.5 Challenges in graphite based nuclear fission reactors

Like nuclear fusion, graphite has significant importance in nuclear fission. In the first and 2nd generation nuclear fission reactors, Graphite was often used as nuclear moderator. The role of moderator is to slow down the speed neutron to make them suitable for interaction with fissile materials. Due to few issues, graphite is no more used as moderator in nuclear reactors. As explained in the previous chapter. In 3rd generation reactor, Graphite is used in zircaloy based fuel elements due to its high melting point. In Gen IV nuclear reactors, Graphite is aspiring candidate to be used as reflectors in molten salt reactors [24].

The use of graphite moderator has declined in 2nd and 3rd generation nuclear plants. Only 20 % of current nuclear reactors works on graphite moderator. More decline is expected in the next few decades. Several issues associated with graphite as moderator made it un popular. Chernobyl incident was one of the causes of public fear.

During emergency scenario, especially when loss of coolant event occurs, reactor operating on graphite moderator will carry on the nuclear fission reaction, as graphite has extremely high heat of sublimation and thus it will be remained working, heat accumulation inside reactor core will occur and it could lead catastrophic scenario of core melt down. But in 3rd generation nuclear reactors, Coolant (Water) itself acts as moderator. So, in case of loss of coolant scenario, there will be no coolant along with moderator and Reactor will stop working [25]. The Chernobyl nuclear disaster occurred in RMBK reactor which used graphite as a moderator. The loss of coolant event leads to catastrophic scenario as core was still active as nuclear reaction keeps happening because of moderation by graphite. It leads to core melt down. On the other hand, both Three Mile Island and Fukushima disaster occurred in light water reactors. Their coolant which itself was moderator was evaporated and nuclear reaction stopped [26].

Another problem associated with graphite-based reactor is that graphite is life limiting component of the reactor [25]. Cracks propagated by irradiated neutrons and creep cause from high temperature fluctuations causes loss in structural integrity by time [26]. Although many challenges are associated with graphite to be used as moderator and other components in nuclear fission-based power plants. But this doesn't render graphite use obsolete. Graphite moderator is supposed to slow down the speed of neutrons by scattering

them. Its moderation ability is way more than light water. In future many opportunities exist for graphite to be used in nuclear power plants. One of them is their potential use in molten salt-based nuclear reactors, where graphite can be utilized as reflector.

In Generation IV nuclear fission-based reactors, molten salt reactors (MSR) are aspiring candidate for future energy exploitation [24]. In this reactor molten fluoride salt circulates in the containment loop and share energy with the coolant present at 2nd loop. Graphite is proposed as moderator and reflector material in that reactor [27]. This graphite undergoes harsh environment in the form of neutrons irradiations and fuel salt. The fluoride salt causes chemical erosion inside graphite matrix and decreases the service life of reflector and moderator material. This was a result of local hotspot formations inside matrix and leads to increase in damage rate of non-replaceable nuclear graphite. So, it is important to protect graphite matrix from infiltration of molten salt.

2.6 Research Needs for Graphite based nuclear fission reactors

Many opportunities are there to improve the use of graphite as moderator in modern reactors [20]. One of them is to increase the oxidation resistance of graphite by diffusing any interstitials in the structure of graphite. Another way is to deposit anti oxidation coating on graphite matrix [28]. This issue can be resolve by make structure of graphite more resilient to halt dislocations caused by high temperature and irradiation hardening and creep.

Another is making the graphite sections more structurally resilient to halt dislocations caused by thermal stress and irradiation creep [25]. Finally, additional areas for fruitful research can be found in creating a simpler system for handling graphite-moderated reactor waste and testing more dependable ways to prevent nuclear meltdowns in graphite-moderated nuclear reactors [25]. Thus, nuclear graphite would benefit from both highly focused materials science research and also broad environmental health and safety research.

2.7 Silicon carbide as corrosion resistant material

Silicon carbide is usually considered as abrasive and heat flux tolerant material. SiC exhibits outstanding advantages in high-voltage, high-frequency and high-temperature

electronic components and devices due to fast saturated electron velocity, wide forbidden band and good radiation resistance. Thin films of SiC and its composites have wide range of technological importance in the field of nuclear engineering [29]. High hardness and very high melting temperatures makes it suitable contender for high temperature reactors. Their applications may range from protective coatings against the corrosion to X-ray mask materials to the protection of thermonuclear reactor walls.

Various studies have been done to analyze silicon carbide performance as protective coatings. In one study SiC was deposited on aluminum matrix by thermal spray technique. And impact of grain size was demonstrated on it. It was found that corrosion resistance increased with an increase in grain size [30]. In another study, silica particle was deposited by Laser cladding on graphite substrate. Ablation test demonstrates that the silica coating has excellent performance compared to the uncoated graphite [31]. In one research, CVD was employed to deposit SiC on graphite. Effect of high temperature annealing was analyzed on impact resistance. The impact strength of the samples increases with deposition temperature, reaching its maximum at 1150 °C, and declines slightly at 1200 °C [32].

Silicon carbide has been recognized as potential material to be used in electronics and as heat sink due to its low density and CTE as well as high thermal conductivity. Mo coated Silicon carbide was developed using sol-gel method using ammonium molybdate tetra hydrate. Method was proved successful to obtain uniform composition and grain structure [15]. In another research, SiC and glassy carbon composite was deposited on graphite using chemical vapor reaction. It was found that SiC/glassy carbon composite coating could be a promising protective coating for nuclear graphite used in MSR [28].

2.8 Different Deposition Techniques

Molybdenum thin film can be deposit using different technique. Electron beam evaporation, DC and RF sputtering and electro deposition can be used for this purpose. Electro deposition is one of the reliable techniques for synthesis of PFC, due to good coating coverage in all sides. Tungsten was coated on Al_2O_3-Cu by electro deposition. Deposition parameters such as current density, duty cycles and periods were optimized. It was concluded that nucleation and electro-crystallization of tungsten coating greatly

depend on the above-mentioned factors [33]. Surface morphological study showed that: smooth grain characters were obtained at 2 ms period and 0.1 duty cycle. Whereas, thickest coating was achieved at 0.5 duty cycles and 1 ms period. Moreover, the current density was 40 mA cm^{-2} . Silicon carbide has been recognized as potential material to be used in electronics and as heat sink due to its low density and CTE as well as high thermal conductivity. Mo coated Silicon carbide was developed using sol-gel method using ammonium molybdate tetrahydrate. Method was proved successful to obtain uniform composition and grain structure [34]. Mo films by electron beam evaporation offers bigger grain size but more surface roughness and higher resistivity [35]. Tungsten coating of micron size thickness was developed on graphite using three different techniques, electron beam evaporation, magnetron sputtering, and arc deposition, the purpose was to select a reliable method for industrial needs. Sputtering has problem with adhesion due to compressive stress which can be cope by plasma etch cleaning. No adhesion losses were observed in later two methods, whereas oxygen impurities were detected in case of electron beam method and carbon impurity is in equal value for all three methods [16]. Characteristic Mo, for example melting temperature 2617°C and vapor pressure 3.47 Pa at 30°C make it more viable to be deposited by sputtering [36]. Rf and DC sputtering has its own benefits like RF sputtered films provide better adhesion due to the fact less energy ion discourages the residual sputtered atom to take part in further crystallite size enhancement and don't over bomb the interface of substrate thus provide better adhesion. Contrary to that, DC sputtering can compensate more energetic ion to sputter more target atom and have bigger grain size that results to get more control over physical and electrical properties of films [37].

In DC sputtering, deposition operation proceeded due to ionized argon atoms resulted by collision of secondary electron from cathode. Higher pressure of Ar in chamber causes tensile stress while lower pressure causes compressive stresses in the films. Surface roughness and adhesion is inversely proportional to the deposition power. The size and density of crystallites varies directly with deposition power [38]. Higher deposition power attributed as the higher grain size and it leads to the columnar structure this lower resistivity [15]. DC magnetron sputtering provides more control over film properties by adjusting the

process parameters [39]. Mainly distance between target to substrate, working gas pressure, deposition power and substrate temperature that effects the characteristic of films. Literature reviews states that pressure of working gas effect the film morphology. Because there will be a greater number of ions to strike target material to enhance sputtering rate. Larger grain size with higher rate of deposition incorporated more foreign atoms result in rough film surface and poor resistivity [18]. The use of molybdenum is well proven back contact electrode for CIGS because they are good conductor. The issues to get good adhesion and less resistivity is tried to overcome. Sputtering deposition technique was used in different modes of operation by varying operational parameter like power gas pressure. By changing parameters and modes of sputtering, samples were characterized to get morphological profiles. RF sputtering give greater resistivity then DC [22]. The crystallanity of Mo thin film is closely related to gas pressure. When gas pressure increases the crystallanity reduces. It can be attributed with atomic peening model. At high gas pressure, due to more collisions and the enhanced scattering leads to unsymmetrical deposition, which lead to low crystallanity. Mixed RF and DC sputter deposition fashion to form bi and tri layered composition gives better resistivity value of $61\times10^{-6}\Omega$ and $61\times10^{-6}\Omega$ respectively. Higher pressure of Ar in chamber causes tensile stress while lower pressure causes compressive stresses in the films [18]. Surface roughness and adhesion is inversely proportional to the deposition power. The size and density of crystallites varies directly with deposition power. Higher deposition power attributed as the higher grain size and it leads to the columnar structure [36].

In our case we have used DC magnetron sputtering for synthesis of Mo thin film. At constant gas pressure, we are changing deposition power by increasing the current that enhance the kinetic energy of ionized species and hence more efficient transfer of sputtered atom to substrate causes larger crystals. However, at constant power, we are changing gas pressure in effort to achieve smoother and highly conductive thin film. In second part we used RF magnetron sputtering to deposit silicon carbide on graphite.

2.9 Summary

The successful recognition of ITER project is critically based upon the efficient material, as well as to verify the credibility of all the integrated system for commercialization of

fusion energy devices. Selection on material should be according to their ability to sustain high heat flux resulting complex thermo mechanical loads and heavy neutron irradiation. Plasma facing components are one of the chief parts of fusion reactor design. PFCs will be exposed in highly adverse environment which is not fully predictable. So, it is vital to mold PFCs design in such a way that could not only with stand all the severe conditions but to achieve required process efficiency. Ion and neutrons of MeV energy ranges strike on the faces that create lattice imperfection. It requires focused set of extensive modeling to judge the simulation of environment and strains in materials. Material examination points are neutron induces activation, sputter erosion, plasma transient response. Solution must fulfill the criteria of an environmentally friendly product with minimum harms to the surroundings, reusable, tolerant to degradation of sputtering and persistent in operation demand. Mo belongs to the refractory metals; it is a block d element of periodic table. Its atomic number is 42, It is one of the distinguish refractory metal because of thermo-mechanical properties as it has melting temperature of 2617°C which make him good candidate for high heat flux application.

In Generation IV nuclear fission-based reactors, molten salt reactors (MSR) are aspiring candidate for future energy exploitation. In this reactor molten fluoride salt circulates in the containment loop and share energy with the coolant present at 2^{nd} loop. Graphite is proposed as moderator and reflector material in that reactor. This graphite undergoes harsh environment in the form of neutrons irradiations and fuel salt. The fluoride salt causes chemical erosion inside graphite matrix and decreases the service life of reflector and moderator material. Many opportunities are there to improve the use of graphite as moderator in modern reactors. One of them is to increase the oxidation resistance of graphite by diffusing any interstitials in the structure of graphite. Another way is to deposit anti oxidation coating on graphite matrix.

2.10 Objectives of Research

- Development of Mo coating on graphite for high heat flux facing applications
- Optimizing synthesis of Mo thin film by varying gas pressure from 7 mTorr to 30 mTorr and deposition power from 100 to 300 watts to get good adhesion and crystallinity

- Conducting ion beam irradiation experiment on optimized thin film using He ions to simulate Mo ability to sustain in plasma environment
- Development of SiC on graphite for corrosion resistant applications in Gen IV nuclear fission power plants
- To study impact of high temperature annealing on corrosion resistance of SiC coated graphite
- To encourage the need of research for future energy sources

References:

[1] J. K. Tripathi, T. J. Novakowski, S. Gonderman, N. Bharadwaj, and A. Hassanein, "The effect of carbon impurities on molybdenum surface morphology evolution under high- fl ux low-energy helium ion irradiation," *J. Nucl. Mater.*, vol. 478, pp. 287–294, 2016, doi: 10.1016/j.jnucmat.2016.06.026.

[2] C. H. Skinner, "Atomic physics in the quest for fusion energy and ITER," *Phys. Scr. T*, vol. T134, 2009, doi: 10.1088/0031-8949/2009/T134/014022.

[3] J. Bucalossi *et al.*, "The WEST project: Testing ITER divertor high heat flux component technology in a steady state tokamak environment," *Fusion Eng. Des.*, vol. 89, no. 7–8, pp. 907–912, 2014, doi: 10.1016/j.fusengdes.2014.01.062.

[4] P. Chra, J. Linke, J. Mate, and P. Chra, "Thermal Spray Coatings for Fusion Applications — Review," *ASM Int. Therm.*, vol. 16, no. March, pp. 64–83, 2007, doi: 10.1007/s11666-006-9007-2.

[5] J. Matějíček and P. Chráska, "Development of advanced coatings for ITER and future fusion devices," *Adv. Sci. Technol.*, vol. 66, pp. 47–65, 2010, doi: 10.4028/www.scientific.net/AST.66.47.

[6] F. Engineering and T. N. E. T. Team, "ITER plasma facing components , design and development," *Fusion Eng. Des.*, vol. 16, no. 1991, pp. 23–34, 2000.

[7] J. Matějíček, Y. Koza, and V. Weinzettl, “Plasma sprayed tungsten-based coatings and their performance under fusion relevant conditions,” *Fusion Eng. Des.*, vol. 75–79, no. SUPPL., pp. 395–399, 2005, doi: 10.1016/j.fusengdes.2005.06.006.

[8] J. Marian, C. S. Becquart, C. Domain, J. Roth, and K. Schmid, “energy conditions Baseline high heat flux and plasma facing materials for fusion,” *Nucl. Fusion*.

[9] J. N. Brooks, L. El-Guebaly, A. Hassanein, and T. Sizyuk, “Plasma-facing material alternatives to tungsten,” *Nucl. Fusion*, vol. 55, no. 4, p. 43002, 2015, doi: 10.1088/0029-5515/55/4/043002.

[10] L. El-guebaly, V. Massaut, K. Tobita, and L. Cadwallader, “Goals , challenges , and successes of managing fusion activated materials,” *Fusion Eng. Des. J.*, vol. d, pp. 928–935, 2008, doi: 10.1016/j.fusengdes.2008.05.025.

[11] M. Tokitani *et al.*, “Evaluation of radiation damages on the first-wall surface in LHD exposed to charge-exchanged helium particles,” *J. Nucl. Mater.*, vol. 386–388, pp. 173–176, 2009, doi: 10.1016/j.jnucmat.2008.12.086.

[12] A. Litnovsky *et al.*, “Smart fi rst wall materials for intrinsic safety of a fusion power plant,” *Fusion Eng. Des.*, vol. 136, no. September 2017, pp. 878–882, 2018, doi: 10.1016/j.fusengdes.2018.04.028.

[13] H. Greuner, H. Maier, M. Balden, B. Boeswirth, and C. Linsmeier, “Investigation of W components exposed to high thermal and high H / He fluxes W-bulk W-VPS on grahite,” *J. Nucl. Mater.*, vol. 417, no. 1–3, pp. 495–498, 2011, doi: 10.1016/j.jnucmat.2010.12.215.

[14] P. Lipetzky, “Refractory metals: A primer,” *Jom*, vol. 54, no. 3, pp. 47–49, 2002, doi: 10.1007/BF02822621.

[15] A. E. B. Kashyout, H. M. A. Soliman, H. Abou, P. Aly, and M. Fathy, “Preparation and characterization of DC sputtered molybdenum thin films,” *Alexandria Eng. J.*, vol. 50, no. 1, pp. 57–63, 2011, doi: 10.1016/j.aej.2011.01.009.

[16] H. Maier, J. Luthin, M. Balden, J. Linke, F. Koch, and H. Bolt, “Properties of tungsten coatings deposited onto the fine grain graphite by different methods,” *Surf.*

Coatings Technol., vol. 142–144, pp. 733–737, 2001, doi: 10.1016/S0257-8972(01)01177-X.

[17] M. Fukutomi *et al.*, "Effect of an intermediate tungsten layer on thermal properties of TiC coatings ion plated onto molybdenum Effect of an intermediate tungsten layer on thermal properties of TiC coatings ion plated onto molybdenum," *J. Vac. Sci. Technol.*, vol. 2650, no. 1985, 2012, doi: 10.1116/1.572806.

[18] N. Ahmed, M. A. Iqbal, Z. S. Khan, and A. A. Qayyum, "DC Magnetron-Sputtered Mo Thin Films with High Adhesion, Conductivity and Reflectance," *J. Electron. Mater.*, 2020, doi: 10.1007/s11664-020-08138-2.

[19] J. A. Shields and P. Lipetzky, "Molybdenum Applications in the Electronics Market," *Jom*, pp. 10–12.

[20] J. Hyun, D. Young, J. Kyung, K. Chakrabarty, and J. Yi, "High temperature crystallized poly-Si on Mo substrates for TFT application," *Thin Solid Film. 345*, vol. 427, no. 02, pp. 303–308, 2003, doi: 10.1016/S0040-6090(02)01156-2.

[21] B. Schwarz, C. Schrank, C. Eisenmenger-sittner, M. Sto, M. Rosner, and E. Neubauer, "Molybdenum interlayers as adhesion promotors for thin copper films on plasma treated glassy carbon," *Surf. Coat. Technol.*, vol. 200, pp. 4891–4896, 2006, doi: 10.1016/j.surfcoat.2005.04.042.

[22] G. Gordillo, F. Mesa, and C. Calder, "Electrical and Morphological Properties of Low Resistivity Mo thin Films Prepared by Magnetron Sputtering," *Brazilian J. ofPhysics*, vol. 36, no. 3, pp. 982–985, 2006.

[23] N. Sun, S. Lang, Y. Zhang, Y. Xu, and H. Liu, "Properties of Electrodeposited Tungsten Coatings on Graphite Substrates for Plasma Facing Components," *J. Fusion Energy*, 2016, doi: 10.1007/s10894-016-0088-8.

[24] J. Serp *et al.*, "The molten salt reactor (MSR) in generation IV: Overview and perspectives," *Prog. Nucl. Energy*, vol. 77, pp. 308–319, 2014, doi: 10.1016/j.pnucene.2014.02.014.

[25] J. J. Lee, J. D. Arregui-Mena, C. I. Contescu, T. D. Burchell, Y. Katoh, and S. K.

Loyalka, “Protection of graphite from salt and gas permeation in molten salt reactors,” *J. Nucl. Mater.*, vol. 534, 2020, doi: 10.1016/j.jnucmat.2020.152119.

[26] M. J. Driscoll and P. Hejzlar, “Reactor physics challanges in Gen IV reactor design,” *Nucl. Eng. Technol.*, vol. 43, no. January 2005, 2015.

[27] R. Bolot, D. Aussavy, and G. Montavon, “Application of FEM to Estimate Thermo-Mechanical Properties of Plasma Sprayed Composite Coatings,” *Coatings*, pp. 1–12, 2017, doi: 10.3390/coatings7070091.

[28] Z. He, J. Song, P. Lian, D. Zhang, and Z. Liu, “Excluding molten fl uoride salt from nuclear graphite by SiC / glassy carbon composite coating,” *Nucl. Eng. Technol.*, vol. 51, no. 5, pp. 1390–1397, 2019, doi: 10.1016/j.net.2019.03.006.

[29] L. Gou, C. Qi, J. Ran, and C. Zheng, “SiC film deposition by DC magnetron sputtering,” *Thin Solid Films*, vol. 345, pp. 42–44, 1999.

[30] R. T. Loto and P. Babalola, “Analysis of SiC grain size variation and NaCl concentration on the corrosion susceptibility of AA1070 aluminium matrix composites Analysis of SiC grain size variation and NaCl concentration on the corrosion susceptibility of AA1070 aluminium matrix composites,” *Cogent Eng.*, vol. 5, no. 1, pp. 1–14, 2018, doi: 10.1080/23311916.2018.1473002.

[31] N. Ma *et al.*, “Fabrication of amorphous silica coating on graphite substrate by laser cladding,” *Ceram. Int.*, vol. 46, no. 8, pp. 10829–10834, 2020, doi: 10.1016/j.ceramint.2020.01.094.

[32] H. Wang and X. Xiong, “Effect of microstructure on impact resistance of chemical vapor deposited SiC coating on graphite substrate,” *Surf. Coat. Technol.*, vol. 380, no. August, p. 125076, 2019, doi: 10.1016/j.surfcoat.2019.125076.

[33] B. I. Khripunov, V. S. Koidan, A. I. Ryazanov, V. M. Gureev, and S. N. Kornienko, “Study of tungsten as a plasma-facing material for a fusion reactor,” *Phys. Procedia*, vol. 71, no. February, pp. 63–67, 2015, doi: 10.1016/j.phpro.2015.08.313.

[34] L. I. Shun, Z. H. U. Mengjian, L. I. U. Meng, and B. A. I. Shuxin, “Preparation of Molybdenum Coating on Surface of SiC Particles by Sol-Gel Method,” *Adv. Mater.*

Res., vol. 721, pp. 224–228, 2013, doi: 10.4028/www.scientific.net/AMR.721.224.

[35] M. A. Mart and C. Guillén, "Comparison between large area dc-magnetron sputtered and e-beam evaporated molybdenum as thin film electrical contacts," *J. Mater. Process. Technol.*, vol. 144, pp. 326–331, 2003, doi: 10.1016/S0924-0136(03)00436-9.

[36] D. Veirman, "Columnar microstructures in magnetron-sputtered refractory metal thin films of tungsten , molybdenum and W - T i - (N)," *Thin Solid Films*, vol. 208, pp. 181–188, 1992.

[37] G. Gordillo, M. Griza, and L. C. Hernandez, "Structural and electrical properties of DC sputtered molybdenum films," *Sol. Energy Mater. Sol. Cells 51*, vol. 51, pp. 327–337, 1998.

[38] M. Khan and M. Islam, "Deposition and Characterization of Molybdenum Thin Films Using DC Plasma Magnetron Sputtering 1," *Semiconductors*, vol. 47, no. 12, pp. 1610–1615, 2013, doi: 10.1134/S1063782613140017.

[39] M. Jubault, L. Ribeaucourt, E. Chassaing, G. Renou, D. Lincot, and F. Donsanti, "Optimization of molybdenum thin films for electrodeposited CIGS solar cells," *Sol. Energy Mater. Sol. Cells*, vol. 95, pp. S26–S31, 2011, doi: 10.1016/j.solmat.2010.12.011.

Chapter 3: Experimental and processing techniques

This chapter includes the brief description of processing and characterization techniques used in research work. First section presents the deposition technique used to deposit Mo and SiC thin films. We used DC magnetron sputtering to deposit Mo thin film on glass and graphite substrate and Rf Magnetron sputtering was employed to deposit Silicon carbide thin film on graphite. Tube furnace was employed for annealing of Mo coated graphite and SiC thin film. Details of equipment and arrangement of deposition process are illustrated. Secondly, matrix of single and dual beam irradiation experiments is described along with information regard ion beam accelerator. UV Vis which was used to estimate reflectance characteristics is also been discuss in this chapter. In the end, all the characterization techniques with their working mechanism are also given in details. XRD, EDS, SEM, AFM and Hall Effect measurements are explained briefly in this section.

3.1 Magnetron Sputtering

Sputtering is vaporization of atoms from a solid surface cause by bombardment of energy particles. This process is independent of temperature as sputtering can be achieved at room temperature because sputtered species are physical ejected by the momentum of incident gaseous ion accelerated by sputter power. The energetic particles that bombard the target are usually ions of a sputtering gas. These ions are produced mostly because of electron collisions with the gas atoms, while moving from cathode to anode via the gaseous medium.

Magnetron sputtering is an advanced form of sputtering. Consist of almost same sputtering setup but having additional magnet. This approach is used to avoid the loss of electron. As electrons drift across the gaseous medium is responsible for producing and sustaining plasma. These electrons ionized the gas atoms. The knocked-out electrons additionally take a role in ionization of gas.

This approach is very widespread for deposition of thin film. With electromagnetic effect, charged plasma is confined in the curve path and it enriches the quantity of electrons in particular volume. And due to influence of constant magnetic field, ions and electrons flows in cycloidal path.

This can be explained by Lorentz equation

$$F = q(E + vB) \qquad (3\text{-}1)$$

Here q is the charge of electron E denoted the electric and B denoted the magnetic field. Moreover, v is the velocity of electron in the confined path. The radius r will b given by

$$r = \frac{mv}{qB} \quad (3\text{-}2)$$

3.1.1 DC Magnetron Sputtering

Generally, DC magnetron sputtering is utilized to deposit metallic substances. This process is one of the most economically viable techniques because it gave high deposition rate and DC power supplies are easier to manufacture. In direct current magnetron sputtering the target conducts the current directly. High crystalline thin films can be achieved using these techniques. In the first part of research all the Molybdenum thin films were deposited by DC magnetron sputtering.

In DC sputtering, deposition operation proceeded due to ionized argon atoms resulted by collision of secondary electron from cathode. Higher pressure of Ar in chamber causes tensile stress while lower pressure causes compressive stresses in the films. Surface roughness and adhesion is inversely proportional to the deposition power. The size and density of crystallites varies directly with deposition power. Higher deposition power attributed as the higher grain size and it leads to the columnar structure this lower resistivity. DC magnetron sputtering provides more control over film properties by adjusting the process parameters. Mainly distance between target to substrate, working gas pressure, deposition power and substrate temperature that effects the characteristic of films.

3.1.2 RF Magnetron Sputtering

For the deposition of insulating or semiconducting targets, we cannot use Direct current magnetron sputtering. The reason is the current cannot pass through non conducting

targets. So, this problem can be resolve by introducing Alternating current at high frequency, so, radio frequency magnetron sputtering was developed to fabricate insulating materials. We can also deposit metallic substances by using this technique.

This deposition technique needs and impedance mating network to make sure that majority of current is immersed in to plasma. Along with this matching network RF source generator is needed to convert current into high frequency. This leads to high manufacturing cost of RF magnetron sputtering equipment. In the second part of research the SiC coating was deposited by using RF Magnetron Sputtering.

3.1.3 Sputtering and Thermal Evaporation System.

NANOVAK NVTS-400 system was used to deposit Mo and SiC on graphite and glass substrate using DC magnetron sputtering. This system is one of the advanced and intelligently controlled system which can be controlled by a computer screen. Three different operations can be performed on this equipment:

- DC Magnetron Sputtering (with DC power capacity of 1560 W)
- RF Magnetron Sputtering (300 W capacity)
- Thermal Evaporation (2000 W capacity)

Different components of this system include stainless steel chamber connected with rotary pump and turbo molecular pump. Vacuum up to 5×10^{-8} torr can be achieved in 3 hours. It has two vacuum gauges which includes a highly précised magnetron pirani vacuum gauge for vacuum measurement from atmospheric pressure to 10^{-9} torr and Capacitance Diaphragm Gauge which is used to measure working gas pressure. Substrate temperature of 500 Celsius can be achieved with sample rotation speed from 5 to 30 rpm. It also possesses thickness controllers which can measure thickness up to 0.1 Å.

Figure 3-1 NANOVAK NVTS-400 hybrid system for Magnetron sputtering and thermal evaporation

3.2 Irradiation Experiment

Mo thin films were tested under the irradiation of heavy and light ion. Using 5 MV Palletron Tandem particle accelerator.

3.2.1 Ion beam accelerator

Ion beam experiments were performed using MV Palletron Tandem accelerator facility available at national center for physics. It has varying ion beam energy from 0.4 MeV to 25 MeV. Ion current ranges between 1nA to 0.2mA. There are two available ports of 15˚

and 30˚. 15˚ is used for ion beam irradiation. Whereas, available ions are: H, He, C, Si, Cu, Ni and Au.

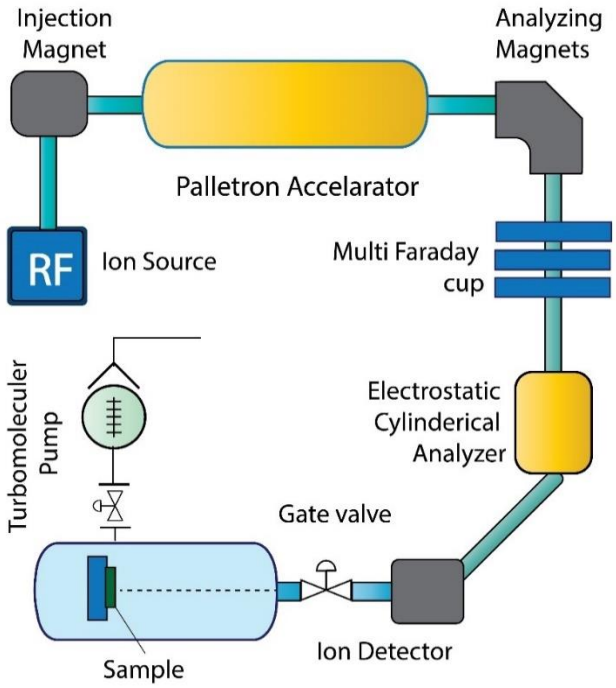

Figure 3-2 Schematic of palletron accelerator for light and heavy ions irradiation

3.3 Heat Treatment

3.3.1 Drying of substrate

Memmert universal drying oven was used to dry substrate material before every deposition. It comes up with many features which includes intuitive and easy-to-use operating menu. It also offers controllable air exchange rates and air flap position electronically. Temperature and air flow ramps are controllable. Temperature fluctuation is control by pre-heating of fresh air. Interior of this oven is made of stainless steel, which is not only corrosion-resistant but very easy to clean.

3.3.2 Annealing and sintering

MTI GSL 1600 tube furnace was used for sintering and reactive annealing of various coated thin films.

Figure 3-3 MTI GSL tube furnace

MTI GSL 1600 tube furnace: GSL-1600X-50-UL contains 5 cm tube with silicon carbide-based heating rods. It can be used in annealing and sintering experiments at elevated temperatures. Under vacuum conditions they can be increased up to 1600 ^{o}C. Temperature is controlled by SCR controller with high precision of 1K. This tube furnace contains high quality tube with 99.99 % pure alumina. It also includes pressure gauges to monitor pressure inside the tube furnace. This tube furnace can be operated with different gases like nitrogen, Argon and helium. Annealing experiments can be performed in the air as well. This tube furnace is highly compatible with glove box as well.

3.4 Electrochemical testing

Different electrochemical techniques like OCPT, TAFEL and electrochemical impedance spectroscopy were used to analyze corrosion resistance behavior of SiC coating on graphite. CH 600 electrochemical work station was employed for this purpose.

3.4.1 Electrochemical work station

CH 600 was employed for all electrochemical testing. This equipment is an electronic general purpose potentiostat /galvanostat. This equipment comprises of a fast-digital function generator and dual-channel data acquisition circuitry. In this workstation the

voltage potential range is between -10 V to +10 V and it can draw a current up to 0.25 A. The precision of measuring currently can be increased up to 10^{-12}Amperes. The generator can produce frequency of 10000 kHz. This equipment provides a very extensive dynamic range of experimental time scales. For example, the scan rate in CV can be up to 1 kV/s with a 0.0.0001V potential increment or 5 kV/s with 0.001 V potential increment. This instrument is capable to perform different sweep techniques, Step techniques, A.C techniques, stripping and control current technique.

3.5 Characterization techniques:

Different characterizations techniques were used to determine morphological and structural characteristics. Chemical composition is detected by EDS. Surface morphology is characterized by scanning electron microscopy and topographic information is calculated by AFM to estimate the surface roughness. Electrical resistivity can be calculated via Van der Pauw method.

3.5.1 X-ray Diffraction

X-ray diffraction is the scattering of electromagnetic waves by a periodic long-range array, resulting in constructive interference at certain angles. Diffraction patterns are representative of the unique microstructure of a material. Bruker D8 advanced X-rays diffractometer was used for structural analysis.

Figure 3-4 Bruker D8 advanced X-rays diffractometer

Atom in the crystal behaves as a coherent scattering point, as the electron in an atom scatter light coherently. The number of electrons in an atom determines the light scattering strength of that atom. As crystals consist of periodic array of long range ordered atoms, thus crystals can diffract X-rays. The X-rays scattered by atoms of a material, contain information of atomic arrangement in the material. Less crystalline or amorphous materials don't have periodic arrangements; thus, x-ray diffraction shows no specific diffraction pattern. For different arrangement of atoms, a different pattern is expected. Several peaks in a single diffraction pattern of a material can be observed. The number of peak and their relative intensity is again dependent upon the crystal structure of the material. As a crystal's structure is defined by its unit cell, whereas, a crystal system describes the shape of the unit cell. Different planes of atoms are identified by Miller indices (hkl).

X-ray diffraction wavelength λ falling on a family of parallel atomic planes, constructive interference occurs only at a specific angle.

$$n\lambda = 2d \sin\theta \qquad (3\text{-}3)$$

Where, n is a positive integer, which indicates the inter-planar distance between two adjacent planes of the (hkl) family. Furthermore, inter-planar spacing (d) using equation

(3-6) and lattice parameter was calculated by Bragg's formula given in the following equation.

$$\frac{1}{d^2} = \frac{h^2+l^2+k^2}{a^2} \quad (3\text{-}3)$$

Where, n is a positive integer, which indicates the inter-planar distance between two adjacent planes of the (hkl) family. Furthermore, inter-planar spacing (d) using equation (3-6) and lattice parameter was calculated by Bragg's formula given in equation.

The crystallite size is calculated using full width half maxima of the characteristic XRD peaks using the Scherer formula

$$D_s = \frac{0.9\lambda}{\beta \cos\theta} \quad (3\text{-}4)$$

D_S is crystallite size, where, λ shows wavelength of the X-Ray which has constant value of 1.54, θ is Bragg diffraction angle, β represent full width at half-maximum (FWHM) in radians.

3.5.2 Scanning Electron Microscopy

Scanning electron microscopy (SEM) works on the principal or interaction of highly energetic electrons in the form of a focused beam, and a sample surface. This incident of electron beam creates multiple signals to create image on the sample. The reflected samples can give knowledge about microstructure, materials orientation, morphology, topography and composition of the sample under observation.

Figure 3-5 TECASN Vega 3 Scanning electron microscopy

A scanning electron microscope typically requires an electron gun to eject electrons. The electron gun typically employs a tungsten filament, which upon heating thermionic ally emits electrons. These electrons are accelerated towards the anode by a high electric field. A portion of the electrons, due to high velocities pass by the anode plate and stream down the column. In the process, the electrons acquire energy typically in the range 0.2 – 40 keV. The electrons are then focused by one or two lenses to a spot of diameter in the range 0.4 to 5 nm. This is followed by the passages of the beam through a pair of scanning coils or deflector plates. Here the beam is deflected in the xy-plane to cause a raster scan of the sample. Selected areas as well as selected points could be analyzed with SEM. Fast and energetic electron interacting with sample surface generates different type of signals that are detected by using specific detectors. Mainly two types of detector are used secondary electron and back scatter electron. SE are especially important for morphology imaging and topography. BSE are often employed for showing compositional.

3.5.3 Cross Sectional SEM analysis

It is one of key method to study interface of thin film with substrate. This tool can also be useful in determining the thickness of thin film. In order to do cross-sectional analysis, sample preparation is an important art. Results can only be elaborative if sample are well prepared and passed through all the necessary step of sample preparation, Careful cutting, grinding and polishing are often required. For grinding and polishing of the samples Metkon FORCIPOL grinding and polishing machine was used.

Sample cleaning is an important step. In this study samples preparation steps were optimized to get desired configuration for cross sectional analysis. Sample preparation involves following steps.

- First of all coated sample is cut down to desire size
- Suitable mold is selected
- Epoxy is prepared by mixing it with hardener in suitable ratio
- Sample is then embedded in the epoxy
- After settling of the sample, grinding and polishing is done with suitable grit size paper
- Sample is then cleaned and stored
- For SEM analysis, sample is coated with gold up to few nanometers
- SEM imaging and processing is done in the end

In addition to it, resolving power of SEM is considerably higher than optical microscope. SEM uses electrons of energies as high as thousands of eV. It can resolve image up to 1nm. In this work, film morphology and cross-sectional analysis was done by using TECASN Vega 3 SEM.

3.5.4 Energy Dispersive X-ray Spectroscopy

Energy dispersive X-ray spectroscopy (EDX) also known as energy dispersive X-ray microanalysis (EDXMA) or energy dispersive X-ray analysis (EDXA), is a technique to analyze the elemental composition of a sample. EDS relies on the principle that each element is made up of atoms of unique atomic structure. Thus, each element has a unique

set of characteristic x-rays that it can emit upon excitation. Emission of X-rays from a sample requires bombardment of the sample with a beam of energetic charged particles (electrons or protons), or X-rays. Thus, EDS involves analysis of the X-ray spectrum obtained as a result of the bombardment for elemental analysis. When particles/radiations fall on a surface, depending upon the energy of the falling particles/radiations and the binding energies of the electrons, electrons might be removed from the surface. Sufficiently energetic particles/radiations can even remove inner shell electrons from the sample atoms. When an inner shell electron is removed, a vacancy (hole) is created in that shell. Electron from an outer orbit falls into that hole. This transition results in X-ray emission, characteristic of that element. X-ray lines are labeled by a capital letter that indicates the shell where the vacancy existed. It may be K, L or M, followed by a Greek letter (α, β etc.). α lines are the most important ones. β lines are less important than but more important than lines indicated by other Greek letters that follow, and so on. The Greek letter is followed by a number (1, 2, etc.) in subscript, that corresponds to the intensity of the line in that peculiar group, such as $K\alpha_1$. Among the numbers, 1 stand for maximum intensity, while others in the sequence represents a correspondingly decreasing intensity. When there is no number mentioned, it represents the combined intensity from all the X-rays in that group, such as Kα. Sometimes, the combined line is represented by mentioning more than one number in subscript, such as $K\alpha_{12}$. All elements with atomic number in the range 4–92, are detectable with EDS. EDS analysis may be qualitative or quantitative. Qualitative analysis is fairly simple, since it involves lines identification in the X-ray spectrum. Quantitative analysis is relatively complicated, because it involves not only line identification but also intensity measurement of each element in the sample as well as of the same elements in calibration standards of known composition. The precision of the quantitative EDS is primarily limited by statistics, since EDS involves photon counting for intensity measurements. For most of the elements, a relative precision of better than ±1% is achievable. However, due to limitations introduced by the standard compositions as well as a set of corrections, the analytical accuracy of EDS is near ±2%. For EDS analysis samples must also be conductive. For insulator a thin layer of gold or carbon are deposited to avoid charging for sample. In this study Oxford EDS detector attached with TESCAN VEGA 3 SEM was used.

3.5.5 Atomic Force Microscopy

Atomic force microscopy (AFM) is also a surface analysis tool used for three dimensional images of the surface to observe the nano metric and sub-nano metric details of a surface. This technique is equally viable for all type of materials independent of their hardness transparency or conductivity. AFM consist of a sample holder a probe fixed at cantilever and laser attached with measuring hardware which controlled and monitored by a computer program. The cantilever can be considered as a spring, whose spring constant along with the distance between the probe and the surface, determine the force experienced by the probe. According to Hook's law force is given by following equation.

$$F = -kx \quad (3\text{-}5)$$

Here x is the displacement from mean position and the value of spring constant and K (~ 0.1 – 1 N/m) is less than that of the surface, a cantilever bending is experienced. In air, the typical range for this force is 10^{-6}µN – 10^{-9}nN. Feedback networks and piezo electronic scanners are used to control the probe motion across the surface. Monitoring the force between the probe and the surface is the primary driver behind the different instrumentation designs today.

Figure 3-6 FLEX Atomic Force Microscopy

Phenomena of light reflection are used to measure deflection of the probe. This method is known as the beam bounce method. Detector measured the bending of cantilever that is mapped by computer pregame to produce 3D image on the surface [7].

It works on two basic modes of operation, the contact and the non-contact mode. In the contact mode of operation repulsive Van der Waals forces are the predominant interactions experienced by the probe. Contrary to that, the probe lies relatively away from the surface; attractive Vander Waals interactions are most influential in non-contact mode. To measure heights, a probe is used. The probe when brought close enough to the sample surface experiences a number of forces, using these forces the height can be calculated. In this study FLEX AFM was used to get topographic images of Mo coated graphite samples. Roughness of the surface was measured and compared with the respective deposition parameters of the samples to determine the relation between them.

3.5.6 Hall Effect Resistivity Measurement:

This is one of the most commonly employed method using Van der Pauw method to determine resistivity, sheet resistance, mobility and material type. The technique requires films of uniform but negligible thickness, developed of materials that are homogeneous and symmetrical. Furthermore, the contacts be equally space, be along the perimeter, and compared to the film area, must be of smaller According to Vander Pauw, if the above conditions are satisfied, then.

$$\boldsymbol{e}^{-(\pi\frac{d+R_{AB,CD}}{\mathcal{P}})} + \boldsymbol{e}^{-\left(\pi\frac{d+R_{BC,AD}}{\mathcal{P}}\right)} = \mathbf{1} \quad (3\text{-}6)$$

Here $R_{AB,\,CD}$ stands for resistance when current in applied at point A and B. Whereas, potential is measured across C and D terminals. Resistance is calculated for the current enter from the point B and leave from C where the potential is measure across A and D point. Thickness of the sample or coating is represented by letter ‘d’ and resistivity is indicated by ‘p’.

$$R_s = \frac{\pi R\Omega}{(ln2)^2} \quad (3\text{-}7)$$

In this study ECOPIA Hall effect measurement system [8] was used to measure resistivity of the films before and after irradiation experiments. Increase in defects density caused by ion irradiation was related to the degradation in conductivity of samples [9]

3.6 Summary

First section presents the deposition technique used to deposit Mo and SiC thin films. We used DC magnetron sputtering to deposit Mo thin film on glass and graphite substrate and RF magnetron sputtering was employed to deposit silicon carbide thin film on graphite. NANOVAK NVTS 400 sputtering system was employed for both depositions. Tube furnace was used for annealing of Mo coated graphite and SiC thin film. Secondly, matrix of single and dual beam irradiation experiments is described along with information regard ion beam accelerator. In the end, all the characterization techniques with their working mechanism are also given in details. XRD, EDS, SEM, AFM and Hall Effect measurements are explained briefly in this section

Chapter 4: Experiments and methods

This chapter contains experimentation matrix of this study, the first part of this chapter is about Mo deposition on graphite. This part accommodates the irradiation experimentation for ITER based plasma facing materials and fabrication of Molybdenum carbide by reactive annealing was one of the parts of this chapter. DC magnetron sputtering was utilized for the deposition of Molybdenum on glass and graphite. The 2nd part is about Silicon carbide thin film on graphite for oxidation resistance-based applications. The RF magnetron Sputtering was utilized for that purpose.

4.1 Mo deposition on graphite at different powers and gas pressures

4.1.1 Sample preparation

Iso-molded graphite was taken as a substrate material and was cut down into a suitable size 3 cm x 4 cm. These substrates were then polished up to 1 micron and cleaned using ethanol and acetone. Molybdenum target of 2-inch diameter with 99.999 % purity was used.

4.1.2 Deposition

DC magnetron sputtering was employed to develop Mo coating on graphite. NANOVAK NVTS-400 hybrid system placed at combined lab USPCASE NUST was utilized for this purpose. Different experimental parameters were used by varying sputtering power and gas pressure. The substrate temperature was kept 300 C with rotation speed of 5 rpm. Moreover, base pressure of 8 x 10^{-7} was achieved. Detail experimental scheme shown in table 4-1.

Table 4-1: Detailed experimental scheme of Mo Deposition on graphite

Sample ID	Power	Gas pressure	Thickness
M1	100	4	1.88
M2	200		1.94
M3	300		2.21
M3A	300	4	2.21
M4		2	1.93
M5		1	2.41

4.1.3 Characterization

The surface morphologies of Mo thin films were monitored with scanning electron microscopy. The impact of process parameters on cryptographic and structural characteristics of molybdenum thin film on graphite was observed with X-Ray Diffraction using CuKα source. The XRD data was analyzed by MDI Jade 6.5 which shows us FWHM, d spacing, peak intensity, and different cryptographic features. Hall Effect was employed to demonstrate the trend of resistivity.

4.2 Ion beam irradiation of Mo Thin film

4.2.1 SRIM Calculation

Irradiation parameters such as the projected range of α-particle in Molybdenum thin film , ion energy and incident angle etc. were predicted using Stopping Range of Ions in Matter (SRIM) program before irradiation experiment. Moreover, the loss in electronic (Se) and nuclear energy (Sn), and damage per atom (DPA) were also calculated [20]. Projected range with respect to ion energy is illustrated in the Fig. 2 a. The projected range for 0.8 MeV was 1.28 micron. The electronic and nuclear energy loss was 713.8 keV/micron and 1.347 KeV/micron respectively. Whereas electronic and nuclear energy loss for 1.6 MeV He ion were 635 and 0.780 KeV/micron with the projected range of 2.41 microns. The irradiation parameters indicate that the electronic energy losses for both experiments were way higher than nuclear energy losses. So, all the expected changes in structure,

morphology, topography and electrical characteristics in the irradiated Mo thin films can be attributed to electronic energy loss.

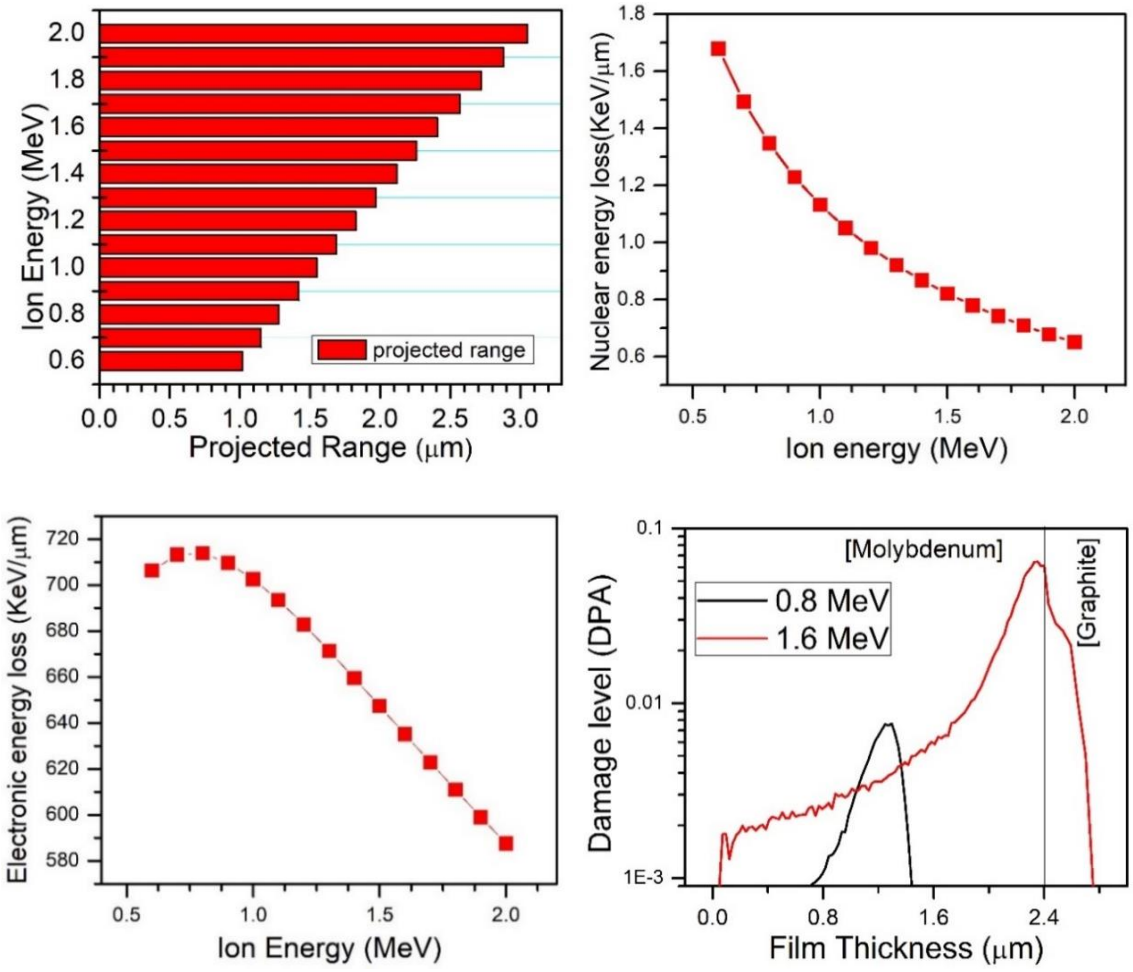

Figure 4-1 a) Projected range of α-particles in the Mo thin film, b) Nuclear energy loss of α-particles in the Mo thin film, c) Electronic energy loss α-particles in the Mo thin film, d) Vacancies per ion (DPA) for both 0.8 and 1.6 MeV irradiated thin film

4.2.2 Irradiation experiment

The ion beam experiment was performed in 5 MV Pelletron Tandem accelerator facility available at National Center for Physics, Islamabad. The schematic diagram of Pelletron Accelerator is shown in fig. 1 b. The first specimen was irradiated with 0.8 MeV He ion with fluence of 5.2 x 10^{15} ions/m^2 and other was irradiated with 1.6 MeV He ion with fluence of 5 x 10^{16} ions/m^2 (as shown in table 4-2). According to SRIM calculations, ion energy for 1st specimen wasn't enough to penetrate through the coating. Whereas for 2nd

specimen, the α- particles was accelerated in a way that they have enough energy to penetrate into the Mo thin film.

Table 4-2: Irradiation parameters for He ion beam irradiation

Sample ID	Ion energy	Fluence	Dose
	MeV	Ion/cm^2	DPA
As-deposited	-	-	-
He 0.8	0.8	5.2 x 10^{15}	0.0765
He 1.6	1.6	5.0 x 10^{16}	0.645

4.2.3 Characterization

Structural analysis of both pre and post irradiated Mo thin films was done to investigate structural changes cause by irradiation of α-particles. Bruker D8 advanced X-rays diffractometer with CuKα (λ = 1.54056 Å) as radiation source was employed for that purpose. The surface morphology observation of the films was made using a TESCAN VEGA3 Field Emission Scanning Electron Microscope (FESEM) at an accelerating voltage of 5 kV. NANOSURF FLEX AFM was used to estimate the change in film roughness and topography on different irradiation doses. The electrical measurement of the Mo thin films was carried out by Hall Effect method.

4.3 RF magnetron sputtered SiC on graphite for anti-corrosive applications

4.3.1 Deposition

Silicon carbide thin film was deposited on graphite by RF Magnetron Sputtering. NANOVAK NVTS 400 was used for this purpose. Molybdenum target of two-inch diameter with 99.999% purity was used. After sample placement, high vacuum was built up to 5×10^{-7} torr by Turbo-molecular pump. The substrate temperature was increased up to 300°C. Moreover, substrate rotation speed was kept at 10 RPM. Gas pressure of 3 Pascal

was used along with RF power of 120 W. 900 nm Silicon carbide thin film was deposited in 2 hours.

4.3.2 Heat Treatment

Three specimens of prepared thin film were annealed at different temperatures for two hours in order to enhance crystallanity of SiC thin film. Tube furnace was employed for that purpose. All heat treatment experiments were done in Argon inert environment. The pressure of 1.05 atm was maintained. Owing to severe heating load at high temperature. Variable heating rate was maintained in different temperature regimes (as shown in table 4-3).

Table 4-3: Annealing scheme of SiC coated graphite

Specimen ID	Annealing temperature	time
1	1000	2 hours
2	1200	2 hours
3	1400	2 hours

4.3.3 Characterization

TESAN VEGA3 scanning electron microscope was used to observe the surface morphology of silicon carbide thin film. Bruker D8 advanced X-rays diffractometer with CuKα as a radiation source was employed to determine the structural properties of thin film. Films resistivity was measured by Ecopia HMS-3000 Hall Effect instrument using the Van der Pauw technique.

4.3.4 Electrochemical testing

Different electrochemical techniques were used to determine corrosive nature of our films. 3.5 % NaCl solution was prepared. Platinum wire was used as counter electrodes along with Ag/AgCl as reference electrode. SiC coatings acted as working electrodes; however, substrate was insulated in a way that only coating was exposed to the solution. For TAFEL analysis, scan rate was maintained at 0.001 V/s and with voltage range of -0.8 to 0.5. OCPT was carried out for 1200 seconds for each sample. Electrochemical Impedance Spectroscopy

(EIS) analysis was also performed. Frequency was kept between 1 and 106 Hz whereas amplitude of 0.01 V was maintained.

4.4 Summary

In this chapter detailed experimental is given. Iso-molded graphite was taken as a substrate material and was cut down into a suitable size 3 cm x 4 cm. These substrates were then polished up to 1 micron and cleaned using ethanol and acetone. Molybdenum target of 2-inch dia with 99.999 % purity was used. DC magnetron sputtering was employed to develop Mo coating on graphite. NANOVAK NVTS-400 hybrid system placed at combined lab USPCASE NUST was utilized for this purpose. Different experimental parameters were used by varying sputtering power and gas pressure. The substrate temperature was kept 300 C and rpm of 5. Moreover, base pressure of 8×10^{-7} was achieved for every deposition. Most optimized thin film was then exposed to two different doses of helium ion to assess their effects on the microstructure, topography and mechanical characteristics. Structural evolution caused by helium ions was analyzed by X-Ray Diffraction. Surface morphology and topography were characterized by scanning electron microcopy (SEM) and atomic force microscopy (AFM), respectively. Micro hardness is used to assess the irradiation hardening behavior of Mo thin film. Moreover, change in conductivity behavior was demonstrated by Hall Effect method. In second part, RF magnetron sputtering was used to deposit SiC thin film on graphite. The substrate temperature was increased up to 300°C. Moreover, substrate rotation speed was kept at 10 RPM. Gas pressure of 3 Pascal was used along with RF power of 120 W. 900 nm Silicon carbide thin film was deposited in 2 hours. Three specimens of prepared thin film were annealed at different temperatures for two hours in order to enhance crystallanity of SiC thin film. Different analytical techniques like SEM, XRD and Hall Effect are used to examine structural and electrical characteristics. Electrochemical methods like OCPT, Tafel and EIS were used to determine corrosive nature of our films. 3.5 % NaCl solution was prepared. Platinum wire was used as counter electrodes along with Ag/AgCl as reference electrode. SiC coatings acted as working electrodes; however, substrate was insulated in a way that only coating was exposed to the solution.

Chapter 5: Results and discussions

5.1 Mo deposition on graphite at different powers and gas pressures

5.1.1 Structural analysis

The X-ray diffraction results reveal that Mo coating maintained a single-phase cubic structure with the preferred orientation (1 1 0). Figure 5-1 shows the XRD patterns of deposited Mo thin film at different sputtering powers and gas pressures. Wider and low intensity peaks were observed at low sputtering powers whereas thin and high intensity peaks were evident for high sputtering power.

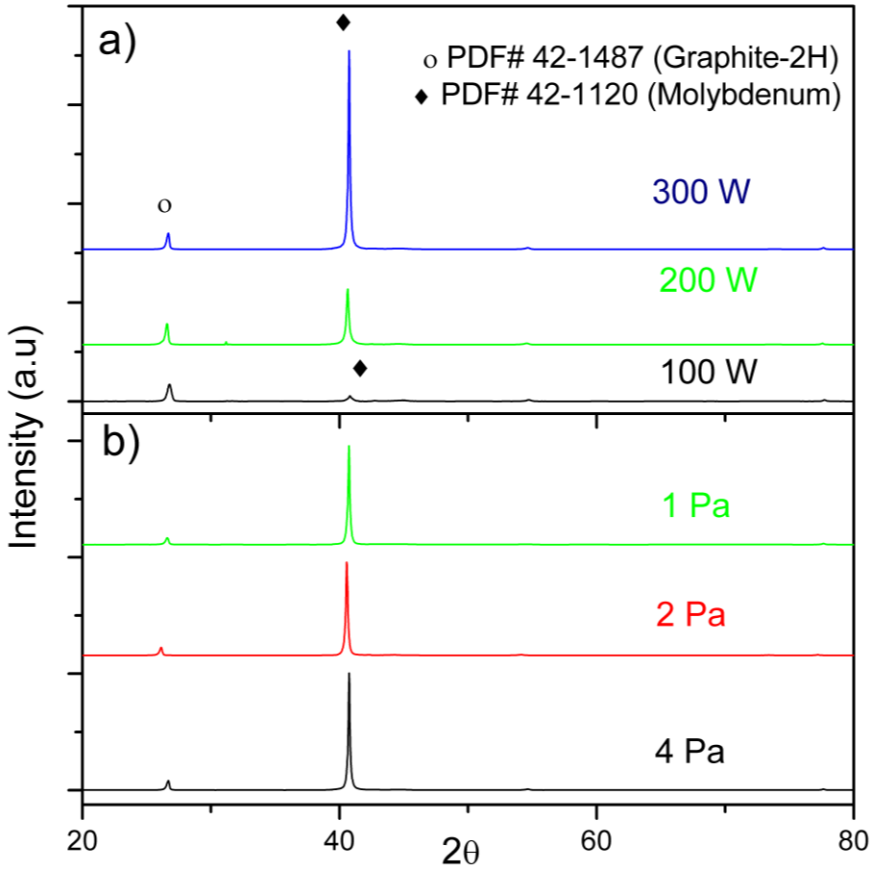

Figure 5-1 X-Ray Diffraction of Mo deposited graphite at different gas pressures and powers

Crystallite size was determined by Scherer formula [1].

$$L = \frac{K\lambda}{B\cos\theta} \qquad (5\text{-}1)$$

K represents the shape factor. For Molybdenum value of K is 0.94. λ represents the wavelength of the X-ray source and *B* represents full-width half maxima (FWHM) of respective peak at angle 2θ. Crystallite size increased with increase in power. The Smallest crystallite size of 24 nm was observed for 100 W whereas it increases up to 37 nm for the sample deposited at 300 W as shown in figure 5-2. This can be explained by higher surface mobility originated by high adatom energy at high power, that reinforced the crystallanity behavior in Mo films [2]. When the sputtering power is low the time between two adatom is more as compare to high sputtering power. So, chances of termination of crystallite are high at low sputtering power. That's why we attained smaller crystallite size at low sputtering power.

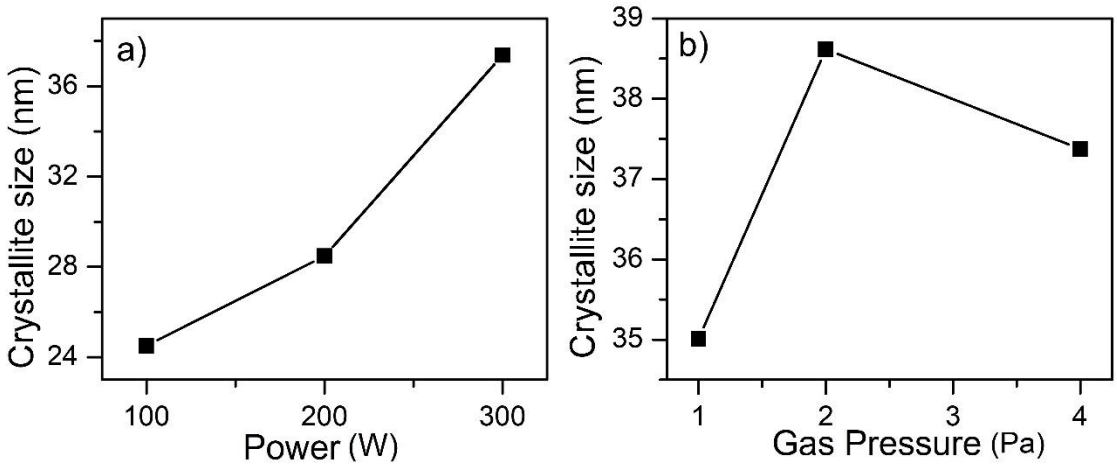

Figure 5-2 crystallite size at different a) Powers and b) gas pressures

Talking about impact of gas pressure on crystallite size, initially increase in crystallite size was observed by increasing the gas pressure [3]. After that further increase in gas pressure the crystallite size decreased. The results are illustrated in the figure. This can be explained by deposition rate.

At low gas pressure of 1 Pa we observed low deposition rate and thus low crystallite size. With an increase in gas pressure up to 2 Pa, owing to more gas atoms the deposition rate increased further. It resulted in greater crystallite size. After further increase to 4 Pa. the collision between target Mo atoms and gas atoms increased, which decreased the mean free path of target atoms. It leads to decrease in deposition rate. Hence smaller crystallite formed at that gas pressure [4].

5.1.2 Surface Morphology

SEM results reveal that porous structure is formed at low sputtering power and dense pack structure was formed at high sputtering power with ellipsoid structure. The SEM micrographs are shown in figure 5-3 At low power, due to low deposition rate, little number of atoms reaches the substrate and hence, the porous structure is formed. Whereas due to high deposition rate at high powers, arrival of sputtered atoms is increased that results in a dense pack structure.

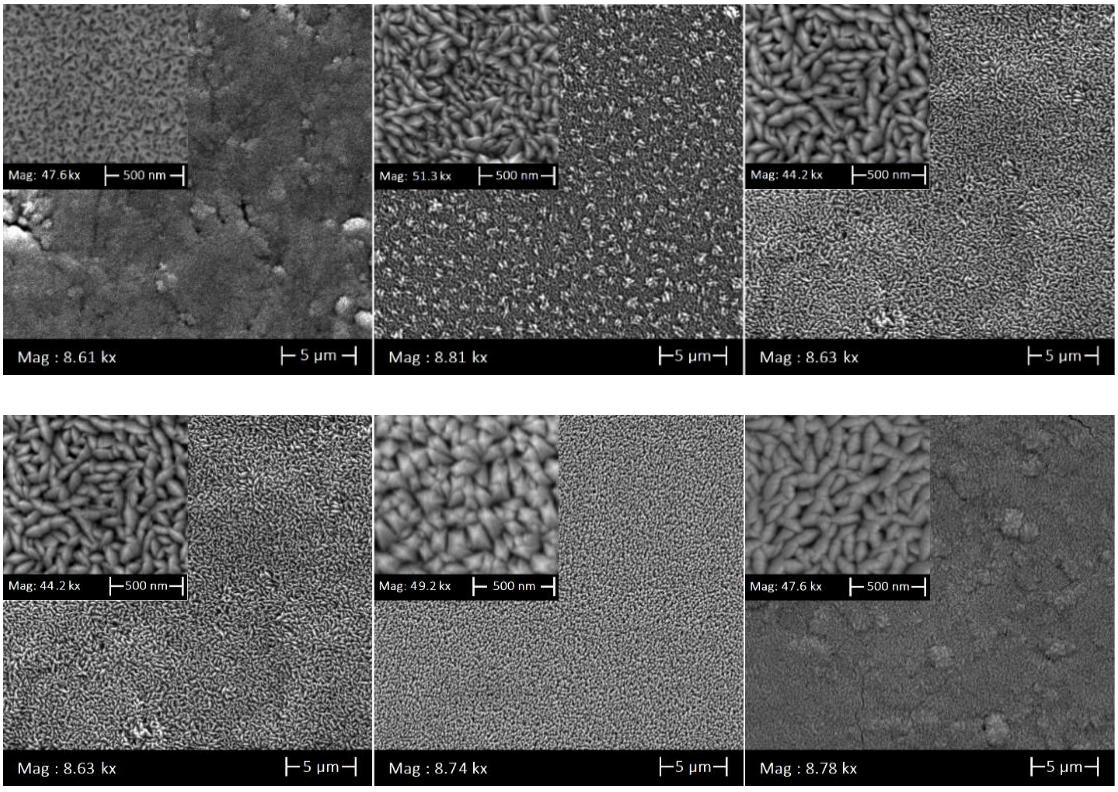

Figure 5-3 SEM images at different Powers and gas pressures

Smoother morphology was observed at low gas pressure. By increasing gas pressure, the surface of the thin film became rougher. This can be explained by kinetic energy of target particles [5]. With the rise of gas pressure, number of inert gas atom increase along with volumetric density of plasma. It enhances the sputter yield of particle. And with least collisions target atoms exhibit high energy and deposited with tightly pack arrangement. On bulk they produce smoother surface. But in case of high gas pressure, enhanced scattering and low mean free path of Mo atoms lead to un symmetric deposition. And it ends up in rougher morphology.

5.1.3 Electrical Characterization

The Hall Effect method was used to demonstrate effect of deposition parameters on the resistivity of Mo thin films. Multiple readings were performed for every thin film and graph with error bars has been plotted between resistivity and process parameters as shown in figure 5-4.

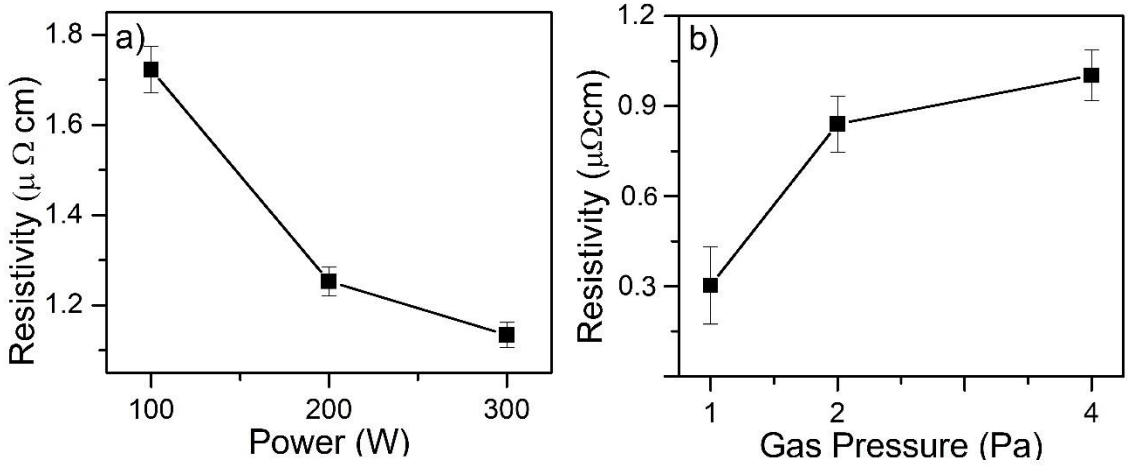

Figure 5-4 Resistivity at different sputtering powers and gas pressures

The Van der Pauw method reveals that with rise in sputtering power the resistivity decreased and it decreased with an increase in working gas pressure. This reduction in resistivity can be associated with the formation of dense pack structure at high sputtering

power and low gas pressure. This trend can also be accompanied by grain size [6]. As grain size increases at high powers and low working gas pressure. It leads to reduction of grain boundaries and decrease the grain boundary potential barrier height. So, during the electronic flow charge carrier has to cross fewer barriers, ultimately it reduced the resistivity of Mo thin film.

5.2 Ion beam irradiation part

5.2.1 Structural analysis:

To study the impact of α-irradiation on the structure of the Mo thin films, XRD measurements were performed. Mo peak matches with JCPDS card no. 42-1120 and (110) plane was observed as shown in figure 5-5. Graphite peak with JCPDS card no. 41-1487 was also observed. Increase in Full width half maxima and decrease in relative intensity was observed with increase in ion beam energy and fluence. However, this impact was not dominant in case of low energy irradiation, where we observed slight change in crystallite size and crystal orientation. Further, the peak intensity decreases for the both irradiated samples due to decrease in defects concentration by the effect of mutual annihilation of defects. At the same time, atoms of Molybdenum again get some space near the defect centers which results in a decrease of crystallinity in this sample. The peak broadening in He irradiated Mo thin film can also attributed to generation of point defects such as vacancies and interstitials [7].

Various parameters like Residual stress, crystallite size (D), dislocation density (δ), micro strain (ε) were calculated. The Residual Stress was calculated using the following equation [2]:

$$Residual\ Stress = \sigma = \frac{E\Delta d}{2\nu d_o} \qquad (5\text{-}2)$$

Where "d_o" is the standard lattice spacing for Mo and Δd is the difference between standard lattice spacing and actual lattice spacing. Actual lattice spacing was calculated by the following relation.

$$d = \frac{a}{\sqrt{h^2+l^2+k^2}} \qquad (5\text{-}3)$$

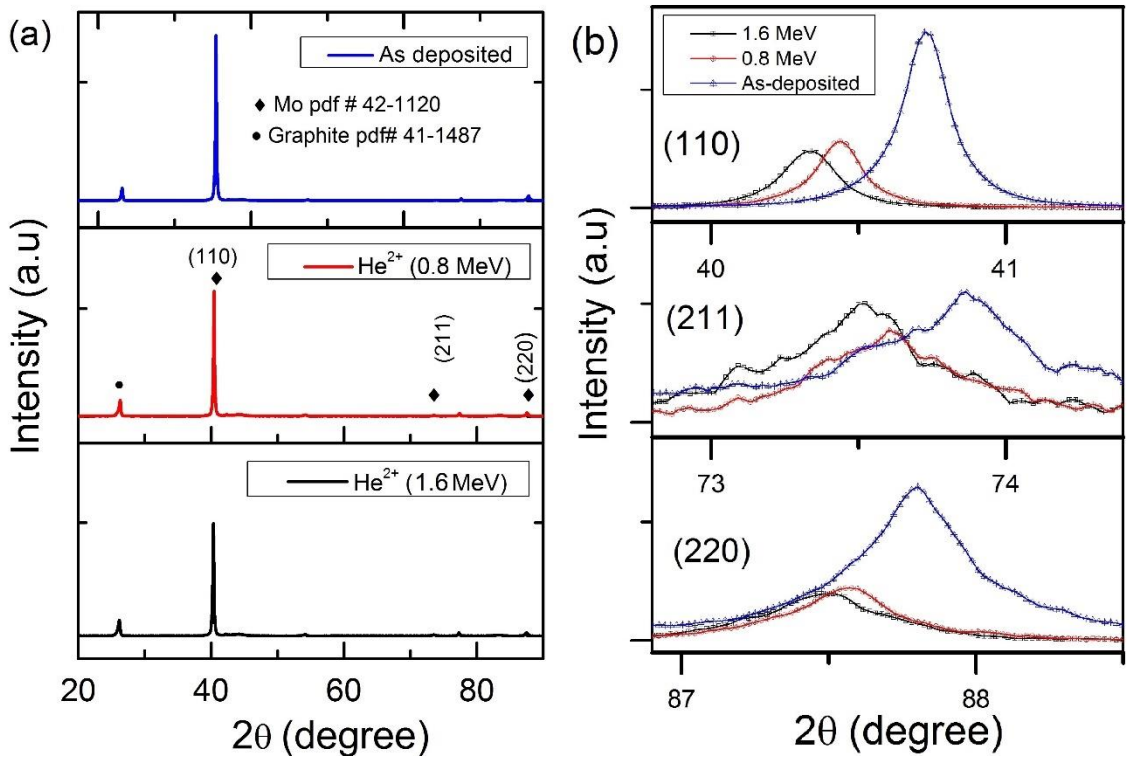

Figure 5-5 XRD spectrum of as deposited and irradiated samples

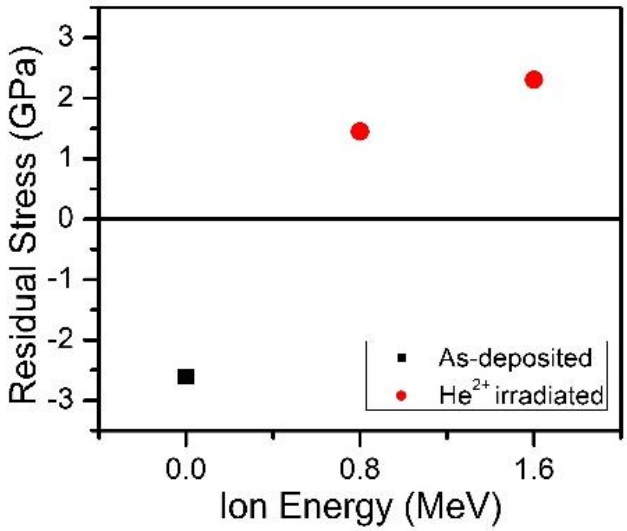

Figure 5-6 Residual stress of all Mo thin films

Where *h, l,* and *k* are lattice phase positions and a is lattice parameter. This equation is only valid for cubic structural systems. The crystal imperfection and distortion produce the lattice strain [8].

Williamson-Hall method has been employed to determine the theeta and strain dependent crystallite size [9]. The general form of Williamson Hall analysis can be written by the following form:

$$\beta \cos\theta = \frac{K\lambda}{D_{WH}} + 4\varepsilon_{WH} \sin\theta \qquad (5\text{-}4)$$

D_{WH} and ε_{WH} are estimated crystallite size and micro strain obtained from Williamson hall method. The Eq. 5-4 is known as Uniform Deformation Model which is very similar to standard linear equation of straight line. To estimate Crystallite size and strain value, βcosθ is plotted against 4sinθ. Slope of straight line obtained from that graph represents strain value, whereas crystallite size is obtained from y-intercept. The values of dislocation density, δ of the samples have been calculated using following relation.

$$\delta = \frac{1}{D^2} \quad (5\text{-}5)$$

Value of Texture co-efficient $TC_{(hlk)}$ has been measured using the following relation.

$$TC_{(hlk)} = \frac{\frac{I_{(hlk)}}{I_{0(hlk)}}}{\frac{1}{n}\sum\frac{I_{(hlk)}}{I_{0(hlk)}}} \quad (5\text{-}6)$$

$I_{(hkl)}$ represents intensity of respective XRD peak, n is the number of reflected orientations in the XRD spectra, and $I_{0(hkl)}$ is the standard intensity of the particular peak taken according to the JCPDS data (PDF#42-1120)

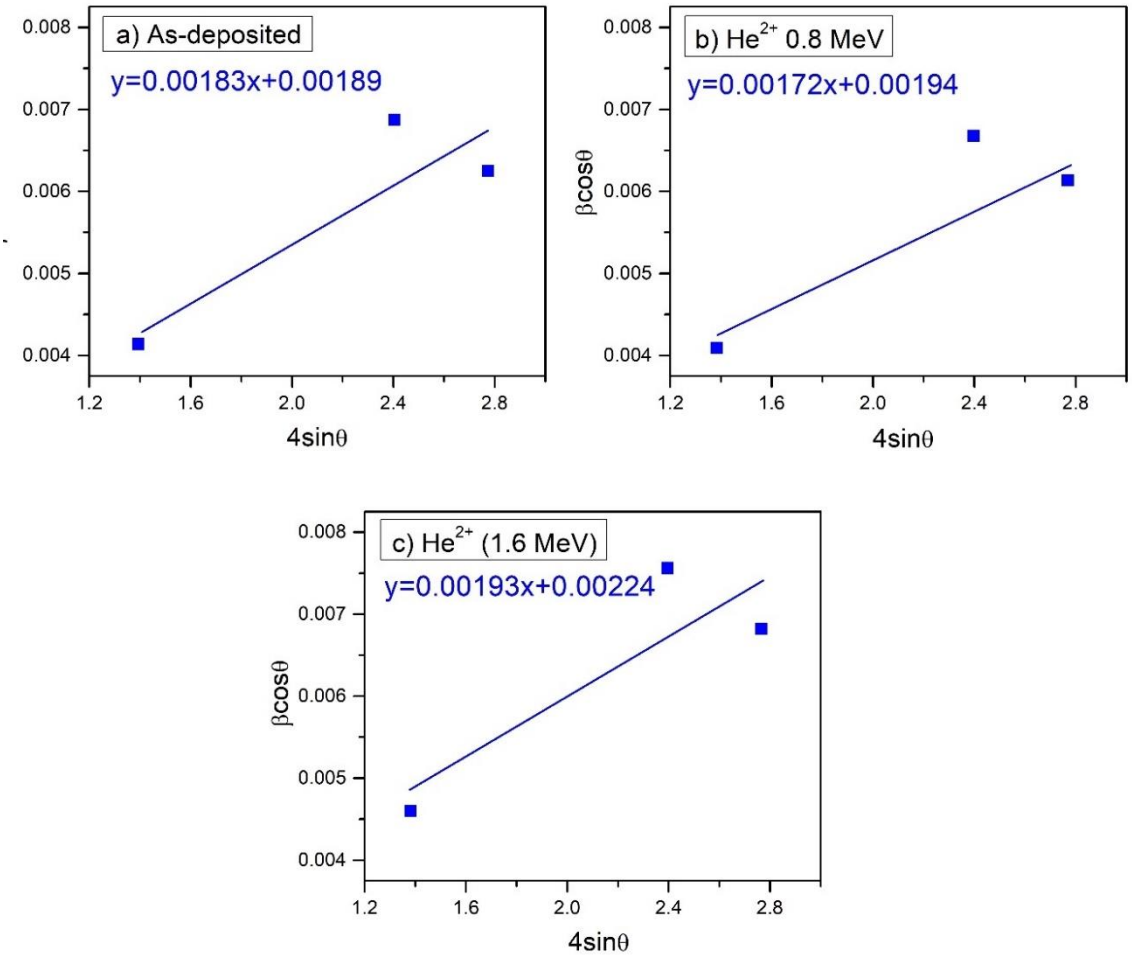

Figure 5-7 Williamson Hall plot of a) As Deposited Mo thin film, b) 0.8 MeV He2+, c) 1.6 MeV He2+

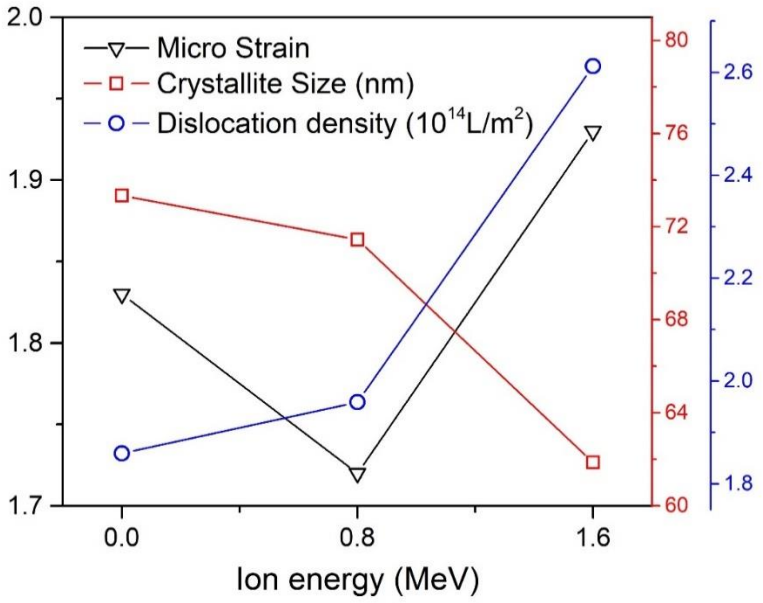

Figure 5-8 Different parameters Micro strain, Crystallite Size and Dislocation Density obtained from Williamson Hall plot

From the estimated values of crystallite size, a deterioration of crystallinity is observed as the crystallite size decreases for irradiated Mo thin films compared with as deposited thin film. The Williamson Hall plot are given in figure 5-7 and the results from Williamson Hall analysis are shown in the figure 5-8. Results shows that crystallite size decreased slightly from 73 nm to 71 nm with low energy irradiation whereas crystallite size decreased significantly to 62 for the sample irradiated with 1.6 MeV helium ion. At higher dose, the process of mutual annihilation of defects occurs by the influence of inelastic collisions and dense electronic excitation results in randomness/disorder in crystallite size and strain of the samples [10]. This decrease in crystallite size can be explained by collision cascade process, when an energetic helium ion interacts with metal by elastic and inelastic collision. In our case inelastic collisions are way too dominant, so inelastic collision takes place between He ion and the electrons of target atoms [11]. The ions lose it energy through ionization and excitation. Other than that, the high energy He ion collides with nuclei of target atom through elastic collision and cause some displacement from its original position. These displaced atoms are known as primary knock on atoms (PKAs) and they

generate vacancies inside the lattice. This happened in very short span of time (10^{-18} s). These atoms either terminate on interstitial sites or collide with neighboring atoms and produce collision cascade. In this way, vacancies and interstitials are produced in irradiated lattice very shortly. In this work, the decrease in crystallite size and increase in strain and dislocation density is due to formation of radiation induced defects in the form of vacancies and interstitials [12].

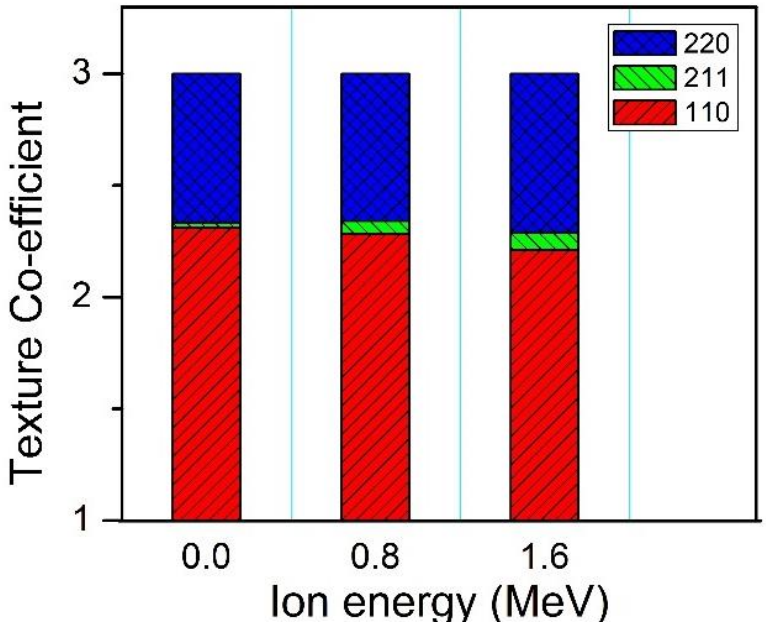

Figure 5-9 Texture coefficient of as-deposited and irradiated samples.

The value of 2.31 was obtained for texture coefficient of characteristic peak of as deposited Mo thin film. The value of 2.28 and 2.20 were obtained for $^{+}$, 0.8 MeV He^{2+} and 1.6 MeV He^{2+} irradiated samples respectively. It can be seen that TC value is greater than 1, which reveals that the grains are preferentially oriented along 110 planes.

5.2.2 Surface morphology

Morphological changes induced by irradiation were evaluated by Scanning electron Microscopy. Fig. 5-10 illustrates comparison of as deposited and irradiated samples. Starting with as deposited sample, relatively smoother surface has been attained and ellipsoid like grains were evident. After irradiation, no delamination has been detected in any sample. However, micro pores and nano fuzz can be observed in the irradiated thin films, but this effect was minor in 0.8 MeV He irradiated Mo thin film and it was dominant

and 1.6 MeV helium ion irradiated thin films [13]. This can be explained by surface sputtering which occurs during the continuous irradiation of He ions at the near-surface, which resulted in micro pores and nano-fuzz [7]. Grain boundaries of He ion irradiated samples appear to decrease after irradiation; it is possible due to amorphization and reduction in grain size.

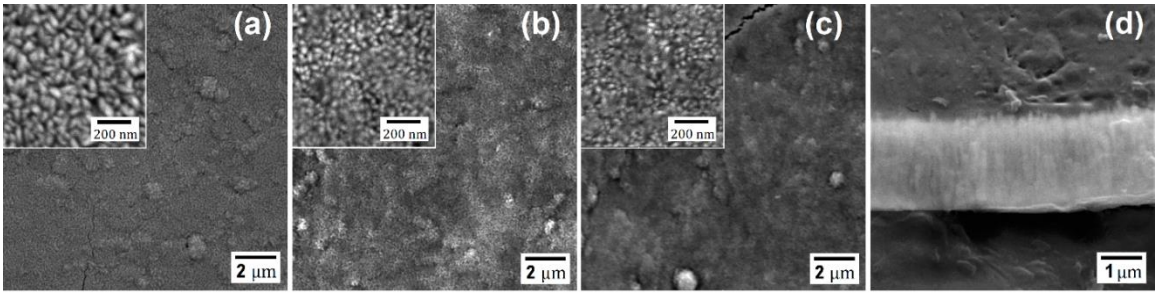

Figure 5-10 SEM Images of a) As-deposited Mo thin film, b)0.8 MeV He2+, c)1.6 MeV He2+

5.2.3 Surface topography

AFM analysis has been done to examine any possible transformation in surface topography of irradiated Mo thin films. Figure 5-11 shows the AFM Images of as deposited and both irradiated samples. It depicts that the as-deposited sample is smoother than all of irradiated samples with least structural features [14]. Root-mean area roughness of irradiated sample was measured. The increase of the surface roughness in the case of the ion irradiated sample is due to the formation of agglomerated structures and micropores on the surface [15].

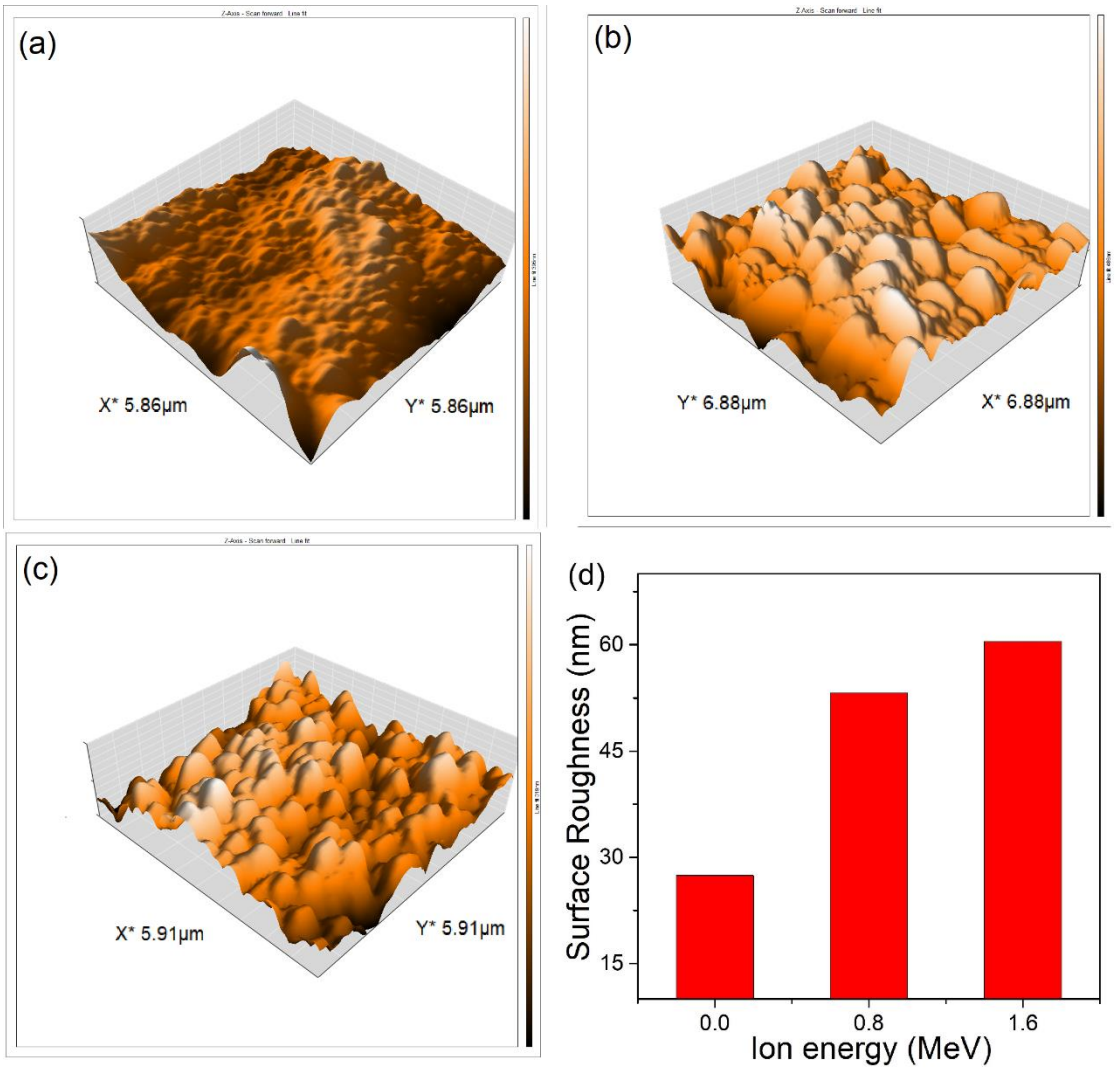

Figure 5-11 Images of a) As-deposited Mo thin film, b)0.8 MeV He2+, c)1.6 MeV He2+ d)Root mean square roughness of as deposited and irradiated samples

5.2.4 Hardness testing

Micro-hardness testing was performed in order to demonstrate irradiation hardening caused by helium ion irradiation on deposited Mo thin film. Since our coating was thin, the hardness measured in this experiment was combined Vickers hardness including substrate effect. Absolute hardness could be calculated as follows:

$$H_f = H_s + (H_c - H_s)/\{\frac{2Ct}{D} - \left(\frac{Ct}{D}\right)^2\} \quad (5\text{-}7)$$

Here H_f is absolute hardness of Mo Thin film, H_s is hardness of bare substrate, whereas H_c is combined hardness of thin film and substrate. D is the depth of scratch which is corresponding to $1/7^{th}$ of impression diagonal d and t represents thickness of thin film which is 2.41 micron. C is the constant which depends on the geometry of the scratch. If thin film harder than substrate then value of C will be $2\sin^2\theta$ (Where $\theta = 11°$). The combined hardness of substrate and thin films on different loads is given in Fig. 8 a. The average hardness values of thin films with error bar against the ion energies are plotted in Fig.8 b. The archived hardness values were 192 HV, 218 HV and 290 HV for as deposited, 0.8 MeV He^{2+} and 1.6MeV He^{2+} irradiated Mo thin films respectively.

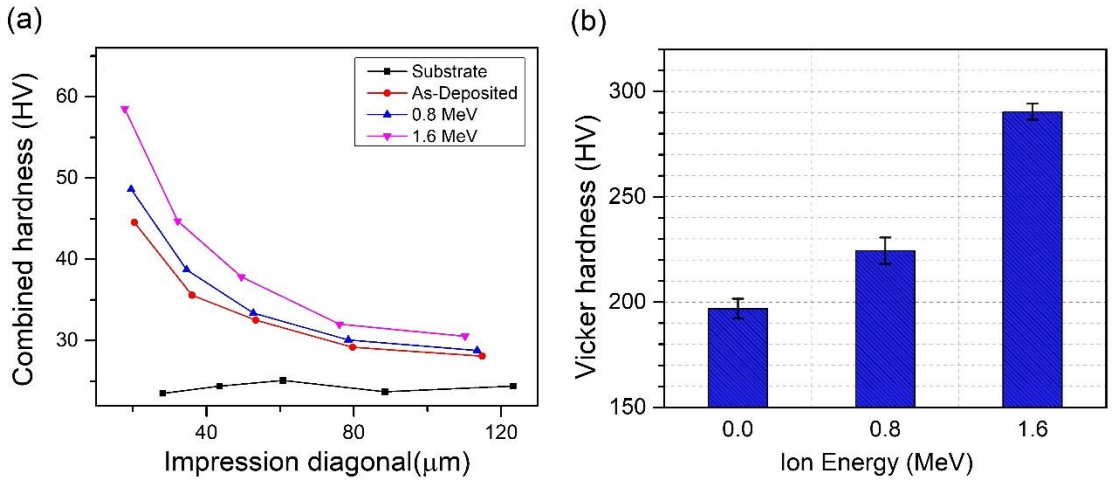

Figure 5-12 a). Combined hardness of substrate and Mo thin films on different loads. b) The average hardness values of thin films with error bar against the ion energies

It is well established that the irradiation hardening behavior of material is associated with the ion energy, fluence and size of irradiation defects which act as obstacles to dislocation glide. In the present study, the irradiation hardening behavior of Mo thin film under helium ion irradiation is analyzed. It is observed that combined hardness of irradiated thin films remained greater than as-deposited thin film on different loads as portrayed in figure 5-12 a. Similarly absolute Vickers hardness showed the same trends [16]. At first, about 17 percent increase in Vickers hardness was observed for the sample irradiated at 0.8 MeV as compare to as-deposited thin film. Since no major change in crystallite size was observed for that sample, so irradiation hardening at this energy can be associated with induced point

defects and dislocation loops. The presence of irradiation induced dislocation loops in Mo thin film increase the critical stress necessary to move the dislocations [8]. However, significant rise in Vickers hardness value was observed for the sample irradiated at 1.6 MeV with equivalent dose of 0.645 DPA. The Vickers hardness increases up to 50 percent. The increased dislocation loops size with increase in irradiation dose strengthens the pinging effect and increases the hardness. This can also be associated with decrease in crystallite size at higher dose as illustrate in figure above.

5.2.5 Electrical characterization:

Hall Effect measurements were carried out in order to demonstrate the effect of irradiation on electrical characteristics of Mo thin film. Increase in resistivity was observed with increase in irradiation dose. Figure 5-13 showed results obtained from Hall effect. The resistivity of 0.23 μΩcm was observed for as-deposited sample which increased to 0.76 μΩcm as a result of 0.8 MeV He irradiation [17]. Highest resistivity of 1.27 μΩcm was found for the specimen treated with α-particles at 1.6 MeV. The reduction in conductivity behavior can be associated with defect annihilation and amorphous nature of thin film as a result of irradiation dose which leads to decrease in crystallite size and increase in number of grain boundaries [2]. The increase in potential barrier heights means charge carriers have to cross more barriers. Hence, conductivity decreased as the irradiation dose increased.

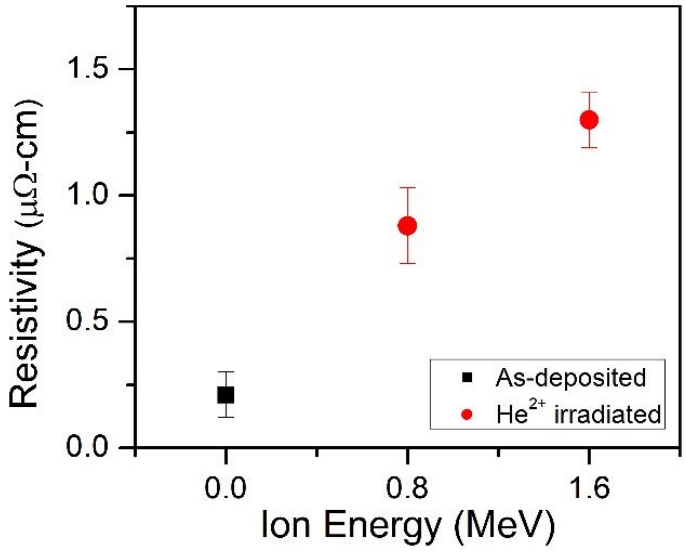

Figure 5-13 Electrical resistivity of as deposited and irradiated Mo thin films.

5.3 RF magnetron sputtered SiC on graphite for anti-corrosive applications

5.3.1 Structural analysis of all films

Structural analysis of pre-annealed and post-annealed thin films were done by using X-Ray Diffraction. All XRD spectrums are shown in figure 5-14 Results show no peak of SiC for pre-annealed sample. All the peaks matched JCPD #41-1487, which indicates presence of graphite 2H. Absence of SiC peak can be associated with amorphous behavior of SiC at relatively low temperature. At high temperature, intensity of graphite peaks increased, but no SiC peak was observed. At 1400 C, some new peaks were evident as XRD spectrum matched with JCPD # 29-1126 indicating Moissanite 2H, one of the crystalline forms of Silicon carbide. Our results matched with literature, as the crystallization of SiC begins after 1350 ºC. X-Ray diffraction study of our thin films showed that crystallanity in SiC coating emerged at high temperature of 1400 ºC.

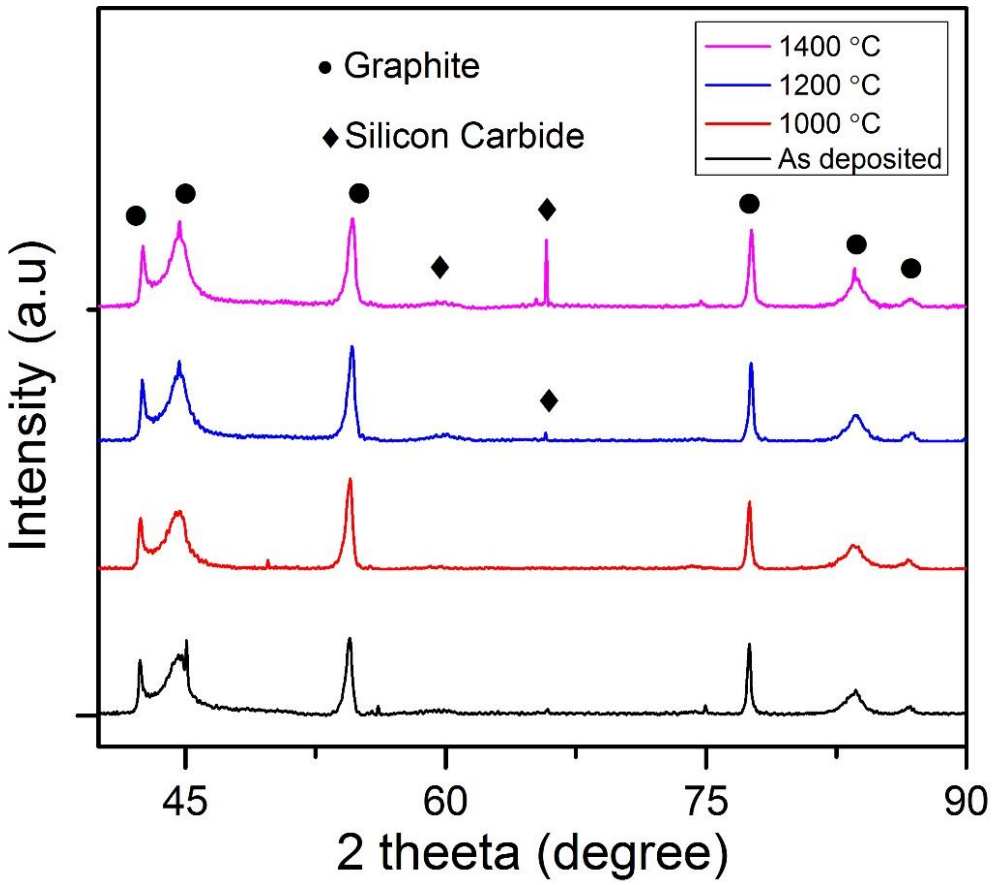

Figure 5-14 XRD of as deposited and Annealed SiC coatings on graphite

5.3.2 Surface morphology of as-deposited film

The surface morphology of SiC coated graphite was studied using scanning electron microscopy. The SEM image of all SiC thin films and EDS of as grown thin film is given in the Fig. 5-16. The micro porous structure was evident in SEM image. Some cracks were also observed. Porosity in the structure could be associated with amorphous nature of SiC coating at low substrate temperature of 300 ºC. Results obtained from EDS confirmed the elemental presence of silicon in as deposited thin film. Few traces of oxygen were also observed [18]. However, excess atomic percent of carbon is observed, which can be associated with graphite substrate. The sample annealed at 1000 ºC showed some micro cracks at the surface. The rougher texture was observed for the sample annealed at 1200 ºC. However, relatively smoother morphology and presence of crystallites was evident at 1400 ºC.

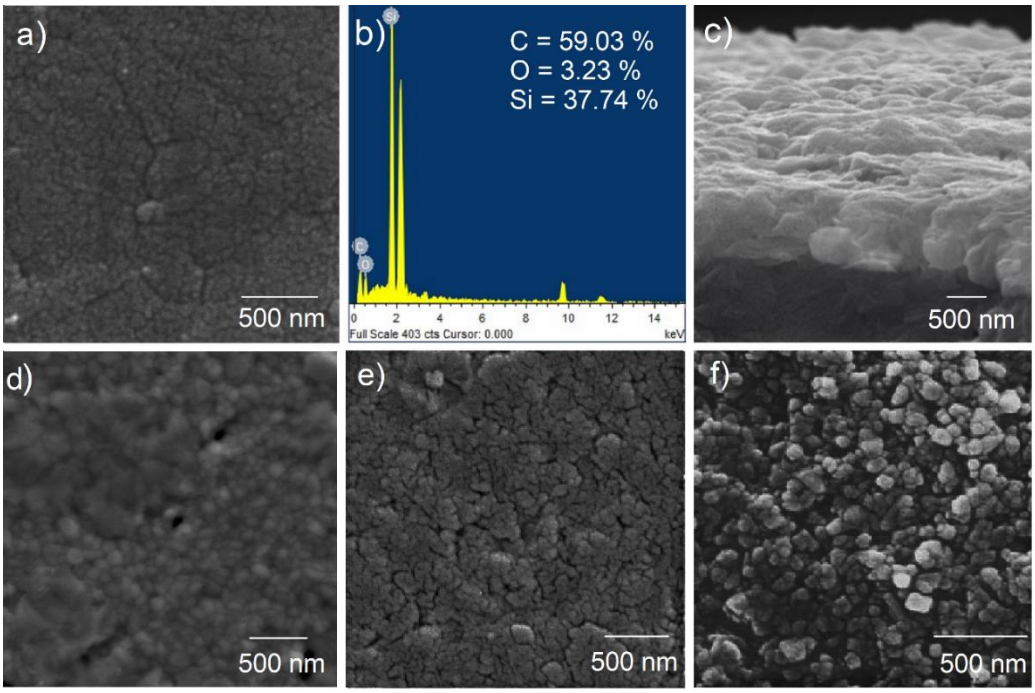

Figure 5-15 SEM image of as deposited and annealed SiC coating on graphite

5.3.3 Electrical characterization

Hall Effect method was employed to determine the electrical characteristics of both pre and post annealed SiC thin films. Electrical resistivity of all SiC samples is given in Fig 5-16. High resistivity of 0.0069 was observed for amorphous and untreated coating. Whereas on annealing of this coating on higher temperature of 1000 and 1200º C results in increase in conductivity of thin films [19]. However, significant decrease in resistivity was evident for the sample annealed at 1400 ºC; this rise in conductivity could be associated with generation of crystallanity in SiC at higher temperatures.

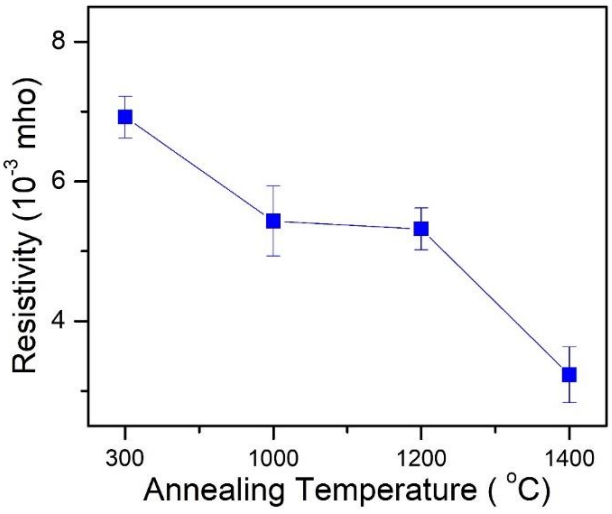

Figure 5-16 Resistivity of as deposited and annealed SiC coatings

5.3.4 Electrochemical testing results

OCPT analysis for 1200 sec was performed for each sample in order to demonstrate the impact of corrosion on annealing temperature. The as deposited SiC coating showed more electronegative behavior on the OCPT plot showed in Fig 5-17. Which showed more corrosive behavior among all SiC coatings. However, significant decrease in electronegative behavior was monitored for the samples annealed at high temperatures. For the sample annealed at 1000 C, initially significant resistant to corrosion was evident, but after some time it started more corrosion. Similar trend was evident for sample annealed at 1200 C. However, sample annealed at 1400 C showed least corrosion and with rise in time the corrosion resistance improved [20].

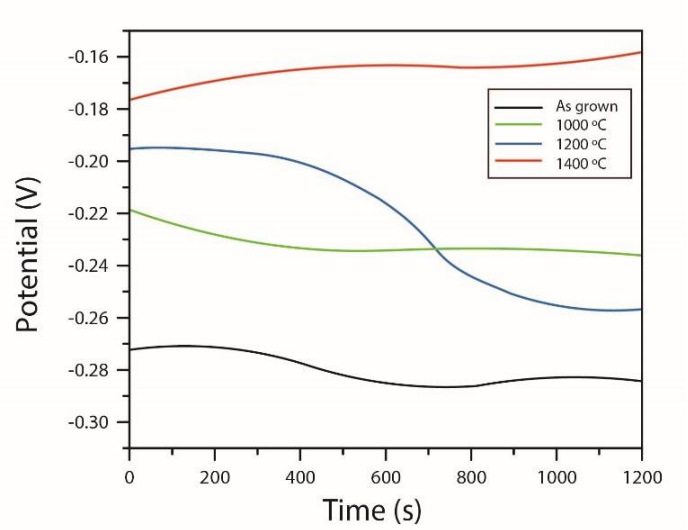

Figure 5-17 OCPT plot of as deposited and annealed SiC Thin films

The electrochemical parameters obtained from fitting experimental Tafel polarization curve are the useful mean to examine the anti-corrosion behavior of coatings. The coating with high ability to sustain corrosion will show less magnitude of current density.

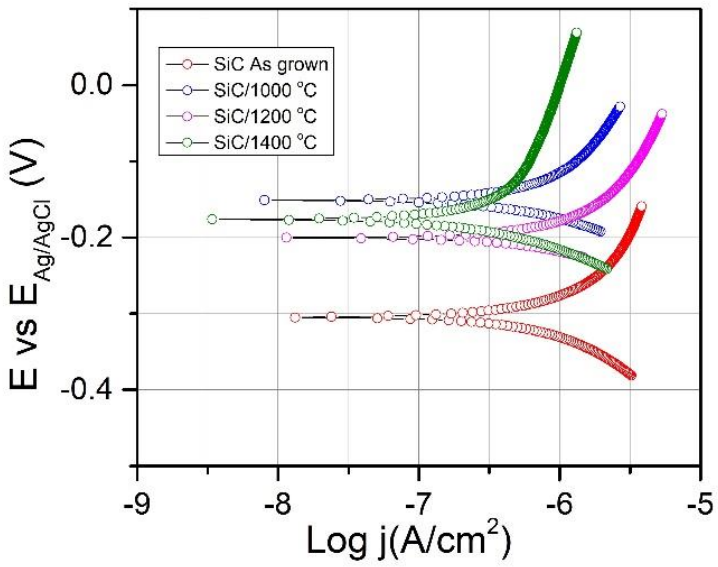

Figure 5-18 Tafel polarization curve of as grown and Annealed SiC samples

To obtain related factors like current density and corrosion potential, Tafel extrapolation was performed. Tafel region was identified by tangent to anodic and cathodic curves. From the Tafel polarization curve showed in Fig 5-18, shift in the corrosion potential was observed for the coatings annealed at high temperatures relative to as-deposited sample and bare graphite sample. An approximately 200 mV shift in E_{corr} between the As- Deposited

and those annealed at high temperature [21]. As compare to graphite. E_{corr} of all thin films are positive. So, we can deduce that the mechanism behind corrosion resistance of these coatings is mainly an anodic process. The decrease in J_{corr} was evident in the presence of SiC thin films after their exposure to NaCl solution for 1 day. The J_{corr} decreased as the annealing temperature increased except for the coating annealed at 1200 ºC where slide decrease in corrosion resistance was observed. This decrease could be associated with phase transformation of SiC at this temperature. The internal stress within thin film enhances the pores inside SiC thin film, whereas for the other cases, the corrosion resistance enhances with rise in temperature due to improvement in gross compactness of thin film [22]. The enhanced particulate compactness limits the permeation of corrosive ions towards graphite substrate. Corrosion rate obtained from Tafel analysis is given in the fig 5-19

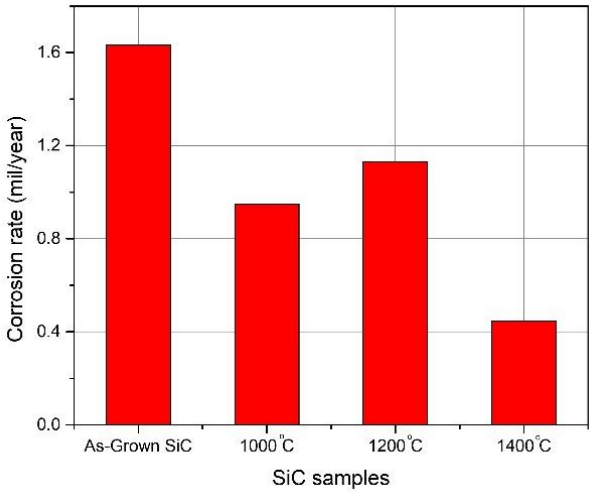

Figure 5-19 Corrosion rate of as grown and annealed SiC coated graphite

Impedance of all SiC coatings was measured using electrochemical impedance spectroscopy. This method almost gave the same trends and complements the results obtained from Tafel plot. Nyquist plot from EIS analysis is given in the Fig 5-20. Other than graphite matrix, Nyquist curve of every SiC thin film is two-time constant semi circles with high frequency capacitive loops [23]. The lower frequency curve represents the diffusion of electrons whereas high frequency curve shows the polarization resistance of thin films. The larger impedance capacitive loop represents the high corrosion resistance ability of thin films [24]. From the figure it has been seen very clearly that the coating annealed at 1400 ºC shows higher impedance as compare to other thin films. And it is complementing our results from Tafel plot.

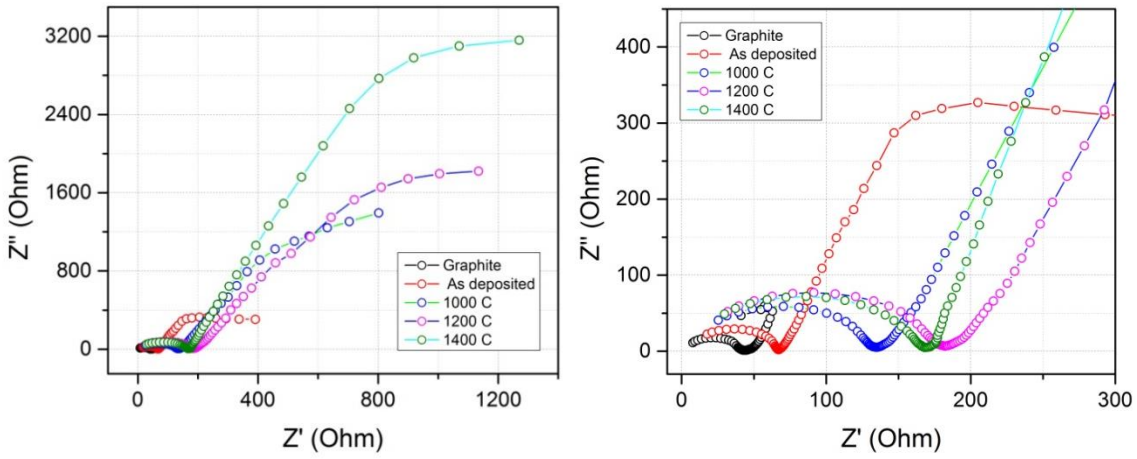

Figure 5-20 Nyquist plot of as deposited and annealed SiC coated graphite

5.4 Summary

Superior quality uniform Mo thin films coated on graphite were achieved by DC Magnetron sputtering. Crystallanity enhanced and crystallite size increases with an increase in sputtering power. More dense structure was obtained with an increase in sputtering power and decrease in gas pressure. However, smoother thin film was attained at low gas pressure. Electrical resistivity decreased with an increase in sputtering power and decrease in gas pressure. We obtained most optimized thin film at high sputtering power and low working gas pressure. Alfa particle irradiation was performed on most optimized thin film at different fluencies and energies. Crystallite size decreased slightly for low dose of irradiation whereas increased significantly for higher dose of irradiation. Compressive thin film turns into tensile thin film. Atomic force microscopy images reveal that surface roughness increased with He ion irradiation whereas micro hardness value increased with increase in irradiation dose. In second part of research, RF Magnetron sputtered SiC thin film showed amorphous behavior. Crystallanity of amorphous thin film was enhanced by annealing at elevated temperatures. The XRD spectrum showed presence of SiC peak for the sample annealed at 1400 ºC. Impact of high temperature annealing on corrosion resistance of SiC coatings was demonstrated. OCPT graph showed that sample annealed at 1400 ºC is less electronegative and its corrosion resistance enhanced with increase in time. However, by Tafel polarization curve, positive shift in the

corrosion potential was observed for the coatings annealed at high temperatures relative to as-deposited sample and bare graphite sample. Highest corrosion rate was observed for as deposited SiC film. Whereas lowest corrosion rate was observed for sample annealed at 1400 ºC. Electrochemical Impedance Spectroscopy also validates the results from Tafel and OCPT.

References

[1] A. Sreedhar, M. H. P. Reddy, S. Uthanna, and J. F. Pierson, "Sputter Power Influenced Structural , Electrical , and Optical Behaviour of Nanocrystalline CuNiO 2 Films Formed by RF Magnetron Sputtering," *Condens. Matter Phys.*, vol. 2013, 2013.

[2] N. Ahmed, M. A. Iqbal, Z. S. Khan, and A. A. Qayyum, "DC Magnetron-Sputtered Mo Thin Films with High Adhesion, Conductivity and Reflectance," *J. Electron. Mater.*, 2020, doi: 10.1007/s11664-020-08138-2.

[3] D. Rafaja *et al.*, "Effect of the deposition process and substrate temperature on the microstructure defects and electrical conductivity of molybdenum thin fi lms," *Thin Solid Films*, vol. 528, pp. 42–48, 2013, doi: 10.1016/j.tsf.2012.06.087.

[4] C. A. O. Hong, Z. Chuanjun, and C. H. U. Junhao, "The effect of working gas pressure and deposition power on the properties of molybdenum films deposited by DC magnetron sputtering," *Sci. China Technol. Sci.*, vol. 57, no. 5, pp. 947–952, 2014, doi: 10.1007/s11431-014-5537-x.

[5] D. M. Mattox and D. M. Mattox, "Particle bombardment effects on thin-film deposition : A review Particle bombardment effects on thin .. film deposition : A review," *J. Vac. Sci. Technol. A*, vol. 1105, no. 1989, 2018, doi: 10.1116/1.576238.

[6] W. Li, X. Yan, A. G. Aberle, and S. Venkataraj, "Analysis of microstructure and surface morphology of sputter deposited molybdenum back contacts for CIGS solar cells," *Procedia Eng.*, vol. 139, pp. 1–6, 2016, doi: 10.1016/j.proeng.2015.09.231.

[7] N. Yoshida, H. Iwakiri, K. Tokunaga, and T. Baba, "Impact of low energy helium irradiation on plasma facing metals," vol. 339, pp. 946–950, 2005, doi: 10.1016/j.jnucmat.2004.10.162.

[8] N. Li, M. Nastasi, and A. Misra, "Defect structures and hardening mechanisms in high dose helium ion implanted Cu and Cu / Nb multilayer thin films," vol. 33, pp. 1–16, 2012, doi: 10.1016/j.ijplas.2011.12.007.

[9] A. Abinaya and B. G. Jeyaprakash, "Materials Science in Semiconductor Processing Structural , surface and mechanical characterization of spray-deposited molybdenum disulfide thin films," *Mater. Sci. Semicond. Process.*, vol. 31, pp. 582–587, 2015, doi: 10.1016/j.mssp.2014.12.045.

[10] S. Das, W. Liu, R. Xu, and F. Hofmann, "Helium-implantation-induced lattice

strains and defects in tungsten probed by X-ray micro-diffraction," *Mater. Des.*, vol. 160, pp. 1226–1237, 2018, doi: 10.1016/j.matdes.2018.11.001.

[11] P. He *et al.*, "Compatibility between high- fl ux helium plasma irradiated molybdenum and liquid lithium," *J. Nucl. Mater.*, vol. 509, pp. 736–741, 2018, doi: 10.1016/j.jnucmat.2018.04.038.

[12] A. Khan, M. Rafique, N. Afzal, Z. Khaliq, and R. Ahmad, "Structural characterization of Zircaloy-4 subjected to helium ions irradiation of variable fluence," *Nucl. Mater. Energy*, vol. 20, no. March, p. 100690, 2019, doi: 10.1016/j.nme.2019.100690.

[13] M. Xu, L. Luo, Y. Zhou, X. Zan, Y. Xu, and Q. Xu, "Helium irradiation behavior of tungsten-niobium alloys under di ff erent ion energies," *Fusion Eng. Des.*, vol. 132, no. April, pp. 7–12, 2018, doi: 10.1016/j.fusengdes.2018.05.015.

[14] S. Huang *et al.*, "Effect of crystal orientation on hardness of He + ion irradiated tungsten," *Nucl. Inst. Methods Phys. Res. B*, vol. 406, pp. 585–590, 2017, doi: 10.1016/j.nimb.2017.04.063.

[15] M. Amirhamzeh, "Damage studies on irradiated tungsten by helium ions in a plasma focus device," no. xxxx, 2019, doi: 10.1016/j.net.2019.10.003.

[16] M. Zhao *et al.*, "Fluence dependence of helium ion irradiation effects on the microstructure and mechanical properties of tungsten," *Nucl. Instruments Methods Phys. Res. Sect. B Beam Interact. with Mater. Atoms*, vol. 414, pp. 121–125, 2018, doi: 10.1016/j.nimb.2017.09.002.

[17] M. Chen, J. P. Best, I. Shorubalko, J. Michler, R. Spolenak, and J. M. Wheeler, "Influence of helium ion irradiation on the structure and strength of diamond," *Carbon N. Y.*, no. xxxx, 2019, doi: 10.1016/j.carbon.2019.10.078.

[18] N. Afzal *et al.*, "influence of carbon ion implantation energy on aluminum carbide precipitation and electrochemical corrosion resistance of aluminum," *Nucl. Inst. Methods Phys. Res. B*, vol. 436, no. September, pp. 84–91, 2018, doi: 10.1016/j.nimb.2018.09.008.

[19] T. Tavsanoglu, E. O. Zayim, O. Agirseven, S. Yildirim, and O. Yucel, "Optical , electrical and microstructural properties of SiC thin fi lms deposited by reactive dc magnetron sputtering," *Thin Solid Films*, vol. 674, no. December 2018, pp. 1–6, 2019, doi: 10.1016/j.tsf.2019.01.047.

[20] R. T. Loto and P. Babalola, "Corrosion polarization behavior and microstructural analysis of AA1070 aluminium silicon carbide matrix composites in acid chloride concentrations Corrosion polarization behavior and microstructural analysis of AA1070 aluminium silicon carbide matrix composites in acid chloride concentrations," *Cogent Eng.*, vol. 10, no. 1, 2018, doi: 10.1080/23311916.2017.1422229.

[21] J. Ding, H. Zhao, Y. Zheng, X. Zhao, and H. Yu, "A long-term anticorrsive coating through graphene passivation," *Carbon N. Y.*, vol. 138, pp. 197–206, 2018, doi:

10.1016/j.carbon.2018.06.018.

[22] C. Chen, C. Lu, X. Feng, and Y. Shen, “Effects of annealing on Al – Si coating synthesised by mechanical alloying,” *Surf. Eng.*, vol. 0, no. 0, pp. 1–11, 2017, doi: 10.1080/02670844.2017.1292706.

[23] S. Ammar *et al.*, “Studies on SiO 2 -hybrid polymeric nanocomposite coatings with superior corrosion protection and hydrophobicity,” *Surf. Coat. Technol.*, vol. 324, pp. 536–545, 2017, doi: 10.1016/j.surfcoat.2017.06.014.

[24] Y. Gao, L. Zhao, X. Yao, R. Hang, X. Zhang, and B. Tang, “Corrosion behavior of porous ZrO 2 ceramic coating on AZ31B magnesium alloy,” *Surf. Coat. Technol.*, vol. 349, no. April, pp. 434–441, 2018, doi: 10.1016/j.surfcoat.2018.06.018.

Conclusions

1. Superior quality Mo coated graphite thin films were achieved as a result of DC magnetron sputtering at different sputtering powers and gas pressures.
2. Optimized thin film with lowest resistivity, high crystallite size and low roughness was obtained at high sputtering power of 300 W and low gas pressure of 7 mTorr.
3. Alfa particle irradiation was performed on most optimized thin film at different doses of 0.076 and 0.645 DPA with equivalent energies of 0.8 and 1.6 MeV respectively.
4. Crystallite size decreased slightly for low dose of irradiation whereas it decreased significantly for higher dose of irradiation.
5. Surface roughness increased for both irradiation doses whereas electrical conductivity decreased significantly with an increase in irradiation dose.
6. RF Magnetron sputtered amorphous SiC thin film was also deposited on graphite substrate. High temperature annealing results in enhancement of crystallanity as the XRD spectrum showed presence of SiC peak for the sample annealed at 1400 ºC.
7. SiC thin films annealed at high temperatures showed good adhesion with substrate
8. Tafel analysis was performed, corrosion rate decreased up to 75% for thin film annealed at 1400 ºC as compared to as grown SiC thin film. Electrochemical Impedance Spectroscopy (EIS) and OCPT also validated the results obtained from Tafel analysis
9. It is concluded that by optimizing deposition parameters, Mo coated graphite configuration can be applicable for PFCs and high temperature annealed SiC thin film can be used as protective coating for graphite in Gen IV reactors.

Appendix A: Research Article 1

DC magnetron sputtered Mo thin films with high adhesion, conductivity and reflectance

Nisar Ahmed[1], Muhammad Azhar Iqbal[1], Zuhair S. Khan[1,2] and Ahmed Abdul Qayyum[1]

1.-U.S.-Pakistan Center for Advanced Studies in Energy, National University of Sciences and Technology, Islamabad 44000, Pakistan, 2.-e-mail: zskhan@ces.nust.edu.pk

Abstract: The main challenge in the deposition of Molybdenum thin films for high efficiency in Copper indium gallium selenide (CIGS) modules lies in gaining adherent coating without compromising conductivity and reflectance characteristics. In this study, Mo thin films were deposited on soda-lime glass by DC magnetron sputtering at different deposition powers (55, 100, 200 and 300 watts) and with high working gas pressure (2 and 4 Pa). Analytical techniques such as X-ray diffraction (XRD), scanning electron microscopy (SEM) and Hall-effect were employed to analyze structure, morphology and electrical resistivity of the deposited films. Ultraviolet-Visible (UV-Vis) spectrometry was performed to find the reflectance and cross-hatch adhesion tape test was employed to know the adhesion behavior of deposited films. With higher sputtering power and reduced gas pressure, an increase in the crystallite size of the deposited films was observed. Films deposited at higher gas pressure were found with tensile stresses and higher adhesion with the substrate. Van der Pauw's method reveals an increase in conductivity at high power and low gas pressure. Improved reflectance was achieved at moderate sputtering power and low gas pressure.

Key words: Molybdenum, DC Magnetron Sputtering, CIGS, Back Contact, Thin films

Introduction

Molybdenum coatings have a wide range of applications in the electronic industry. It is used as the gate electrode in GaAs-based metal gate field-effect transistors (MESFETs), silicon-based metal–oxide semiconductor (MOS) devices and different photovoltaic cells. Molybdenum is well known because of its inert chemical behavior, good adhesive property, low roughness and contact resistance [1]. These characteristics allow Molybdenum coating to be used as a back-contact layer for copper indium gallium selenide (CIGS) and cadmium zinc telluride (CZT) based solar cells, which have a massive photo-conversion efficiency of more than 20% [2]. Owing to this high conversion efficiency [3], these solar cells can be considered as an aspiring contender to be commercialized [4].

CIGS based solar cells have a layered structure starting from Mo back contact to $CuInGaSe_2$ layer, followed by CdS and ZnO layers (Fig. 1) [5]. For this solar cell to deliver high photo-conversion efficiency, the performance of every layer including back contact matters as the entire device is fabricated on a back contact, which acts as a base to the cell. During the formation of the absorber layer of CIGS, Mo coating undergoes harsh heat treatment, which alters the residual stress and other morphological characteristics of the thin film thus, leading to poor adhesion of CIGS module with the back contact. Furthermore, molybdenum also forms a resistance layer of $MoSe_2$ between the interface of the CIGS layer and Mo thin film at high substrate temperature [6]. This could be avoided by using lower substrate temperature; however, this strategy decreases the conductivity and adhesion of Mo back contact Like Adhesion and resistivity, reflectance is another major characteristic which plays a vital role in determining the efficiency of CIGS solar cell. The literature demonstrates that reflectance improves as the gas pressure is diminished. But in that case, adhesion is undermined which has equivalent significance [7]. So, optimizing process parameters to achieve high reflectance, good adhesion, and low resistivity is crucial.

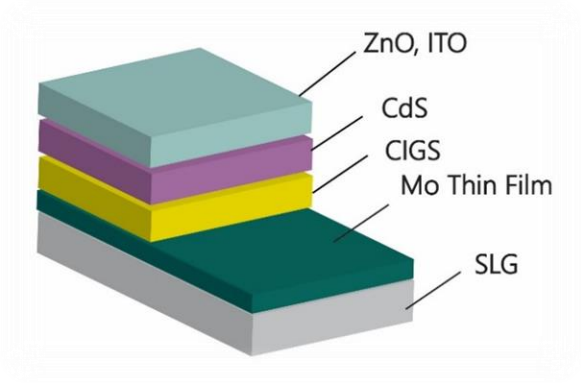

Fig. 1. Schematic of CIGS solar cell showing different layers

Different physical vapor deposition methods can be employed to deposit Mo thin films on SLG including e-beam evaporation, DC and RF magnetron sputtering. Deposition through e-beam evaporation results in a highly crystalline thin film [8]. The film deposited by RF magnetron sputtering usually shows smoother morphology and high reflectance as compared to other techniques [9]. DC magnetron sputtered thin films are more conductive than RF Sputtered thin and also it is a commercially viable technique because of greater deposition rate. A great deal of research work has been done to optimize conductivity, adhesion, and reflectance of Mo back contacts. Generally, different deposition parameters like sputtering power, gas pressure, deposition time, and substrate temperature are varied to achieve optimized thin film. Starting with substrate temperature, crystallinity enhances with an increase in substrate temperature along with grain size which ends up in the reduction of resistivity. Increasing the rotation speed of the substrate enhances the columnar growth of grains. Deposition time effects directly on the thickness of the film, and the surface roughness [10]. As thickness increases, the more compressive film is attained. But this influence can be neglected for the higher thicknesses. Increase in thickness also leads to a decrease in the resistivity [1].

Sputtering power has an immense effect on molybdenum thin film due to its physical characteristics such as nucleation and surface morphology [11]. When sputtering power is increased, working gas atoms get energized and in turn delivers appropriate kinetic energy to adatoms. Then these adatoms because of their increased kinetic energy diffuses more into the surface of thin films thus, enhancing nucleation and growth mechanism [3]. Furthermore, the increase in power increases uniformity in grain size distribution [11]. It

has been reported that sputtering power also affects surface morphology. At low power, rice-like grain structure with microporous morphology is attained however, lower energy atoms produce porous microstructures which lead to higher roughness. At moderate power range, the grain looks triangular-shaped and a relatively smoother surface is obtained and at high sputtering power [12], the grain size becomes elongated in shape thus, decreasing the surface roughness again. The smoothening of surface at intermediate power range can be attributed to the densification of molybdenum thin film [13]. Cross-section analysis reveals that columnar grains have more of an open type structure but tightly packed structure is obtained at high power hence, it decreases porosity. Moreover, It has already been observed that crystallinity increases with an increase in sputter power because adatoms with high kinetic energy can impart higher momentum during the deposition process, packing up voids and vacancies, which increases crystallite size [14]. This increase in crystallite size leads to the formation of larger grain [15], which decreases the number of grain boundaries that are present in the structure and hence, decreases resistivity [16].

Working gas pressure also has a vital influence on different characteristics of Mo thin films. At low gas pressure, a thin film with a smooth surface is attained whereas, porous morphology with a loose microstructure is evident at increased gas pressure [13]. Moreover, the growth rate of a thin film increases by increasing gas pressure up to certain values. This can be ascribed to either increase in the number of gas atoms or to the kinetic energy of target particles. increasing gas pressure enhances the sputter yield of particles due to increase in volumetric density of plasma, which increases growth rate to a certain point and then decreases. This decrease in growth rate happened due to the increased number of gas molecules at high pressure colliding with Mo sputtered atoms and reducing its mean free path. But logically, both effects prevented major changes in the growth rate. So, gas pressure has a minor effect on the surface morphology and growth rate as compared to sputtering power [13]. When it comes to resistivity, this reduced mean free path of Mo sputtered atoms at high pressure increases the resistivity of thin-film because they get deposited with a low K.E, which increases the number of grain boundaries that are present in it [17]. Furthermore, residual stress that generate in Mo thin film increases with an increase in gas pressure and becomes more tensile and this is mostly preferred due to its ability to provide high adhesion strength [14].

Residual stress plays a significant role in the mechanical performance of Mo thin films [18] and sometimes it is deliberately induced in a thin film to enhance its adhesive property of [19]. So, it is vital to inspect and control the degree of residual stress being induced in thin films. Generally, the optimum range of residual stress for CIGS back contact is between stress-free and slightly tensile. Desired residual stress can be achieved by changing different process parameters like sputtering power, substrate temperature and most importantly working gas pressure [18]. This study is focused on the optimization of Mo thin film prepared by DC Magneton Sputtering. Since gas pressure is one of the essential factors in fabricating adhesive thin film for the back contact, we analyzed the impact of different sputter powers at high working gas pressure (2 Pa, 4 Pa) on resistivity, adhesion and reflectance characteristics of the films.

Materials and Method.

Molybdenum thin films were deposited on SLG by DC Magnetron Sputtering. NANOVAK NVTS 400 was used for this purpose. First of all, substrates were cleaned with acetone and then sonicated in ethanol solution. Molybdenum target of a two-inch diameter with 99.999% purity was used. After sample placement, high vacuum was built up to 5×10^{-7} torr by Turbomolecular pump. The substrate temperature was increased up to 300°C and, substrate rotation speed was kept at 10 RPM. These parameters were controlled by automatic control of the NVTS-400, NANOVAK. The system employs a K-type thermocouple coupled with a heater to control heat the substrate. Moreover, the total eight experiments were performed with four different sputtering powers 55W, 100W, 200W and 300W at two different working pressures i.e. 2 Pa and 4 Pa. Detailed experimental scheme is shown in Table. I. The film thickness of 1 micrometer was achieved in every deposition. After deposition, Cross-section was prepared by embedding samples in epoxy mold followed by grinding on grinding papers of different grit sizes and polishing on 3 µm polishing cloth.

TESAN VEGA3 scanning electron microscope was used to observe the surface morphology of Mo thin film. Bruker D8 advanced X-rays diffractometer with CuKα as a radiation source was employed to determine the structural properties of thin film. Films resistivity was measured by Ecopia HMS-3000 hall effect instrument. using the Van der Pauw technique.

The reflectivity behavior was monitored with Ultraviolet-visible spectrophotometer. The crosshatch tape test (hatch cutter) was used to estimate the adhesion characteristic of the deposited Molybdenum films on the SLG. This method is chosen because it is very useful for quick analysis between low adhesion and strong adherent thin films. Different cuts were produced on coated samples by using a blade. 2mm of distance between every successive cut was maintained. Scotch tape was applied for 60 seconds for every coating. A comparison was made of qualitative base between the Molybdenum thin films and a reference classification chart from 0 to 5 [1]. These qualitative results were then compared with residual stress obtained from XRD results.

Table I. Experimental scheme for different thin films deposition

Sample ID	Substrate Temp. °C	Gas Pressure (Pa)	Sputtering Power (Watts)
a	300	2	55
b			100
c			200
d			300
e		4	55
f			100
g			200
h			300

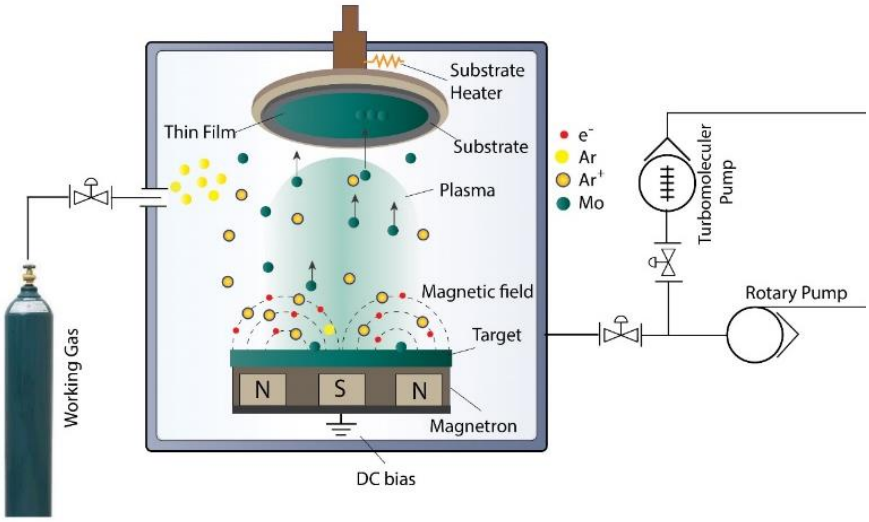

Fig.2. Schematic of Mo deposition through DC Magnetron Sputtering

Results & Discussions

Structural and Morphological Analysis

Impact of sputtering power:

XRD results show that molybdenum thin film maintained a single-phase cubic structure. Mo (1 1 0) preferred orientation has been identified in all spectrums. Fig. 1 illustrates the XRD patterns of deposited Molybdenum thin film at different process parameters. The intensity of Mo peaks is measured as a quantitative degree of crystallinity. Values of different parameters like full-width half maxima (FWHM) and lattice spacing are given in Supplementary Table A. Trends show wider peaks at low deposition powers, while thin and high-intensity peaks were observed for high powers which indicates an increase in crystallinity. The intensity of peak increases with the increase in DC sputtering power, indicating relatively better crystallization along the corresponding direction at higher power. Theoretically, the high kinetic energy of molybdenum atoms at higher sputtering power impart higher momentum during the deposition, It fills up vacancies and micropores, resulting in Mo thin film with a higher degree of crystallinity and larger grain size. At low sputtering power, a decline in crystallinity may be observed for the sputtered particles don't have that much energy adequate for particle movement to preferred low energy sites. Other than the presence of small crystallite size (indicated by the broad peak), non-uniform micro-

strain with respect to Mo thin film depth might also have contributed to the broadening of the XRD peak [11]. The grain size was determined by the Scherrer equation [20].

$$L = \frac{K\lambda}{B\cos\theta} \qquad (1)$$

where K is Scherrer constant is also known as shape factor and its value for spherical particles is 0.94 [17], L indicates the size of the crystal, λ represents the wavelength of the X-ray source (which is 1.5403 Å for CuK_{α}) and B is as full-width half maxima (FWHM) of diffraction peak at angle 2θ. It is found that crystallite size increases by increasing sputtering power except for thin film prepared at 200 W. Trends of change in crystallite size are shown in Fig. 4. The increase in crystallite size with an increase of deposition power shows that the higher surface mobility originated by high adatom energy, which reinforced the crystallinity behavior in Mo films [21]. In the case of low sputtering power, the time between successive adatom deposition is more as compare to high sputtering power. The probability to terminate formation of complete crystal is high so, early termination leads to low crystallite size. Whereas in other scenarios, the limited time between successive adatom deposition is low. Thus, larger island formation at the early stages results in a larger crystallite size later [22]. Thin-film deposited at 200 W and 2 Pa gave us different behavior. This can also be explained by the reduction of the mean free path. Although power was increased from 100 W to 200 W, but it increases the collisions with working gas atoms and it limits the coalescence process. Consequently, a smaller grain size is obtained as compared to 100 W [14].

Residual stress was also calculated by the following relation

$$Residual\ Stress = \sigma = \frac{E\Delta d}{2\nu d_o} \qquad (2)$$

where "d_o" is the standard lattice spacing for Mo and Δd is the difference between standard lattice spacing and actual lattice spacing. Actual lattice spacing was calculated by the following relation.

$$d = \frac{a}{\sqrt{h^2+l^2+k^2}} \qquad (3)$$

Where *h, l,* and *k* are lattice phase positions and a is lattice parameter. This equation is only valid for cubic structural systems. Residual stress initiates from the deposition process they do not depend upon the difference between the coefficient of thermal expansion of target and substrate material [7]. Moreover, compressive stress was detected for low power depositions while tensile stress for high power deposition. Residual stress for different deposition powers and gas pressure are illustrated in Fig. 4.

Results from scanning electron microscopy show formation of ellipsoid like structure at 100W and 200W and dense close-packed structure at 300 W for 4 Pa working gas pressure. For the samples prepared at 2 Pa, the formation of a star-like structure for low powers and dense pack structure for higher powers was observed. SEM images of Molybdenum thin films are shown in Fig. 5. Whereas cross-sectional SEM images of deposited Mo thin films are given in supplementary figure A. The formation of porous microstructure at low power and dense pack structure at relatively higher powers is evident in literature [23]. At low sputtering power, the deposition rate was low, so a small number of atoms reached the substrate and hence, the porous structure is formed. On the other hand, the deposition rate was higher at elevated powers. Therefore, the arrival of sputtered atoms was increased that results in a dense pack structure [24].

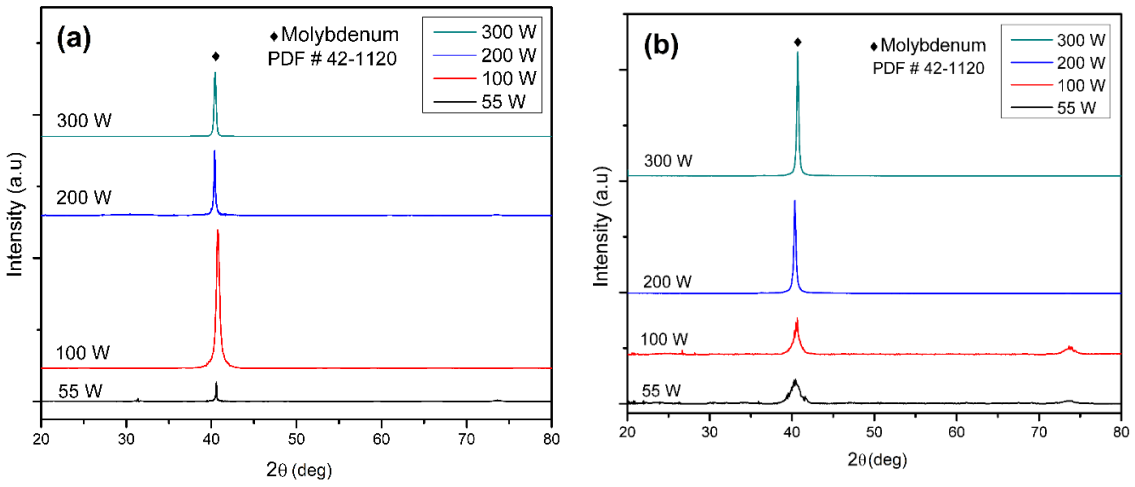

Fig.3(a) XRD results at different powers at 2 Pa, (b) XRD results at different powers at 4 Pa

Impact of gas pressure:

Decrease in crystallite size was observed with increase in working gas as shown in Fig 4. At high gas pressure, regular collisions and low mean free path lower ions energy which leads to low adatom mobility, this lower mobility offers kinetically limited coalescence process. Thus, it leads to smaller sized islands at initial stages, therefore, smaller crystallite size later. Whereas in a moderate range of gas pressure, adatoms gain more energy due to the least collisions and they can move more energetically, as a result, the large crystallite size was formed [3].

Mo coatings deposited at high gas pressure of 4 Pa showed more tensile behavior. The shift of compressive stress towards tensile stress as gas pressure increases can be described by the atomic-peening model [4]. At low gas pressure, due to the low quantity of argon gas, the Mo atoms undergo the least collisions with Ar atoms. The high energy Mo atoms were deposited on substrate with tightly packed arrangement. Eventually, the compressive thin film was attained at low gas pressure as shown in Fig. 8 a. However, in the case of high gas pressure, owing to the high amount of Ar in the chamber, there were more collisions among the sputtered particles and the working gas. Hence, Mo atoms lost most of their energy and low energy deposition resulted in loosely packed arrangement, ultimately, we got tensile stress at high gas pressure as shown in figure 8 b. Although dense pack structure is desirable because it gives good electrical properties but films with tensile stress are not only flexible but also gives good adhesion properties with soda-lime glass. As well as such films show resistance against salinization at high temperatures [25].

At low gas pressure, smoother surface is attained. On increasing the gas pressure, porous morphology with loose microstructure with smaller grain size is evident [26]. This can be explained by the number of gas molecules and the kinetic energy of target particles. When gas pressure increases, it also increases the number of molecules and volumetric density of the plasma. It leads to enhancement in the sputtered yield of particles at a particular time. Thus, initially increase in growth rate was observed along with larger grain size. It increased up to one point. After that growth rate decreased. This happened due to the fact that increase in gas molecules increases the probability of collision of sputtered atoms with gas molecules, hence reduction in the mean free path leads to more scattering of sputtered atoms. With lower adatom bombardment energy and lower growth rate, we got a lower

grain size. But logically, both contrary effects prevented major changes in the growth rate. So, gas pressure has a minor effect on surface morphology and growth rate as compared to sputtering power [27].

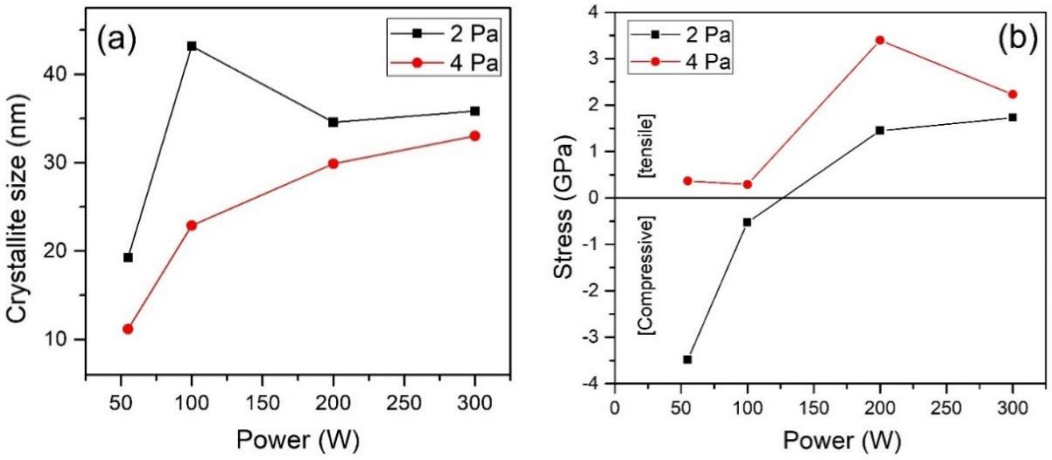

Fig.4. a) Gas pressure and deposition dependence on crystallite size, 4 b) Residual stress for different deposition powers and gas pressure

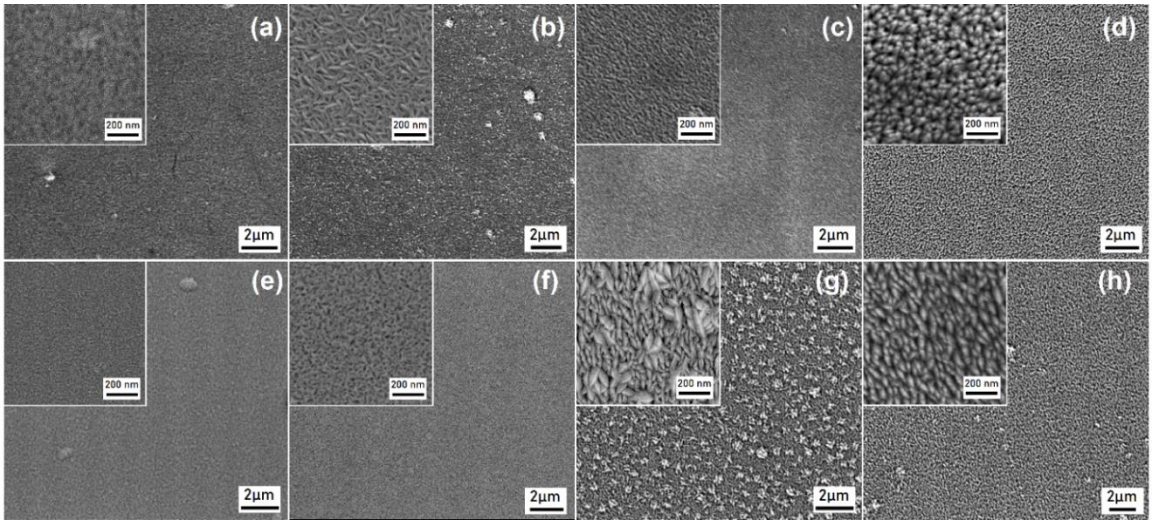

Fig. 5. SEM images of Mo thin films deposited at 2 Pa and 4 Pa at deposition power of (a & e)55W; (b & f)100W; (c & g) 200W; (d & h)300W.

Electrical characterization

The Van der Pauw method was used to measure electrical characteristics. Both current and thickness were kept constant while measuring resistivity in order to have symmetric results. The impact of different deposition powers and working gas pressure on the electrical

resistivity were considered in an effort to find the deposition parameters that can be utilized to obtain high conductive Mo thin films.

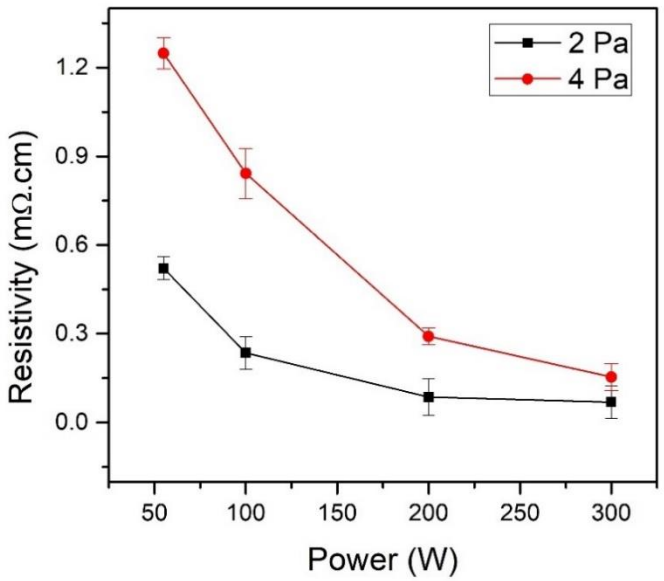

Fig.6. Gas pressure and deposition dependence on resistivity

A decrease in resistivity was observed with an increase in power while the increase in resistivity was evident with an increase in gas pressure. Reduction in resistivity is due to the formation of the dense microstructure at high deposition power which improves the rapid growth of fairly thick film [21]. The resistivity of Mo thin film on different deposition parameters is shown in Fig. 6. The highest resistivity of 1.25 mΩ.cm was observed for 55 W and 4 Pa pressure, which follows a decreasing trend with increasing power. Talking about the effects of increased gas pressure, the lowest resistivity of 0.069 mΩ.cm was obtained on 2 Pa and 300 W which increased by increasing the gas pressure to 4 Pa for the same power. The same trends were achieved for other samples, so it can be stated that resistivity increases with an increase in gas pressure. This trend can also be accompanied by grain size [24]. With the rise of sputtering power and a decrease in gas pressure increase in grain size was observed and a denser structure obtained. This not only increases carrier concentration but also reduces the grain boundaries. The rise of the grain size leads to a decrease in grain boundary potential barrier heights. So, during the electronic flow charge carrier has to cross fewer barriers, ultimately it increases the conductivity of the film [28].

Reflectance:

Reflectance characteristics of back contact plays a dynamic role in the overall conversion efficiency of the CIGS based solar cell. Reflectivity behavior of our film was demonstrated with UV-vis. Reflectivity was increased with an increase in deposition power. Whereas, at high powers reduction in reflectance was observed. Whereas the percentage reflectance reduced as the gas pressure was increased. Fig. 7 a and Fig. 7 b illustrates the reflectance capability of Mo thin film at different deposition conditions. The rise in reflectance with an increase in sputtering power can be explained by the grain boundaries. Excess grain boundaries are the main barrier in reflectivity. As deposition power increases, grain size increased, which reduced the number of grain boundaries. Ultimately, high reflective thin films was observed at moderate sputtering powers [29]. But in case of relatively high power (300 W) very large grains make coating surface rougher which decreases reflectance capability of Mo thin film. Comparing results among different gas pressures, it is observed that percentage reflectance decreased with an increase in gas pressure. With increasing gas pressure, the deposition rate increased, resulting in more rougher samples for the atoms that don't find considerable time to settle in their preferred low energy positions. For a rougher surface, Lambertian reflectance is more pronounced, compelling an electromagnetic ray to undergo several reflections with the sample surface features prior to leaving it thus losing a part of its total energy with each reflection. As a consequence, the absorbed/transmitted component increases relatively to a non-Lambertian smoother surface [30]. In literature it has been shown that an increase in power or working gas pressure leads to a reduction of reflectance characteristic [29].

Adhesion testing

Scotch test method (Table II) revealed that thin films which were prepared at high working gas pressure and high sputtering power has good adhesive properties. Surface images of cross-cut area after scotch tape removal are shown in Fig. 9. Each thin film developed at high gas pressure shows excellent adhesion behavior while those which were deposited at low gas pressure and low sputtering power delaminated and failed adhesion tape test. The film deposited at 55 watts and 2 Pa delaminated up to 70% and ranked 5th in our standard reference classification chart which is the worse scale for adhesion [1]. Film produced at 100 watts and 2 Pa delaminated up to 20 % and was placed 3rd. The failure of Mo thin film

adhesion at low gas pressure can be related with the build-up of internal compressive stress during the nucleation process [29]. Film with compressive stress tends to buckle up and delaminate from the underlying substrate. At low sputtering power, the lack of adhesion can be associated with incomplete coalescence processes, porous structure, and formation of microcracks. All the films deposited at high gas pressure showed excellent adhesion behavior. At gas pressure of 4 Pa, due to tensile stress and smaller grain size, strong adhesion was observed between the substrate and thin films.

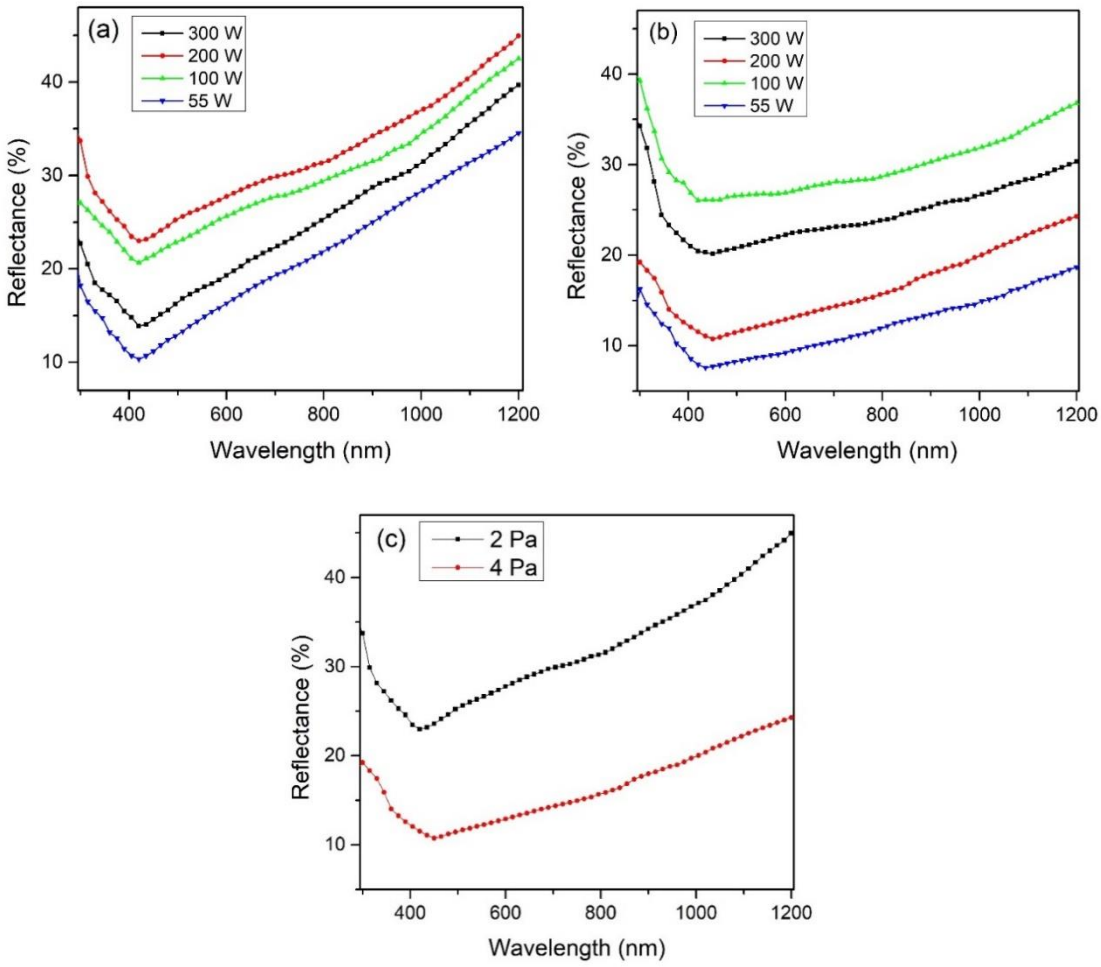

Fig.7. Deposition power dependence on reflectance for gas pressure of a)2 Pa, b) 4 Pa, c) dependence of gas pressure on reflectance at 200 W.

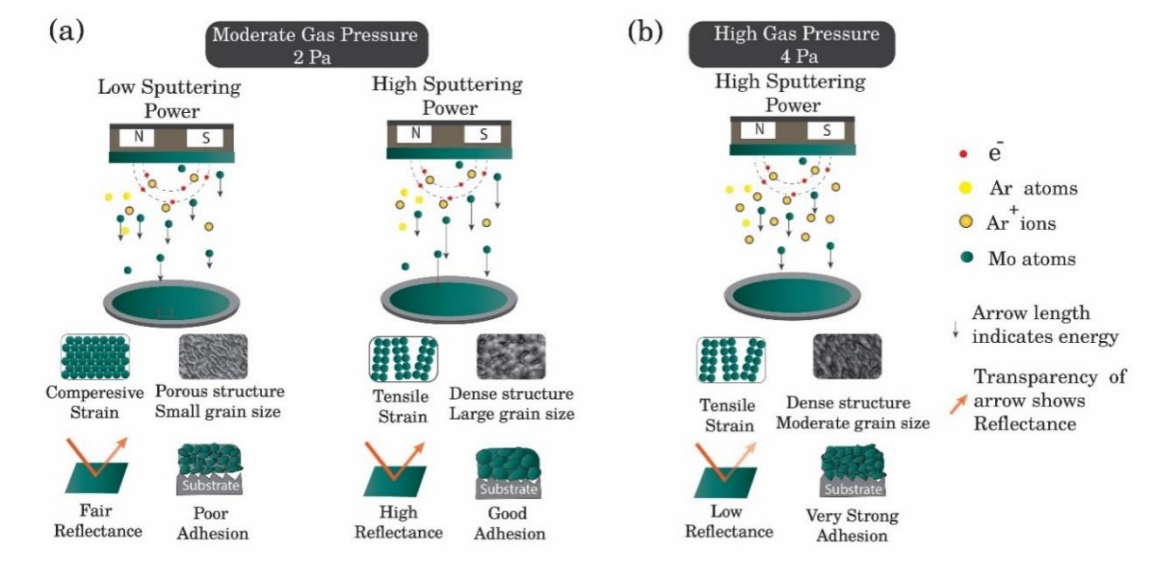

Fig. 8. Detail Schematic of impact of process parameter on desire characteristics

Table. II. Adhesion behavior of Mo thin films using tape adhesion test

Sample ID	Gas pressure (Pa)	Sputtering power (W)	Percentage of area removed	ISO Damage level	Performance
a	2	55	Greater than 65 %	5	Fail
b		100	Greater than 20 %	3	Fail
c		200	Less than 5%	1	Pass
d		300	0 %	0	Pass
e	4	55	Less than 5%	1	Pass
f		100	Less than 5%	1	Pass
g		200	Less than 5%	1	Pass
h		300	0 %	0	Pass

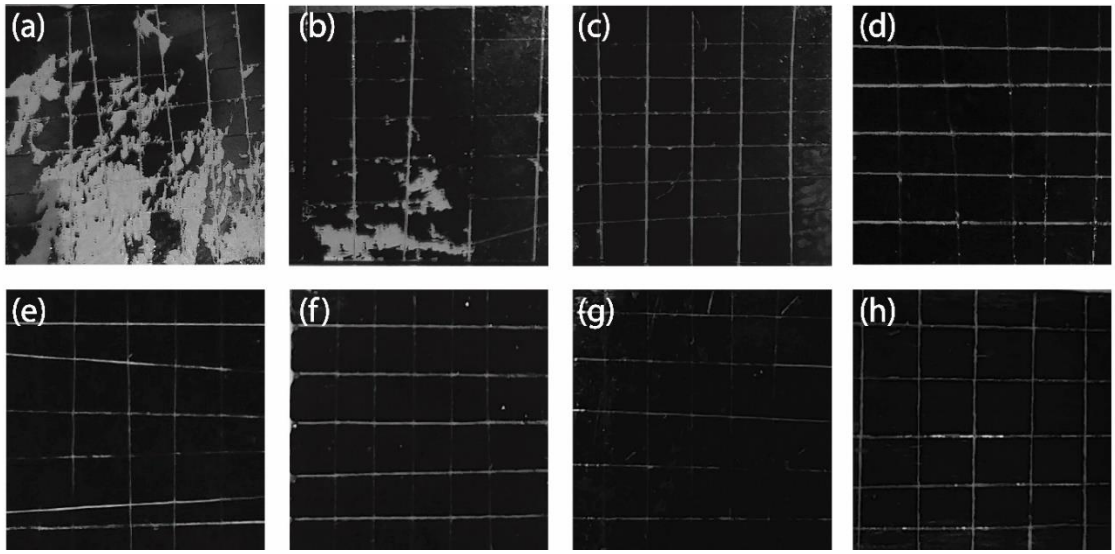

Fig. 9. Surface images of cross-cut area after scotch tape removal of Mo thin film deposited at 2 Pa with deposition power of a) 55 W, b) 100 W, c) 200 W, d) 300 W and at 4 Pa with deposition power of e) 55 W, f) 100 W, g) 200 W, h) 300 W.

Conclusion

DC magnetron sputtered Mo thin films were developed on the SLG substrate. To demonstrate the impact of varying deposition power and gas pressure on the crystallite size, residual stress, resistivity and reflectance properties. Scanning electron microscopy shows improvement in grain size with an increase in power, while XRD results demonstrate that crystallites of the film are oriented in (110) phase. Enhanced crystallinity was achieved at 100 W and 2 Pa pressure while high power and high gas pressure results in tensile thin films. Highly conductive films were obtained at 2 Pa and 300 W. Improved reflectance was achieved at low pressure and moderate power ranges. Reduction in the mean free mean path leads to smooth transfer of sputter flux that enhanced film quality. Improved adhesion was observed at high gas pressure and high sputtering powers. Decisively, adequate class thin films suitable for back contact of CIGS were obtained at high sputter power and low gas pressure.

Acknowledgments: This work was financially supported by the Research and PGP Directorates of National University of Sciences and Technology (NUST), Islamabad, Pakistan.

References:

[1] A. E. B. Kashyout, H. M. A. Soliman, H. Abou, P. Aly, and M. Fathy, "Preparation and characterization of DC sputtered molybdenum thin films," *Alexandria Eng. J.*, vol. 50, no. 1, pp. 57–63, 2011, doi: 10.1016/j.aej.2011.01.009.

[2] H. Ahn, D. Lee, and Y. Um, "Substrate Temperature Effects on DC Sputtered Mo thin film," *Appl. Sci. Converg. Technol.*, vol. 26, no. 1, pp. 11–15, 2017, doi: 10.5757/ASCT.2017.26.1.11.

[3] D. Rafaja *et al.*, "Effect of the deposition process and substrate temperature on the microstructure defects and electrical conductivity of molybdenum thin fi lms," *Thin Solid Films*, vol. 528, pp. 42–48, 2013, doi: 10.1016/j.tsf.2012.06.087.

[4] P. Blösch *et al.*, "Sodium-doped molybdenum back contact designs for Cu (In , Ga) Se 2 solar cells," *Sol. Energy Mater. Sol. Cells*, vol. 124, pp. 10–16, 2014, doi: 10.1016/j.solmat.2014.01.020.

[5] M. Theelen *et al.*, "Influence of deposition pressure and selenisation on damp heat degradation of the Cu (In , Ga) Se 2 back contact molybdenum," *Surf. Coat. Technol.*, vol. 252, pp. 157–167, 2014, doi: 10.1016/j.surfcoat.2014.05.001.

[6] S. Lee *et al.*, "Effect of sputtering parameters on the adhesion force of copper / molybdenum metal on polymer substrate," *Curr. Appl. Phys.*, vol. 11, no. 5, pp. S12–S15, 2011, doi: 10.1016/j.cap.2011.06.019.

[7] N. Akcay, N. A. Sonmez, E. P. Zaretskaya, and S. Ozcelik, "Influence of deposition pressure and power on characteristics of RF- Sputtered Mo fi lms and investigation of sodium diffusion in the fi lms," *Curr. Appl. Phys. J.*, vol. 18, 2018, doi: 10.1016/j.cap.2018.02.014.

[8] M. A. Mart and C. Guillén, "Comparison between large area dc-magnetron sputtered and e-beam evaporated molybdenum as thin film electrical contacts," *J. Mater. Process. Technol.*, vol. 144, pp. 326–331, 2003, doi: 10.1016/S0924-0136(03)00436-9.

[9] F. Jingxue *et al.*, "Preparation and optimization of a molybdenum electrode for CIGS solar cells Preparation and optimization of a molybdenum electrode for CIGS solar cells," *AIP Adv.*, vol. 115210, 2016, doi: 10.1063/1.4967427.

[10] O. Briot *et al.*, "Solar Energy Materials and Solar Cells Optimization of the properties of the molybdenum back contact deposited by radiofrequency sputtering for Cu (In 1 − x Ga x) Se 2 solar cells," *Sol. Energy Mater. Sol. Cells*, vol. 174, no. September 2017, pp. 418–422, 2018, doi: 10.1016/j.solmat.2017.09.019.

[11] R. Latif, M. F. Aziz, and B. Y. Majlis, "Control of physical and microstructural properties in molybdenum by direct current magnetron sputtering deposition producing bilayer thin fi lm," *Thin Solid Films*, vol. 665, no. August, pp. 17–28, 2018, doi: 10.1016/j.tsf.2018.08.043.

[12] M. Khan and M. Islam, "Deposition and Characterization of Molybdenum Thin

Films Using DC Plasma Magnetron Sputtering," *Semiconductors*, vol. 47, no. 12, pp. 1610–1615, 2013, doi: 10.1134/S1063782613140017.

[13] X. Dai, A. Zhou, L. Feng, Y. Wang, J. Xu, and J. Li, "Molybdenum thin films with low resistivity and superior adhesion deposited by radio-frequency magnetron sputtering at elevated temperature," *Thin Solid Films*, vol. 567, pp. 64–71, 2014, doi: 10.1016/j.tsf.2014.07.043.

[14] M. G. Faraj *et al.*, "Investigation on Molybdenum Thin Films Deposited by DC-Sputtering on Polyethylene Terephthalate Substrate Investigation on Molybdenum Thin Films Deposited by DC-Sputtering on Polyethylene Terephthalate Substrate," vol. 4037, no. August 2017, 2010, doi: 10.1080/00914031003760733.

[15] B. Guo, Y. Wang, and X. Zhu, "Molybdenum thin films fabricated by rf and dc sputtering for Cu (In , Ga) Se 2 solar cell applications," *Chinese Opt. Lett.*, doi: 10.3788/COL201614.043101.The.

[16] G. Gordillo, F. Mesa, and C. Calder, "Electrical and Morphological Properties of Low Resistivity Mo thin Films Prepared by Magnetron Sputtering," *Brazilian J. ofPhysics*, vol. 36, no. 3, pp. 982–985, 2006.

[17] D. Zhou *et al.*, "Sputtered molybdenum thin films and the application in CIGS solar cells," vol. 362, pp. 202–209, 2016, doi: 10.1016/j.apsusc.2015.11.235.

[18] T. Jörg, M. J. Cordill, R. Franz, O. Glushko, J. Winkler, and C. Mitterer, "The electro-mechanical behavior of sputter-deposited Mo thin films on flexible substrates," vol. 606, pp. 45–50, 2016, doi: 10.1016/j.tsf.2016.03.032.

[19] R. Das, M. Deo, J. Mukherjee, and M. S. R. Rao, "Strain induced FCC to BCC structural change in sputtered molybdenum thin films," *Surf. Coat. Technol.*, vol. 353, no. August, pp. 292–299, 2018, doi: 10.1016/j.surfcoat.2018.08.065.

[20] P. Chelvanathan *et al.*, "Effects of RF magnetron sputtering deposition process parameters on the properties of molybdenum thin fi lms," *Thin Solid Films*, vol. 638, pp. 213–219, 2017, doi: 10.1016/j.tsf.2017.07.057.

[21] C. Roger *et al.*, "Characteristics of molybdenum bilayer back contacts for Cu (In , Ga) Se 2 solar cells on Ti foils," *Thin Solid Films*, vol. 548, pp. 608–616, 2013, doi: 10.1016/j.tsf.2013.09.080.

[22] M. Jubault, L. Ribeaucourt, E. Chassaing, G. Renou, D. Lincot, and F. Donsanti, "Optimization of molybdenum thin films for electrodeposited CIGS solar cells," *Sol. Energy Mater. Sol. Cells*, vol. 95, pp. S26–S31, 2011, doi: 10.1016/j.solmat.2010.12.011.

[23] W. Li, X. Yan, A. G. Aberle, and S. Venkataraj, "Analysis of microstructure and surface morphology of sputter deposited molybdenum back contacts for CIGS solar cells," *Procedia Eng.*, vol. 139, pp. 1–6, 2016, doi: 10.1016/j.proeng.2015.09.231.

[24] B. S. Yadav, A. C. Badgujar, and S. R. Dhage, "Effect of various surface treatments on adhesion strength of magnetron sputtered bi-layer Molybdenum thin films on soda lime glass substrate," *Sol. Energy*, vol. 157, no. September, pp. 507–513, 2017,

doi: 10.1016/j.solener.2017.08.068.

[25] O. Poncelet, R. Kotipalli, B. Vermang, A. Macleod, L. A. Francis, and D. Flandre, “Optimisation of rear reflectance in ultra-thin CIGS solar cells towards > 20 % efficiency,” *Sol. Energy*, vol. 146, pp. 443–452, 2017, doi: 10.1016/j.solener.2017.03.001.

[26] B. Vermang *et al.*, “Highly reflective rear surface passivation design for ultra-thin Cu (In , Ga) Se 2 solar cells,” *Thin Solid Films*, vol. 582, pp. 300–303, 2015, doi: 10.1016/j.tsf.2014.10.050.

[27] D. Rafaja *et al.*, “Effect of the deposition process and substrate temperature on the microstructure defects and electrical conductivity of molybdenum thin fi lms,” vol. 528, pp. 42–48, 2013, doi: 10.1016/j.tsf.2012.06.087.

[28] S. Karthikeyan, L. Zhang, S. Hwang, and S. A. Campbell, “Experimental scheme for a stable molybdenum bilayer back contacts for photovoltaic applications,” *Appl. Surf. Sci.*, vol. 449, pp. 647–653, 2018, doi: 10.1016/j.apsusc.2017.11.277.

[29] H. Cao, C. Zhang, and J. Chu, “The effect of working gas pressure and deposition power on the properties of molybdenum films deposited by DC magnetron sputtering,” *Sci. China Technol. Sci.*, vol. 57, no. 5, pp. 947–952, 2014, doi: 10.1007/s11431-014-5537-x.

[30] S. A. Jesuraj, P. Kuppusami, T. Dharini, P. Panda, and D. Devapal, “effect of substrate temperature on microstructure and nanomechanical properties of Gd 2 Zr 2 O 7 coatings prepared by EB-PVD technique,” *Ceram. Int.*, vol. 44, no. 15, pp. 18164–18172, 2018, doi: 10.1016/j.ceramint.2018.07.024.

Appendix B: Research Article 2

Structural evaluation and irradiation hardening in alfa-particles irradiated DC magnetron sputtered Mo thin film

Nisar Ahmed, Zuhair S. Khan, Muhammad Azhar Iqbal, Asghar Ali

U.S.-Pakistan Center for Advanced Studies in Energy, National University of Sciences and Technology, Islamabad 44000, Pakistan.

Abstract: This study is an account of the irradiation effects on the microstructure, morphology, topography, hardening behavior, and electrical characteristics of molybdenum (Mo) films deposited over graphite. For the purpose, almost 2.4 μm thick Mo films were deposited employing DC magnetron sputtering and were irradiated with He ions of 0.8 MeV and 1.6 MeV, with an equivalent dose of 0.0765 and 0.645 DPA, respectively. A decrease in the film crystallinity was observed with an increase in the radiation dose. In fact, there was a minimal decrease in the crystallite size for the low dose α-particles radiation, however, the crystallite size decreased significantly with the high dose radiation. Furthermore, it was deduced that the irradiation induced lattice strain turns compressive thin films into tensile thin films. The micrographs reveal the presence of micro-pores and fuzz in the irradiated samples. The topographical analysis depicts the formation of hill like structure and an increase in surface roughness with the enhanced radiation dose. Some degree of hardening was observed for samples irradiated with the 0.8 MeV α-particles; however, significant hardening was demonstrated by the sample irradiated with the 1.6 MeV radiation. Moreover, the electrical conductivity was found to significantly decrease with an increase in the radiation dose.

Graphical Abstract:

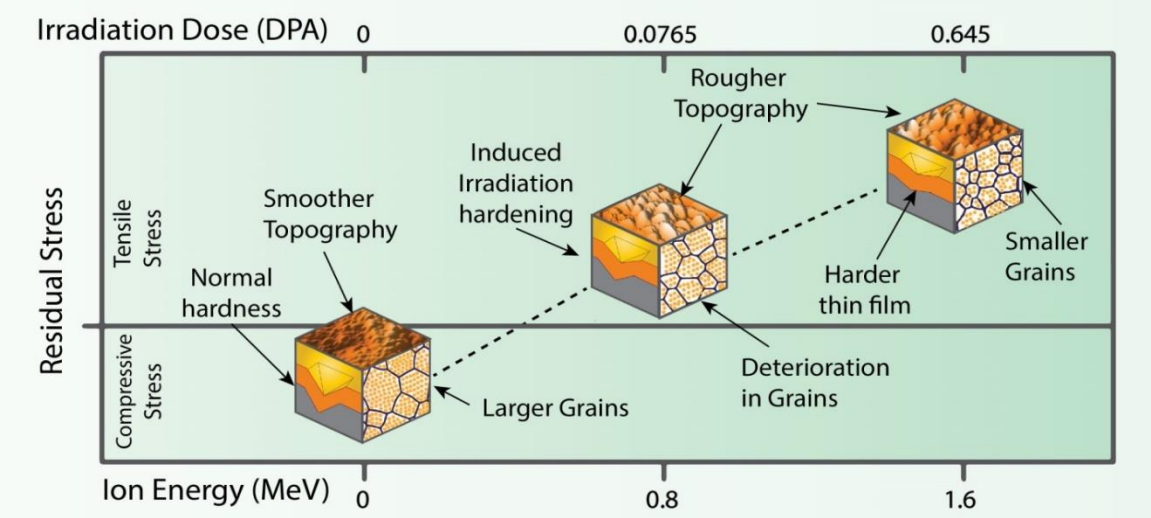

Keywords:

Molybdenum, Thin films, ITER, Plasma Facing Components, Ion beam irradiation

1. Introduction:

In magnetically confined nuclear fusion, diverter is one of the key components, where field lines are straightly incident on an area of the vessel wall and it is subjected to steady-state heat fluxes in the shape of high energy radiations, neutrons and α-particles [1]. Generally, Low Z elements such as Beryllium and Graphite are used for the development of PFCs because of their tolerable concentration in the fusion plasma. Graphite is often considered as an aspiring candidate for the development of PFCs components due to its high heat flux tolerance [2]. But relatively large erosion of graphite during bombardment of α-particles in fusion plasma is critical matter. Other than physical sputtering, enhanced erosion which leads to the formation and release of hydrocarbons, is the key issue [3]. So, protecting graphite from direct erosion and light ion sputtering is crucial. This can be done by depositing appropriate material with low sputtering yield on graphite. High Z number elements like refractory metals can be suitable option because very high energy is required for these elements to undergo light ion sputtering [4]. So refractory metals have been proposed for development of plasma facing components.

Tungsten has been considered as potential contender for first wall and plasma-facing component due to its high melting point and very low sputtering yield [5]. But brittleness

due to neutron irradiation and loss of strength during recrystallization are the limitations associated with tungsten. Molybdenum also belongs to Refractory metals and is similar to tungsten in terms of thermo electrical properties and a potential substitute contender for PFCs materials [6]. Mainly, difference in Co-efficient of thermal expansion (CTE) of thin film and substrate material prompts adhesion loses, which can lead to instability of PFCs. CTE of Mo (4.8 μm/m °C) and graphite (5.9 μm/m °C) is more matching than that of tungsten (4.5 μm/m °C), that can enhance stability of Mo films [7]. However, activation of molybdenum as a result of neutrons in real time scenarios is the key issue [6]. Helium often forms as a result of transmutation reactions (n, a) during reactor operations specifically in neutron irradiation environment and it cause embrittlement and swelling. This has been a cause of concerns in term of structural integrity. For feasible commercial fusion power plants, to estimate functional characteristics and integrity of plasma facing components under the harsh environment, it is important to understand generation and retention of irradiation-induced defects. The irradiation experiments of helium ions (α-particles) in metals by ion beam accelerator have been extensively used to find out valuable data for elementary knowledge of the damage behavior of irradiated materials, as it gives a suitable way of concurrently mimicking damage caused by high energy neutron irradiation and α-particles [8]. The micro structural evolution in the material as a result of irradiation has been studied by varying different factors like energies, fluence and irradiation. Helium release and lattice swelling were typical phenomena reported by many investigations in the irradiated materials. This phenomenon often leads to generation of lattice strain which itself is cause of residual stress. They can be on the order of few Giga Pascals [9]. These stresses will add to structural in-service loads, it leads to stress-offset. So, it is important to include them in estimating the overall fatigue performance of structural components [10]. However, the concerned knowledge and mechanisms are not yet fully understood, which need to be further explored. So, the evolution of helium in molybdenum and its relative research have been research hotspot [11].

In this study, molybdenum thin film has been deposited on graphite by DC magnetron sputtering and then exposed to two different doses of helium ion to assess their effects on the microstructure, topography and mechanical characteristics. Structural evolution caused by helium ions was analyzed by X-Ray Diffraction. Surface morphology and topography

were characterized by scanning electron microcopy (SEM) and atomic force microscopy (AFM), respectively. Micro hardness is used to assess the irradiation hardening behavior of Mo thin film. Moreover, change in conductivity behavior was demonstrated by Hall Effect method.

2. Experimentation Method:

2.1.Sample Deposition:

Molybdenum thin film was deposited on graphite substrate using direct current Magnetron Sputtering. NANOVAK NVTS 400 was employed for this purpose. Graphite substrate with thickness of 1.5 mm was polished up to one micron and moisture removal was ensured by heating substrate at 200 Celsius in the vacuum oven prior to deposition. Molybdenum target with two-inch diameter and 99.9% purity was utilized. High vacuum of 5×10^{-7} torr was achieved using Oerlikon TURBOVAC 450 turbo-molecular pump. Substrate was heated up to 300 C and substrate rotation speed was maintained at 15 rpm. Sputtering power was kept 300 W with working gas pressure of 1 Pa . Thickness of 2.4 micron was achieved in 40 minutes with deposition rate of 10 Å/s.

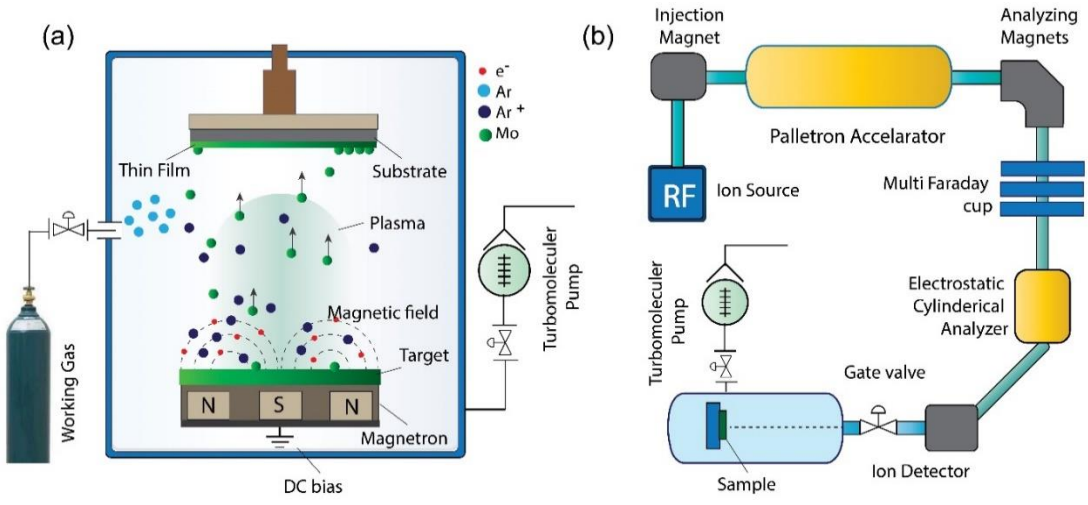

Fig.1 a). Illustration of Molybdenum thin film deposition through Direct Current Magnetron Sputtering, b). Schematic of equipment for irradiation experiment [12]

2.2.SRIM Calculations:

Irradiation parameters such as the projected range of α-particle in Molybdenum thin film, ion energy and incident angle etc. were predicted using Stopping Range of Ions in Matter (SRIM) program before irradiation experiment. Moreover, the loss in electronic (S_e) and nuclear energy (S_n), and damage per atom (DPA) were also calculated [13]. Projected range with respect to ion energy is illustrated in the Fig. 2 a. The projected range for 0.8 MeV was 1.28 micron. The electronic and nuclear energy loss was 713.8 keV/micron and 1.347 KeV/micron respectively. Whereas electronic and nuclear energy loss for 1.6 MeV He ion were 635 and 0.780 KeV/micron with the projected range of 2.41 microns. The irradiation parameters indicate that the electronic energy losses for both experiments were way higher than nuclear energy losses. So, all the expected changes in structure, morphology, topography and electrical characteristics in the irradiated Mo thin films can be attributed to electronic energy loss [13].

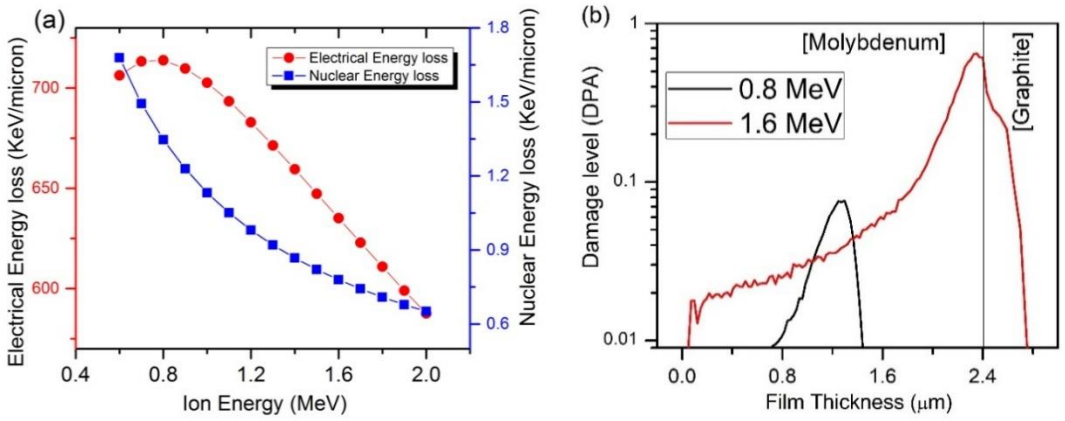

Fig. 2 a) a) Nuclear and electronic energy loss by α-particles in the Mo thin film, b) Vacancies per ion (DPA) for both 0.8 and 1.6 MeV irradiated thin film

Irradiation experiment:

The ion beam experiment was performed in 5 MV Pelletron Tandem accelerator facility available at National Center for Physics, Pakistan. The schematic diagram of Pelletron accelerator is shown in fig. 1 b.

Table I: Irradiation parameters

Sample ID	Ion energy MeV	Fluence Ion/cm^2	Dose DPA
As-deposited	-	-	-
He 0.8	0.8	5.2 x 10^{15}	0.00765
He 1.6	1.6	5.0 x 10^{16}	0.0645

Characterization:

Structural analysis of all pre and post irradiated Mo thin films was done to investigate structural changes cause by irradiation of α-particles. Bruker D8 advanced X-rays diffractometer with CuKα (λ = 1.54056 Å) as radiation source was employed for that purpose. The surface morphology of Mo thin films was analyze using a TESCAN VEGA3 Field Emission Scanning Electron Microscope (FESEM) with an accelerating voltage 5 kilovolt. NANOSURF FLEX AFM was used to estimate the change in film roughness and topography on different irradiation doses. The electrical characterization of Mo thin films was done by Van der Pauw. Ecopia HMS-3000 Hall effect instrument was used for that purpose. Micro-hardness test was performed in order to demonstrate irradiation hardening caused by helium ions.

3. Results and discussion:

Structural characterization:

Impact of α-irradiation on the structure of the Mo thin films was studied using X-ray Diffraction. Mo peak matches with JCPDS card no. 42-1120 and (110) plane was observed. Graphite peak with JCPDS card no. 41-1487 was also observed. The decrease in relative intensity was observed with an increase in ion beam energy and fluence. The full width half maxima of low energy irradiated Mo thin remained unchanged. However, significant increase in FWHM was observed in case of high energy He ion irradiation. The decrease in peak intensities of irradiated samples can be attributed to decrease in defects

concentration by the effect of mutual annihilation of defects. The peak broadening in He irradiated Mo thin film can also cause by formation of point defects like vacancies and interstitials [14].

Various structural parameters were calculated using X-ray diffraction data. The Residual Stress was calculated using the following equation [15]:

$$Residual\ Stress = \sigma = \frac{E\Delta d}{2\nu d_o} \qquad (1)$$

where "d_o" is the standard lattice spacing for molybdenum and Δd is referred to variation between d_o and d. d is actual lattice spacing and can be obtained from following equation.

$$d = \frac{a}{\sqrt{h^2+l^2+k^2}} \qquad (2)$$

Above relation is only applicable for cubic system. *h, l,* and *k* imply to miller indices, where a is lattice parameter.

The un-irradiated (as-deposited) thin film showed compressive stress because this Mo thin film was fabricated at relatively low working gas pressure of 1 Pa (7 mTorr) . The compressive behavior of thin film can be explained by atomic peening model. At low working gas pressure, owing to low amount of working gas, the target atoms will undergo limited collisions with working gas atoms. Hence very small energy loss will occur. The high energy target atoms will deposit on graphite with tightly pack arrangement. Ultimately, compressive film was formed. However, when Mo thin film was irradiated with alfa particles, this compressive thin film turns in to tensile thin film. This is due to formation of radiation induced defects in the form of vacancies and interstitials [16].

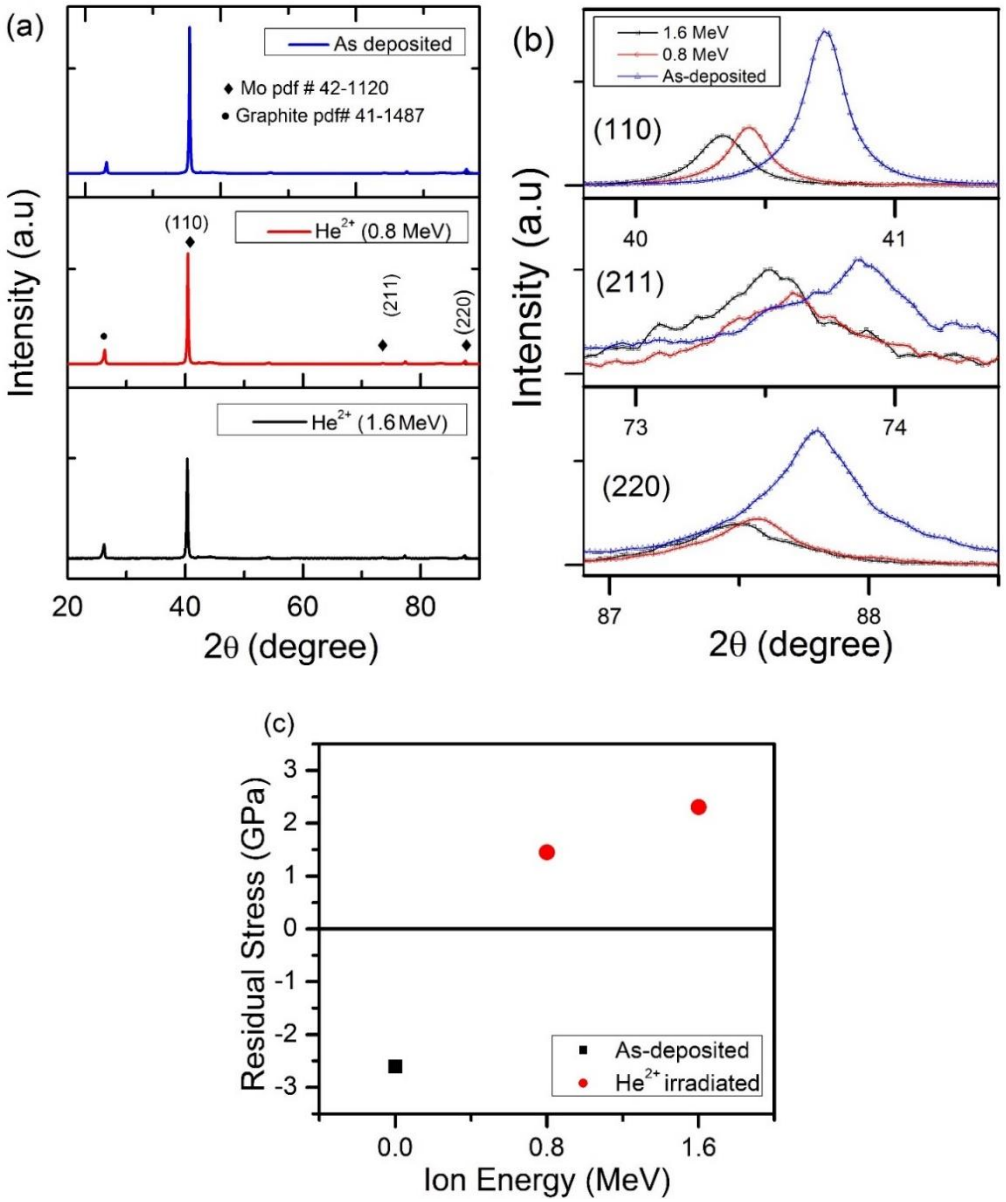

Fig 3. a) XRD spectrum of as deposited and irradiated samples, b) Magnified XRD spectrum of different Mo phases c) Residual stress of all Mo thin films.

Williamson-Hall method has been employed to determine the theeta and strain dependent crystallite size [12]. The general form of Williamson Hall analysis can be written by the following form:

$$\beta \cos\theta = \frac{K\lambda}{D_{WH}} + 4\varepsilon_{WH} \sin\theta \qquad (3)$$

D_{WH} and ε_{WH} are estimated crystallite size and micro strain acquired from Williamson hall method.$\beta$is full width half maxima (FWHM) of respective peak, K is Scherer constant, and λ is wave length of radiation source (for Cukα, λ = 0.154 nm). The Eq. 3 is known as Uniform Deformation Model which is very similar to standard linear equation of straight line. To estimate Crystallite size and strain value, βcosθ is plotted against 4sinθ. Slope of straight line obtained from that graph represents strain value. Whereas crystallite size is obtained from y-intercept. The values of dislocation density, δ of the samples have been calculated using following relation.

$$\delta = \frac{1}{D^2} \quad (4)$$

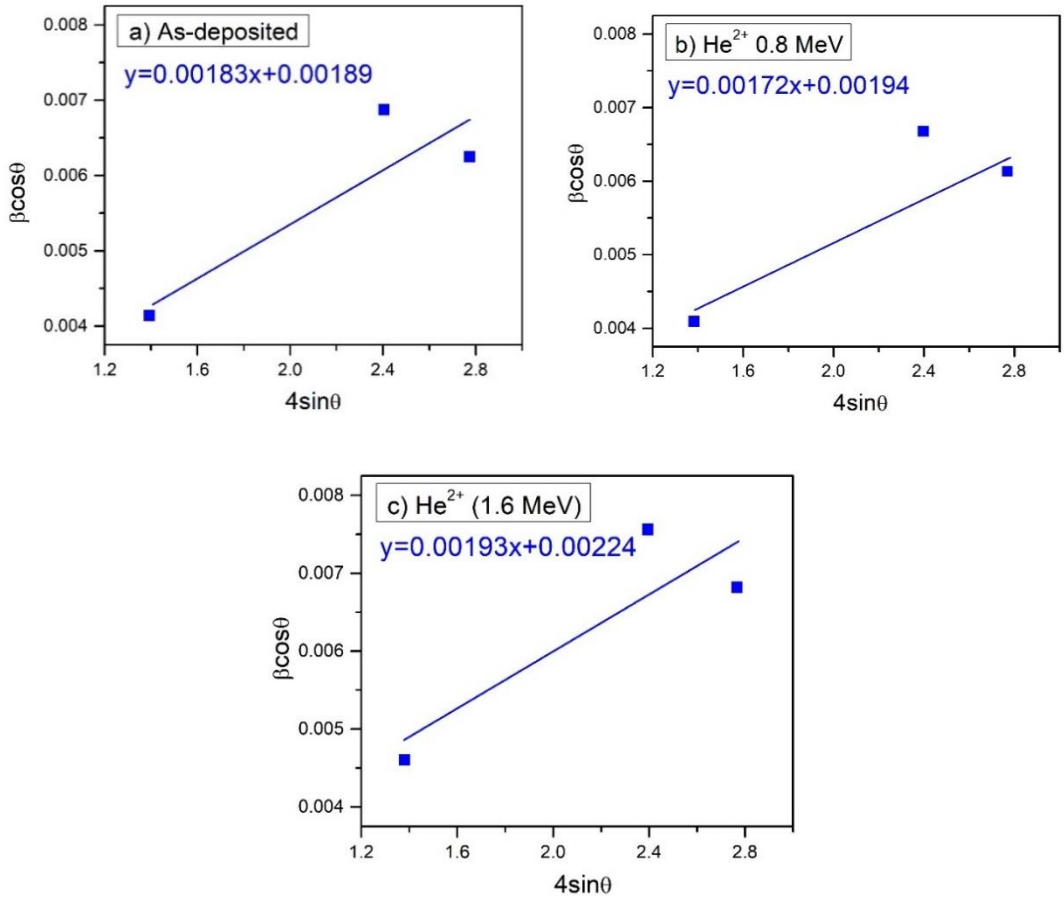

Fig.4. Williamson Hall plot of a) As Deposited Mo thin film, b)0.8 MeV He^{2+}, c)1.6 MeV He^{2+}

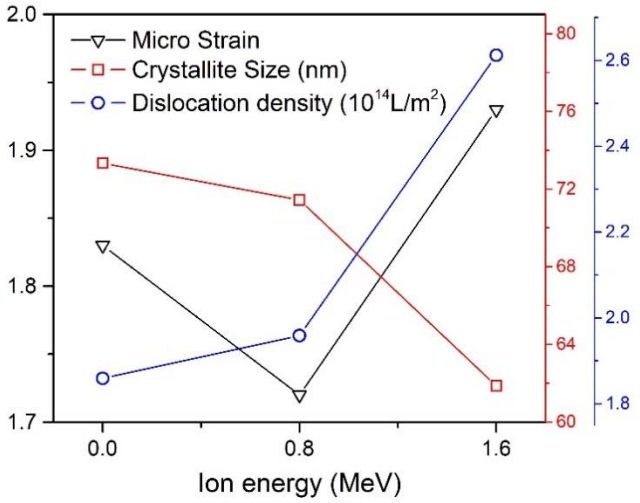

Fig.5. Micro strain, crystallite size, and dislocation density attained from Williamson Hall plot

Williamson hall method reveals deterioration in crystallinity as the irradiation dose was increased. The crystallite size decreased from 73 nm to 71 nm when irradiated with He ion at 0.8 MeV. Whereas, a considerable decrease to 62 nm was observed with 1.6 MeV. As shown in the Fig. 5. At this energy and fluence, the mutual annihilation of defects and dense electronic excitation leads to disorder crystallite size and strain values. This decrease in crystallite size can also be explained via collision cascade process. Energetic Helium ion interacts with the metal via elastic and inelastic collisions. In our case, inelastic collisions are dominant, that took place between He ion and the electrons of target atoms [17]. However, high energy He ions make elastic collisions with nuclei and displace them from their mean positions. Consequently, atoms either terminate on interstitial sites or collide with neighboring atoms and form vacancies in collisional cascade. So, the deteriorated crystallite size, micro strain and increase in dislocation density can be attributed to such radiation-induced defects. Similarly, grain boundaries restrict the growth of dislocations, which is associated to grain size. Decrease in density of crystallite size refers to an increase in grain boundaries. Thus, smaller grain size suggests higher density of smaller dislocations [18].

Surface morphology and topography:

Morphological changes induced by irradiation were evaluated by Scanning electron Microscopy. Fig.8 illustrates comparison of as deposited and irradiated samples. Starting with as deposited sample, relatively smoother surface has been attained and ellipsoid like grains were evident. After irradiation, no delamination has been detected in any sample. However, micro-pores and nano fuzz can be observed in the irradiated thin films, but this effect was minor in 0.8 MeV He irradiated Mo thin film and it was dominant and1.6 MeV helium ion irradiated thin films. This can be explained by surface sputtering which occurs during the continuous bombardment of alfa particles at the near-surface, which leads to micro-pores and nano-fuzz [19]. Grain boundaries of He ion irradiated samples appear to decrease after irradiation, it is possible due to amorphization and reduction in grain size.

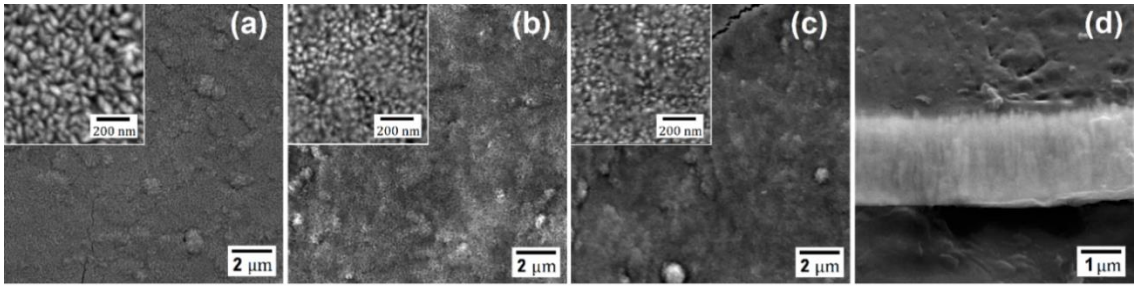

Fig. 6. SEM Images of a) As-deposited Mo thin film, b)0.8 MeV He^{2+}, c)1.6 MeV He^{2+}d) cross section image of as deposited Mo thin film

AFM analysis have been done to examine any possible transformation in surface topography of irradiated Mo thin films. Fig. 7 shows the AFM Images of as deposited and both irradiated samples. It depicts that the as-deposited sample is smoother than all of irradiated samples with least structural features. Root mean area roughness of irradiated sample was measured, Fig. 8 a) shows root mean square roughness of all as deposited and irradiated samples. The increase in area roughness after helium ion irradiation is due to the formation of agglomerated structures and micro-pores on the surface.

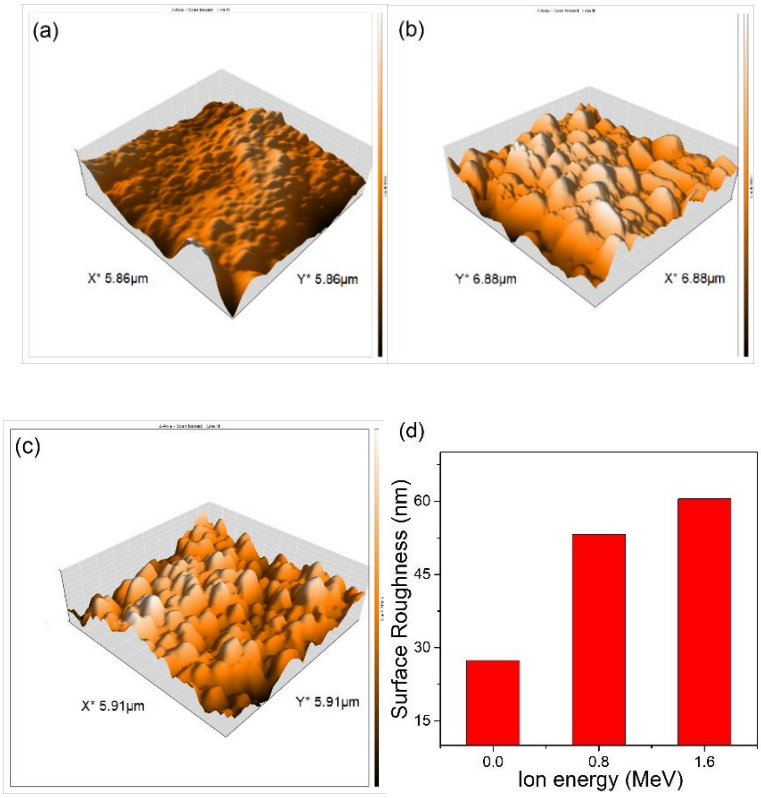

Fig. 7. AFM Images of a) As Deposited Mo thin film b) 0.8 MeV He^{2+}, c)1.6 MeV He^{2+}d) Area roughness of all thin films

Hardness testing

Micro-hardness testing was performed in order to demonstrate irradiation hardening caused by helium ion irradiation on deposited Mo thin film. Since our coating was thin, the hardness measured in this experiment was combined-Vickers hardness including substrate effect. Absolute hardness was calculated by given equation [20]:

$$H_f = H_s + (H_c - H_s)/\{\frac{2Ct}{D} - \left(\frac{Ct}{D}\right)^2\} \quad (5)$$

Here H_f is absolute hardness of Mo Thin film, H_s is hardness of bare substrate, whereas H_c is combined hardness of thin film and substrate. D is the depth of scratch which is corresponding to $1/7^{th}$ of impression diagonal d and t represents thickness of thin film which is 2.41 micron. C is the constant which depends on the geometry of the scratch. If thin film harder than substrate then value of C will be $2\sin^2\theta$ (Where $\theta = 11°$). The

combined hardness of substrate and thin films on different loads is given in Fig. 8 a. The average hardness values of thin films with error bar against the ion energies are plotted in Fig.8 b. The archived hardness values were 192 HV, 218 HV and 290 HV for as deposited, 0.8 MeV He^{2+} and 1.6 MeV He^{2+} irradiated Mo thin films respectively.

It is observed that combined hardness of irradiated thin films remained greater than as-deposited thin film on different loads as portrayed in fig. 8 a. Similarly, absolute Vickers hardness showed the same trends. At first, about 17 percent increase in Vickers hardness was observed for the sample irradiated at 0.8 MeV as compare to as-deposited thin film. Since no major change in crystallite size was observed for that sample, so irradiation hardening at this energy can be associated with induced point defects and dislocation loops. The presence of irradiation induced dislocation loops in Mo thin film increase the critical stress necessary to move the dislocations. However, significant rise in Vickers hardness value was observed for the sample irradiated at 1.6 MeV with equivalent dose of 0.645 DPA. The Vickers hardness increases up to 50 percent. The increased dislocation loops size with increase in irradiation dose strengthens the pinging effect and increases the hardness [21]. This can also be associated with decrease in crystallite size at higher dose as illustrate in fig. 5 b.

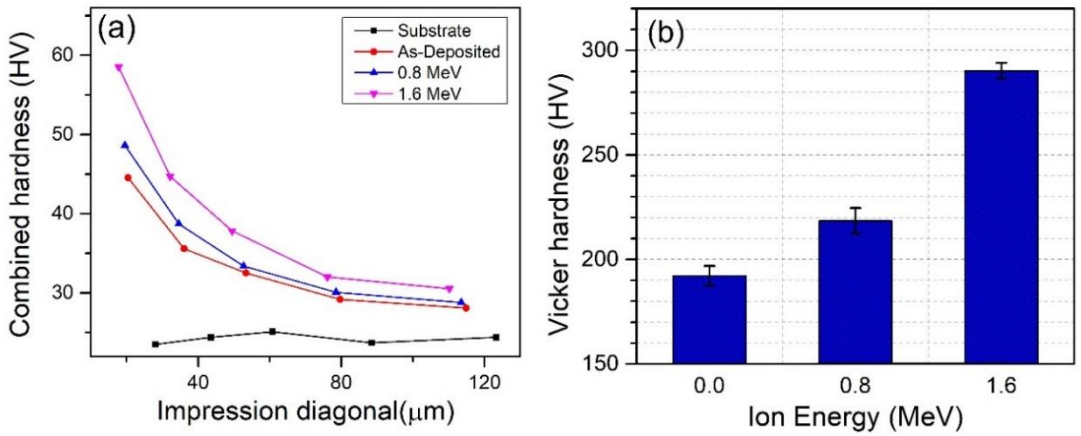

Fig. 8 a). Combined hardness of substrate and Mo thin films on different loads. b). The average hardness values of thin films with error bar against the ion energies

Electrical characterization:

Hall effect measurements were carried out in order to demonstrate the effect of irradiation on electrical characteristics of Mo thin film. Increase in resistivity was observed with increase in irradiation dose. Fig 9 showed results obtained from Hall effect. The resistivity of 0.23 μΩcm was observed for as-deposited sample which increased to 0.76 μΩcm as a result of 0.8 MeV He irradiation. Highest resistivity of 1.27 μΩcm was found for the specimen treated at 1.6 MeV. The reduction in conductivity behavior can be associated with defect annihilation and amorphization as a result of irradiation dose which leads to decrease in crystallite size and increase in number of grain boundaries. The increase in potential barrier heights means charge carriers have to cross more barriers [16]. Hence, conductivity decreased as the irradiation dose increased.

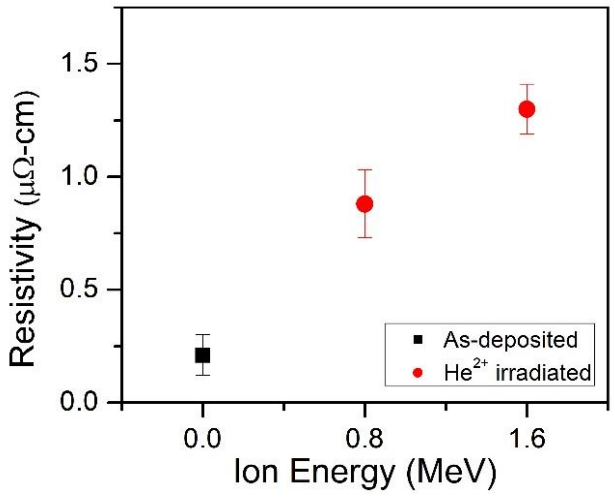

Fig 9. Electrical resistivity of pre and post irradiation Mo thin films.

4. Conclusion:

Molybdenum film was deposited on the graphite substrate via DC magnetron sputtering. Irradiated samples were evaluated by changing the dose of He ions (0.0765 and 0.645 DPA) and following results were drawn. Irradiations cause changes in surface morphology such as micro pores were evolved. Moreover, root mean roughness increases with the increase in irradiation energy. High dose (1.6 MeV) irradiation caused a significant decrease in crystallite size. Furthermore, residual stress increased with increase in the irradiation dose so that compressive films turned into tensile. Irradiation produces

hardening in the samples: values were small with 0.8 MeV. However, a prominent rise up to 50 percent was observed at 1.6 MeV irradiation. As well as, decrease in conductivity was evident with an increase in irradiation dose.

Acknowledgments:

This research was financially supported by the Research and PGP Directorates of National University of Sciences and Technology (NUST), Islamabad, Pakistan.

Data availability:

The raw data required to reproduce these findings are available to download from [https://drive.google.com/open?id=1HPl5VyQensCFDFDlSBArhYkd3KCTUeyY]. The processed data required to reproduce these findings are available to download from [https://drive.google.com/open?id=1hkT7FN0QhTgkvfMwdDqK9hO9c_wxehxM].

References:

[1] M. Turnyanskiy *et al.*, "European roadmap to the realization of fusion energy: Mission for solution on heat-exhaust systems," *Fusion Eng. Des.*, vol. 96–97, pp. 361–364, 2015, doi: 10.1016/j.fusengdes.2015.04.041.

[2] J. Roth, "Sputtering of limiter and divertor materials," *J. Nucl. Mater.*, vol. 176–177, no. C, pp. 132–141, 1990, doi: 10.1016/0022-3115(90)90035-L.

[3] J. Roth, "Chemical erosion of carbon based materials in fusion devices," *J. Nucl. Mater.*, vol. 266, pp. 51–57, 1999, doi: 10.1016/S0022-3115(98)00658-8.

[4] B. V. Mech, A. A. Haasz, and J. W. Davis, "Model for the chemical erosion of graphite due to low-energyH+ and D+ impact," *J. Appl. Phys.*, vol. 84, no. 3, pp. 1655–1669, 1998, doi: 10.1063/1.368235.

[5] R. Neu *et al.*, "Final steps to an all tungsten divertor tokamak," *J. Nucl. Mater.*, vol. 363–365, no. 1–3, pp. 52–59, 2007, doi: 10.1016/j.jnucmat.2006.12.021.

[6] D. Hancock, D. Homfray, M. Porton, I. Todd, and B. Wynne, "Refractory metals as

structural materials for fusion high heat flux components," *J. Nucl. Mater.*, vol. 512, pp. 169–183, 2018, doi: 10.1016/j.jnucmat.2018.09.052.

[7] G. S. Cho and K. H. Choe, "Characterization of plasma-sprayed tungsten coating on graphite with intermediate layers," *Surf. Coatings Technol.*, vol. 209, pp. 131–136, 2012, doi: 10.1016/j.surfcoat.2012.08.051.

[8] H. Trinkaus and B. N. Singh, "Helium accumulation in metals during irradiation - Where do we stand?," *J. Nucl. Mater.*, vol. 323, no. 2–3, pp. 229–242, 2003, doi: 10.1016/j.jnucmat.2003.09.001.

[9] F. Hofmann *et al.*, "Lattice swelling and modulus change in a helium-implanted tungsten alloy: X-ray micro-diffraction, surface acoustic wave measurements, and multiscale modelling," *Acta Mater.*, vol. 89, pp. 352–363, 2015, doi: 10.1016/j.actamat.2015.01.055.

[10] F. Hofmann *et al.*, "Micro-beam Laue alignment of multi-reflection Bragg coherent diffraction imaging measurements," *J. Synchrotron Radiat.*, vol. 24, no. 5, pp. 1048–1055, 2017, doi: 10.1107/S1600577517009183.

[11] S. Huang *et al.*, "Effect of crystal orientation on hardness of He+ ion irradiated tungsten," *Nucl. Instruments Methods Phys. Res. Sect. B Beam Interact. with Mater. Atoms*, vol. 406, pp. 585–590, 2017, doi: 10.1016/j.nimb.2017.04.063.

[12] A. Khan, M. Rafique, N. Afzal, Z. Khaliq, and R. Ahmad, "Structural characterization of Zircaloy-4 subjected to helium ions irradiation of variable fluence," *Nucl. Mater. Energy*, vol. 20, no. March, p. 100690, 2019, doi: 10.1016/j.nme.2019.100690.

[13] V. Chauhan, T. Gupta, P. Singh, P. D. Sahare, N. Koratkar, and R. Kumar, "Influence of 120 MeV S9+ ion irradiation on structural, optical and morphological properties of zirconium oxide thin films deposited by RF sputtering," *Phys. Lett. Sect. A Gen. At. Solid State Phys.*, vol. 383, no. 9, pp. 898–907, 2019, doi: 10.1016/j.physleta.2018.12.013.

[14] I. Yamada, "Progress, demands and prospects for advanced ion beam processing," *Mater. Chem. Phys.*, vol. 54, no. 1–3, pp. 5–14, 1998, doi: 10.1016/S0254-0584(98)00112-6.

[15] H. Cao, C. Zhang, and J. Chu, "The effect of working gas pressure and deposition power on the properties of molybdenum films deposited by DC magnetron sputtering," *Sci. China Technol. Sci.*, vol. 57, no. 5, pp. 947–952, 2014, doi: 10.1007/s11431-014-5537-x.

[16] N. Ahmed, M. A. Iqbal, Z. S. Khan, and A. A. Qayyum, "DC Magnetron-Sputtered Mo

Thin Films with High Adhesion, Conductivity and Reflectance," *J. Electron. Mater.*, 2020, doi: 10.1007/s11664-020-08138-2.

[17] N. Afzal *et al.*, "Influence of carbon ion implantation energy on aluminum carbide precipitation and electrochemical corrosion resistance of aluminum," *Nucl. Instruments Methods Phys. Res. Sect. B Beam Interact. with Mater. Atoms*, vol. 436, no. September, pp. 84–91, 2018, doi: 10.1016/j.nimb.2018.09.008.

[18] F. A. Mir and K. M. Batoo, "Effect of Ni and Au ion irradiations on structural and optical properties of nanocrystalline Sb-doped SnO2 thin films," *Appl. Phys. A Mater. Sci. Process.*, vol. 122, no. 4, pp. 1–7, 2016, doi: 10.1007/s00339-016-9948-3.

[19] Q. Yang *et al.*, "Nanostructured fuzz growth on tungsten under low-energy and high-flux He irradiation," *Sci. Rep.*, vol. 5, pp. 1–9, 2015, doi: 10.1038/srep10959.

[20] B. Jönsson and S. Hogmark, "Hardness measurements of thin films," *Thin Solid Films*, vol. 114, no. 3, pp. 257–269, 1984, doi: 10.1016/0040-6090(84)90123-8.

[21] M. Zhao *et al.*, "Fluence dependence of helium ion irradiation effects on the microstructure and mechanical properties of tungsten," *Nucl. Instruments Methods Phys. Res. Sect. B Beam Interact. with Mater. Atoms*, vol. 414, pp. 121–125, 2018, doi: 10.1016/j.nimb.2017.09.002.